UNDERSTANDING OF CHARGE EFFECTS IN PICKERING EMULSIONS AND DESIGN OF DOUBLE PICKERING EMULSION TEMPLATED COMPOSITE MICROCAPSULES

A Dissertation
Presented to
The Academic Faculty

by

Hongzhi Wang

In Partial Fulfillment
of the Requirements for the Degree
Doctor of Philosophy in the School of
Chemical & Biomolecular Engineering

Georgia Institute of Technology

December, 2013

UNDERSTANDING OF CHARGE EFFECTS IN PICKERING EMULSIONS AND DESIGN OF DOUBLE PICKERING EMULSION TEMPLATED COMPOSITE MICROCAPSULES

Approved by:

Dr. Sven Holger Behrens, Advisor
School of Chemical and Biomolecular Engineering
Georgia Institute of Technology

Dr. Alberto Fernandez-Nieves
School of Physics
Georgia Institute of Technology

Dr. Victor Breedveld
School of Chemical and Biomolecular Engineering
Georgia Institute of Technology

Dr. Carson Meredith
School of Chemical and Biomolecular Engineering
Georgia Institute of Technology

Dr. Yulin Deng
School of Chemical and Biomolecular Engineering
Georgia Institute of Technology

Date Approved: Nov 11th, 2013

[To my family for their love and support]

ACKNOWLEDGEMENTS

There are many people I would like to thank for their support throughout my Ph.D. study at Georgia Tech. I would like first express my tons of gratitude to my advisor Dr. Behrens for his invaluable support that I will remember for ever. I will remember his great guidance whenever I encounter a problem in my thesis work; I will remember his encouragements whenever I feel frustrated in my life; I will remember his great suggestions in my job seeking; I will remember his generous help in securing my funding for the last semester. In one word, I feel great honored to be a student working with Dr. Behrens, and he is more than a super advisor for research, also a friend for life, a mentor for career, and a role model for follow. I also would like to thank my thesis committee members, Dr. Victor Breedveld, Dr. Yulin Deng, Dr. Alberto Fernandez-Nieves, and Dr. Carson Meredith for their comments, suggestions, and time throughout the completion of my thesis work.

I am very grateful to my past lab mates, Dr. Virendra Singh, Dr. Adriana San Miguel, Dr. Qiong Guo and Carlos Espinosa, for imparting their knowledge and skills to me and training me for the use of equipment when I entered the lab in my first year; I also would like to thank my current lab mates, Joohyung Lee, Abiola Shitta, Joanna Tsao, and Yi Zhang for their help and being such great colleagues. I wish you all a successful future in both research and career!

Special thanks should be given to our collaborators, Dr. Nguyen from Vietnam National University for modeling the dipole field of a charged particle at oil-water interfaces and Dr. Isa from ETH for contact angle measurements with FreSca cryo-SEM

methods; To Dr. Jennifer Curtis, Dr. Jan Scrimgeour and Dan Kovari for suggestions in confocal microscopic measurements; To Weinan Xu for helpful discussions about AFM measurements; To Nabil Kleinhenz for the spin-coating training; To Chen Zhang and Chunhong Ye for SEM measurements; To Dr. Johnson for suggestions in the selection of polymers; To Dr.Drake from Dow Chemical, for suggestions in preparing microcapsules; and to everyone who has assisted me during my Ph.D. research.

I would like to thank Dr. Virendra Singh, Xiaoyu Min, Dr. Delong Song, Dr. Qiong Guo, Liwei li, Xiaojuan(Roxy) Zhou, Chen Zhang, Wei Mu and Dr. Haoxi Ben for their helpful discussions, suggestions and encouragements during my job seeking process. I would also like to thank all my Chinese friends in Yuntao group, and you make my life outside research in Atlanta fabulous and memorable!

Finally, I would like to thank my family for their love and unconditional support always. Without their love and support, this work cannot have been possible! Especially, I would like to thank my wife, Qin Sun, who sacrificed her career and has accompanied me here for two years, whose love, trust, encouragements and support have always been my biggest motivation to go forward.

TABLE OF CONTENTS

LIST OF TABLES

LIST OF FIGURES

LIST OF SYMBOLS

G	Free energy
γ	Interfacial tension
A	Area
R	Radius
θ	Contact angle
Pc,max	Maximum capillary pressure
ε	Dielectric constant
q	Surface charge
ρ	Density
W	Interaction energy
Φ	Electric potential
κ^{-1}	Debye screening length
ζ	Zeta potential
E	Electric field
p	Dipole moment
σ	Surface charge density
$\mathrm{E_r}$	Reduced young modulus
H	Hardness
P	Permeability
τ	Diffusion/permeation time constant
I	Bessel function
h	Distance
T_g	Glass transition temperature

LIST OF ABBREVIATIONS

HLB	Hydrophilic-Lipophilic Balance
o/w	Oil in water
w/o	Water in oil
w/o/w	Water in oil in water
GTT	Gel trapping technique
Pc,max	Maximum capillary pressure
PDMS	Polydimethylsiloxane
IPA	Isopropyl alcohol
SEM	Scanning Electron Microscopy
AFM	Atomic Force Microscopy
LbL	Layer by layer
EDTA	Ethylenediaminetetraacetic acid
EA	Ethyl acetate
PNIPAM	Poly(N-isopropylacrylamide)
PS	Polystyrene
APTES	(3-Aminopropyl) triethoxysilane
IEP	Isoelectric point
MTMS	Methyltrimethoxysilane
FITC	Fluorescein isothiocyanate
MDI	Methylene diphenyl diisocyanate
FRAP	Fluorescence Recovery After Photobleaching
HPLC	High-performance liquid chromatography
PVAc	Polyvinyl acetate

SUMMARY

My thesis work addresses fundamentals and applications of particle stabilized emulsions, also known as Pickering emulsions. Pickering emulsions play an important role in many applications such as food technology, oil recovery, surfactant-free cosmetics and skin care products, and more recently, they have become popular as precursors and templates for the assembly of novel materials, including microcapsules, micro-reactors, foams, and metal organic frameworks (MOFS). Compared to classical surfactants as emulsifiers, particles often achieve better emulsion stability, they can prevent undesired foaming, and do not cause the allergic reactions associated with certain surfactants used in skin care products. While the breadth of potential applications for Pickering emulsions keeps growing, our fundamental understanding of Pickering emulsions is still poor. It is currently impossible, for instance, to predict whether particles of a given type will be effective in stabilizing emulsions of a given oil and water phase, even when all material parameters are known; in fact, it is not even possible to reliably predict whether mixing of equal amounts of oil and water in the presence of the particles will lead to the formation of oil droplets in water or water droplets in oil.

It has been established beyond doubt, however, that emulsion stabilization relies on the adsorption of particles at the oil-water interface, and that the contact angle between this interface and the particle surface plays an important role both for the type of emulsion formed and for the emulsion stability that can be achieved. An obvious shortcoming of the existing models for this all-important contact angle is that they do not account for the influence of electric particle charge, even though particle charging is

almost unavoidable in aqueous systems. Therefore, the primary objective of this thesis was to gain insights into the effect of particle charge on the particle adsorption and the particle contact angle, and to investigate the ensuing consequences for the stability of Pickering emulsions. In a separate, more application oriented part of this thesis work, I have explored the use of double emulsions, in which both liquid interfaces are stabilized by colloidal particles, as precursors for controlled release microcapsules, and investigated novel design strategies for liquid core microcapsules with two solid shells of a composite material.

In the fundamental part of this thesis work, emulsification experiments were carried out with particles of systematically varied surface charge and at varied concentration of charge screening salt ions. It was found that depending on their charging state the same particles could stabilize either oil-in-water emulsions, or water-in-oil emulsions, or fail to provide any noticeable stabilization against phase separation after mixing. Studies of particle adsorption to a macroscopic oil-water interface revealed that a complete failure to stabilize emulsions, observed for highly charged and weakly screened particles of either sign of charge, directly correlates with a failure of the particles to adsorb to the liquid interface. A simple theoretical model calculation for the forces driving and hindering particle adsorption under conditions of turbulent mixing showed that the so-called image forces acting on the particle charge near the dielectric discontinuity of the oil-water interface can give rise to an insurmountable barrier to particle adsorption. While the presence of image charge interaction is not surprising from a theoretical standpoint, the potentially critical impact on short-term emulsion stability had not been recognized before.

For the conditions in which particle adsorption to the liquid interface does occur, it was found that the equilibrium contact angle with the liquid interface can differ dramatically from the contact angle accessible via macroscopic measurements using a flat proxy substrate representing the particle surface. An improved protocol for the widely used "gel-trapping method" for determining the actual particle contact angle was developed in this study. The improved experimental approach, which avoids significant preparative artifacts, showed that charged polymer microparticles can assume contact angles identifying them as "hydrophilic" even though macroscopic measurements would suggest "hydrophobic" wetting behavior, and they reveal a systematic dependence of the contact angle on the particle size. We hypothesized that this size dependent "hydrophilic shift" of charged particles in an oil-water interface is due to a position dependent free energy contribution from the electric field set up by the charged interfacial particle and its counterions in the aqueous phase. Treating this field as a simple dipole field in the leading order approximation and treating the water phase as a perfect conductor compared to the nonpolar oil, we found that the field contribution to the particle free energy can qualitatively explain the hydrophilic shift as well as its particle size dependence – provided that some particle charges are assumed to exist on the particle-oil interface (a somewhat controversial assumption).

In the application oriented part of this thesis work, we have fabricated microcapsules from double Pickering emulsions and demonstrated that the combined use of hard silica particles and pH-responsive dissoluble polymer particles at the emulsion interface imparts a combination of pH-responsiveness (stimulated pore opening) and structural integrity to resulting capsules. We have further demonstrated the first double

Pickering emulsion templated capsules in which interfacial polymerization was carried out at both emulsion interfaces, yielding a capsule with two composite shells, composed of polyurethane and silica particles, and characterized the transport of a model cargo through the capsules walls as well as the capsules' mechanical properties.

CHAPTER 1

INTRODUCTION

1.1 Emulsions

An emulsion is a mixture of two normally immiscible liquids, typically oil and water, formed when an energy input is provided through shaking, stirring, homogenizing or power ultrasound[1]. The emulsions contain a dispersed droplet phase within a continuous phase, with a liquid-liquid interface formed by the droplet surfaces. In order to minimize the interfacial free energy, the emulsion droplets tend to coalesce over time, thus reducing the interfacial area of two phases, until complete phase separation is achieved. This process can be slowed down dramatically, however, in the presence of emulsion stabilizers: commonly speaking, surfactants or colloidal particles. They both introduce a kinetic barrier to coalescence and stabilize the large interface of the emulsion state through lowering the interfacial free energy, but in a different way. The free energy of liquid-liquid interfaces can be expressed as:

$$G_{L-L} = \gamma_{L-L} \times A_{L-L}, \qquad \text{Eq.1-1}$$

where G_{L-L}, γ_{L-L} and A_{L-L} represent free energy, interfacial tension and interfacial area of liquid-liquid interfaces respectively. The adsorption of surfactants to interfaces induces a decrease of the interfacial tension γ_{L-L} and therefore lowers the free energy of liquid-liquid interfaces. In contrast, the adsorbed particles as emulsifiers lower the interfacial free energy primarily by reducing the interfacial area A_{L-L} between two phases.

Compared to surfactants as emulsifiers, particles often achieve better emulsion stability, reduce undesired foaming, and avoid the risk of allergic responses to certain surfactants commonly used as emulsion stabilizers in skin care products[2].

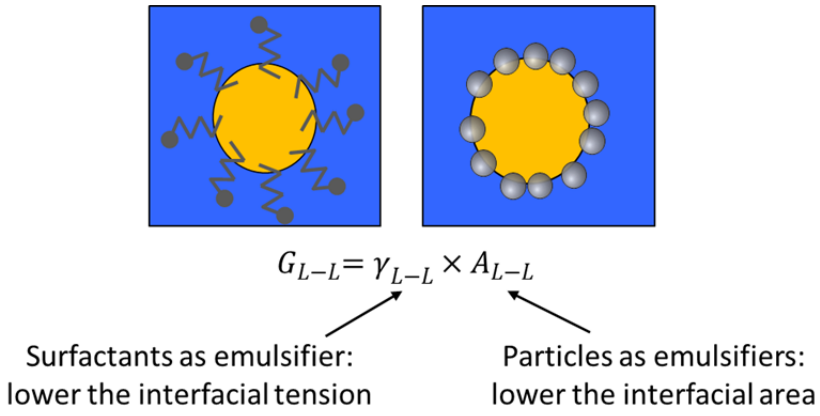

Figure 1.1 Scheme for emulsion droplets stabilized by adsorption of surfactants (left) and particles (right)

1.1.1 Emulsion type

Whether mixing of oil and water will result in an "oil-in-water" emulsion or "water-in-oil" emulsion depends on the volume ratio of the oil and water phases and on the type of emulsifier used. For an equal mixture of two phases, the Bancroft rule generally applies and states "the phase in which an emulsifier is more soluble constitutes the continuous phase"[3]. For surfactant-stabilized emulsions, consistently with the Bancroft rule, more oil-soluble surfactants tend to stabilize water-in-oil emulsions, and more water-soluble surfactants tend to stabilized oil-in-water emulsions. The so-called Hydrophilic-Lipophilic Balance (HLB) value is the parameter most commonly used to determining whether for practical purposes a surfactant or surfactant mixture may be

considered more lipophilic or more hydrophilic. HLB values can be estimated based on calculating the mass ratio of hydrophilic part over the total mass of surfactant molecules, as first proposed by Griffin[4]. The method produces values on a scale from 0, as the lipophilic extreme, to 20, for the most hydrophilic surfactants.

For particle-stabilized emulsions, the type of emulsion depends on the particle wettability, as quantified by measuring the three phase contact angle. The Bancroft rule can be interpreted as saying that hydrophilic particles – those with a contact angle smaller than 90° measured through the water phase – prefer to stabilize oil-in-water emulsions, whereas particles with a contact angle greater than 90° are lipophilic or hydrophobic and tend to stabilize water-in-oil emulsions[5]. The type of emulsion formed upon mixing of equal volumes of oil and water phase follow the Bancroft rule and can be thought as the "preferred" emulsion type; it is the only emulsion type with the potential for long term stability. The type of emulsion can be altered by changing the volume ratio of the two phases. Increasing the volume of the dispersed phase dramatically over the continuous phase will lead to so-called "catastrophic phase inversion"[6,7] and into the "non-preferred" emulsion type, but such anti-Bancroft rule emulsions are unstable against coalescence[8].

1.1.2 Double emulsions

Double emulsions are emulsion systems where the dispersed phase of the outer emulsion also serves as a continuous phase for the inner emulsion. Double emulsions are practically helpful to achieve a system which requires the inner emulsion droplets to have the same composition as the external phase, for example, a controlled release system calling for a release of aqueous actives into an aqueous environment.

Two types of emulsifiers are often required to prepare double emulsions, a more hydrophobic one stabilizing water in-oil-emulsions and a more hydrophilic one stabilizing oil-in-water emulsions. Double emulsions with surfactants have been successfully achieved in several previous studies, but one key problem of surfactant-based double emulsions is their relative instability, as these double emulsion often evolve into single emulsions over time as a result of coalescence[8,9]. An effective way to produce stable double emulsions is to use particles as stabilizers. Binks et al.[10] patented a method of preparing double emulsions with two types of silica particles which have different wettability via surface modifications. Producing double emulsions via combining both particles and surfactants is also reported[11]. Double emulsions produced via bulk emulsification are usually very polydisperse, and microfluidic emulsification is therefore employed to produce monodisperse double emulsions. Researchers from David Weitz'[12,13,14,15,16] group at Harvard published several papers about producing monodisperse double emulsions for various applications via microfluidic emulsification.

One new emerging application of double emulsion droplets is their use as templates for microcapsules, which offers benefits in controlling shell thickness or dispersing microcapsules in the target phase with higher encapsulation efficiency than other alternative techniques that rely on diffusive loading.[17]

1.2 Pickering emulsions

Particle-stabilized emulsions are also called "Pickering emulsions" after S.U Pickering who presented a first systematic study on emulsions stabilized by adsorbed particles in 1907[18], although this phenomenon had already been reported by Ramsden in

1903[19]. Their studies demonstrated that solid particles can adsorb to oil-water interfaces and prevent droplet coalescence and thus stabilize emulsions. They also showed that particles can yield better emulsion stability compared to surfactant based emulsions. Despite these advantages of particles over surfactants as emulsifiers, research in Pickering emulsions stalled for a long period after their first disclosure. Only recently, research interest in Pickering emulsions has been rekindled along with considerable scientific and technical advances. Pickering emulsions have so far been used widely in many industrial applications such as food technology[9,20], cosmetic products, oil recovery[21,22], and more recently, in drug delivery[23,24].

1.2.1 Particle as emulsifiers

The effectiveness of particles in stabilizing emulsions depends on their size, shape, wettability, pH, and electrolyte concentration. To obtain effective stabilization, the particle size should be at least one order of magnitude smaller than the droplets to make particle locate properly around the droplets[25]. The reported size of particles that successfully stabilize emulsions ranges from nanometers[26] to micrometers[27]. There is also a strong dependence of emulsion stability on the particle shape. Shape induced capillary forces between interfacially adsorbed particles and packing effects[28] lead to a trend of increasing emulsion stability with increasing aspect ratio of the particles. Particle wettability, quantified by measuring the three phase contact angle, is another crucial parameter to the emulsion stability. A good particle emulsifier should be able to wet both phases. Kaptay[29] suggests the optimum contact angle for the stabilization of Pickering

emulsions is around 70° for oil-in-water emulsions, and around 110° for water-in-oil emulsions.

Many types of particles, inorganic or organic, have been reported as Pickering emulsifiers. Examples are inorganic silica[30], calcium carbonate[31,32], clays[33], gold[34] and carbon black particles[35], organic latex[26,36], starch[37], hydrogels[38] and copolymer particles[39]. Some non-traditional particles are also used as Pickering emulsifiers, such as proteins[40,41], bacteria[42] and spore[43] particles. Functional emulsions are achieved by using specific particles according to customizable requirements, for example, poly(methyl methacrylate-co-ethyl acrylate) particles can add pH-responsive properties to emulsions, and poly(N-isopropylacrylamide)[44] particles can give temperature-sensitive properties to emulsions. In general, fundamentals of Pickering emulsions with inorganic particles have been extensively studied and are well understood, but many fundamentals of Pickering emulsions with polymeric particles are still less well understood. Especially, particles often carry electric surface charge in aqueous solution, and the role of charge on the stability of Pickering emulsions is not well understood and will be investigated in this work.

1.2.2 Pickering emulsion stabilization mechanism

Emulsions can be stabilized thermodynamically or kinetically. The thermodynamically stable emulsions, called "micro-emulsions", form spontaneously without any external energy inputs. Micro-emulsions are formed when oil-water interfacial tensions are sufficiently reduced by adding high concentrations of surfactants[45]. Thermodynamically stable Pickering emulsions have also been reported

recently under specific conditions which require very low oil-water interfacial tensions, adsorbed amphiphilic ions and specific type of colloidal particles[46,47].

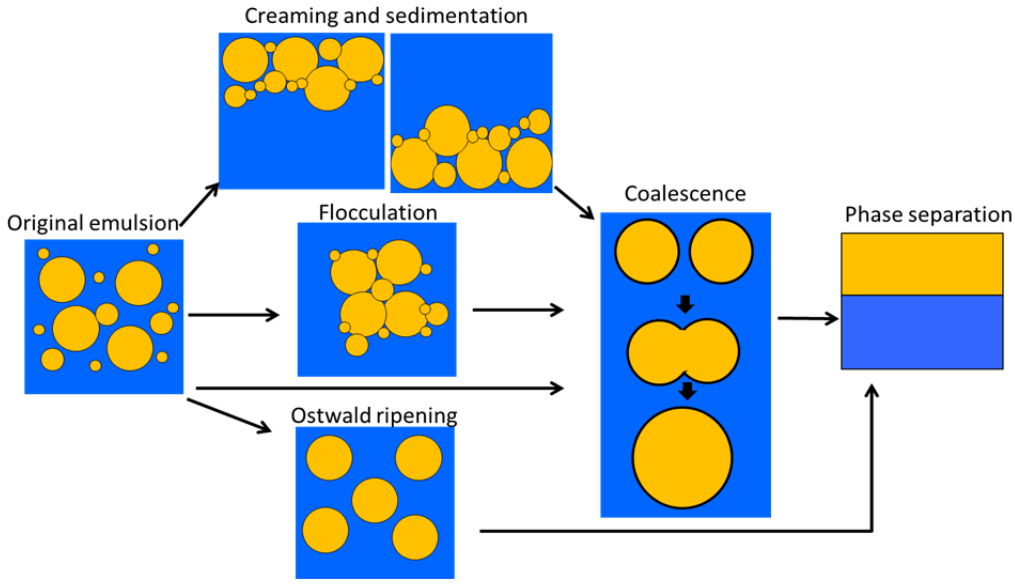

Figure 1.2 Scheme of various breakdown processes in emulsions[48]

With the exception of these special cases, Pickering emulsions are thermodynamically unstable and are only kinetically stabilized. To understand the stabilization mechanism in Pickering emulsions, we need first know how emulsion destabilization occurs. In general, the destabilization of emulsions can involve several mechanisms illustrated in Fig. 1.2[48]. The creaming and sedimentation result from gravity effects caused by the density difference between the dispersed phase and the continuous phase. Flocculation occurs when there is not sufficient repulsion to keep the emulsion droplets apart and the van der Waals attraction force dominates the interaction. The above two processes bring the emulsion droplets together, but coalescence and Ostwald ripening ultimately lead to phase separation. Coalescence is the process beginning with the

thinning and rupture of the liquid film between two droplets, and ending with the fusion of the droplets into a larger one. Ostwald ripening is caused by the finite solubility of dispersed phase in the continuous phase. In emulsions, which are usually polydisperse, the smaller droplets exhibit a greater solubility than larger droplets due to curvature effects. Over time, the smaller droplets disappear and the larger droplets expand as molecules of smaller droplets diffuse into the surface of larger droplets. The Ostwald ripening will be suppressed when the dispersed phase has less solubility in the continuous phase. In our work, the used oil phase is hexadecane, a very non-polar oil with ultra-low solubility in water, and thus Ostwald ripening will not play an important role in the evolution towards phase separation. In a Pickering emulsion system, even for more water-soluble oils, particles can effectively prevent Ostwald ripening when particles are densely packed at the oil-water interface, which results in a very flat interstitial space with no curvature effects[49].

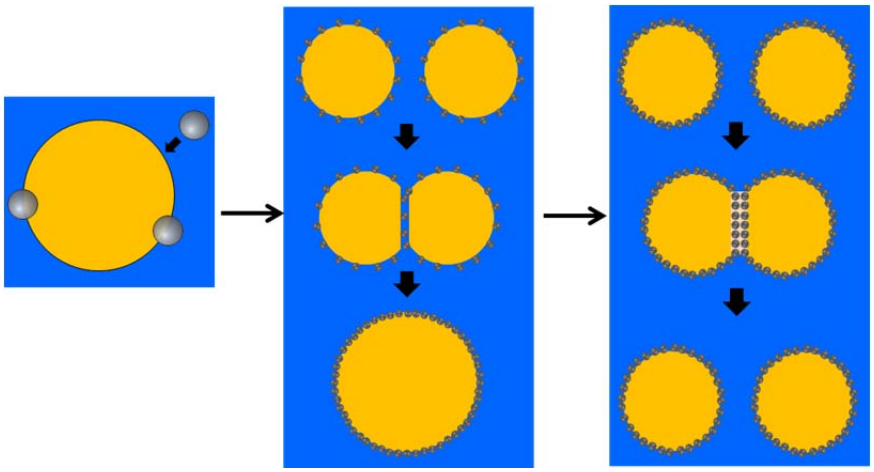

Figure 1.3 Scheme of Pickering emulsion stabilization mechanisms

Coalescence is therefore the only mechanism which leads to phase separation in our case. Based on the understanding of emulsion destabilization mechanisms, the Pickering emulsion stabilization process can be illustrated as shown in Fig. 1.3. Particles adsorb to the oil-water interface of the small emulsion droplets first generated by the mixing or homogenization process, and, for reasons discussed in more detail below, the particles can be considered strongly (irreversibly) bound to the interface. Droplets with incomplete particle coverage can coalescence as indicated in the center scheme of Fig. 1.3. Since the coalescence of two droplets decreases their combined interfacial area, to which the adsorbed particles remain strongly bound, every coalescence event increases the particle concentration in the interface – until the coverage is so high that further coalescence would require particle desorption. At this point the strong binding of adsorbed particles to the droplet surface strongly suppresses further coalescence. Different factors contributing the stability of Pickering emulsions will be discussed in detail below.

1.2.2.1 Electrostatic barrier to the particle adsorption

Particle adsorption is the first step for the Pickering emulsion stabilization. In our work, since particles are initially dispersed in the water phase, we will only consider the case that particles adsorb from the water phase to the oil water interface.

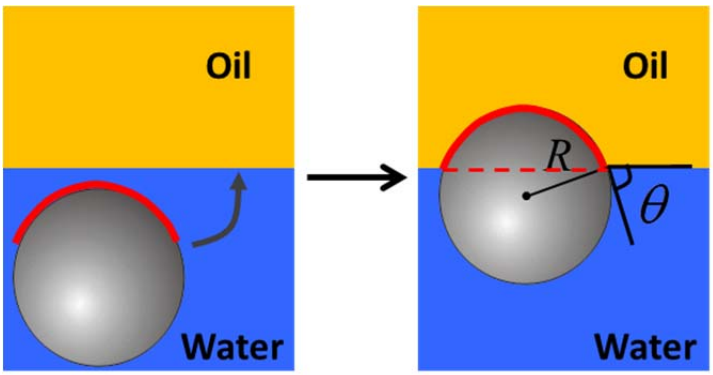

Figure 1.4 Adsorption of a particle from the water phase to the interface replaces the oil-water contact area with particle-oil contacts

When a particle moves from the water phase to the oil-water interface, the particle replaces the oil-water contact area with particle-oil contacts (Fig. 1.4), reducing the total interfacial free energy. The reduction of interfacial free energy is given by[8]:

$$\Delta G = -\pi R^2 \gamma_{ow}(1 - cos\theta_{ow})^2 \qquad \text{Eq. 1-2}$$

where R is the particle radius; $\gamma_{ow}$is the oil-water interfacial tension; θ_{ow} is the three phase contact angle measured through the water phase. Such energy reduction can also be interpreted as an energy cost of detaching a particle, once at the interface, from the interface. For particles with the sizes above 10 nm, the typical adsorption energy ΔG is much larger than the thermal energy kT, and thus the adsorption of particles to oil-water interfaces is considered irreversible[5], a behavior unlike surfactants, which are in a dynamic equilibrium of adsorption and desorption to interfaces on a very fast timescale. This is the reason why particle emulsifiers produce more stable emulsions than surfactant emulsifiers. From Eq. 1-2, we can tell that the detachment energy depends on the contact

angle and exhibits a maximum at the contact angle of 90°. Accordingly, a particle with a contact angle close to 90° achieves high detachment energy and benefits the emulsion stability, which motivates researchers to prepare amphiphilic particles, also known as 'Janus' particles, defined originally as particles with equal parts of hydrophilic and hydrophobic surface. The theoretical prediction of the increased detachment energy for 'Janus' particles is supported by experimental evidence. Binks et al.[50] reported that the detachment energy increased significantly wtih increasing amphiphilicity of the particle and produced a maximum three-fold increase for contact angles around 90°, as compared to homogeneous particles. Recently, theoretical calculations indicated that Janus particles can generate thermodynamically stable Pickering emulsions[51].

Though the adsorption energy favors to locate the particle at the interface, particle adsorption to the interface should not be taken for granted. The oil-water interface is generally considered negatively charged due to the preferential adsorption of hydroxide ions[52], although this explanation remains controversial[53,54].

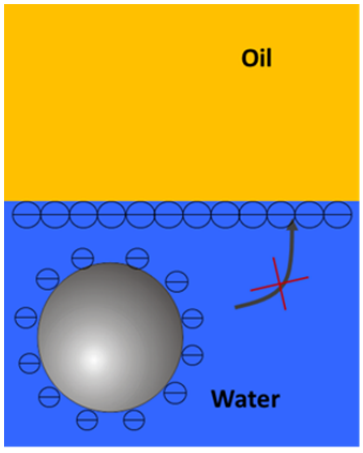

Figure 1.5 Scheme for a adsorption barrier to a negatively charge particle created by a negatively charged interface

At low electrolyte concentrations, significant electrostatic repulsion appears when a negatively charged particle approaches the oil-water interface that is also negatively charged (Fig. 1.5). Such repulsion can create an energy barrier preventing particle adsorption to the interface, and prevent the formation of emulsions. For example, K. Golemanov et al.[55] found that sulfate polystyrene particles could not stabilize emulsions at low electrolyte concentrations and assumed that the failure to form emulsions was caused by the electrical repulsion by the negatively-charged interface. Danov et al.[56] also discussed the electrical repulsion barrier that can prevent the particle from adsorbing even when the adsorption energy is favorable.

1.2.2.2 Maximum capillary pressure of coalescence

If particles can overcome the electrostatic barrier and adsorb to the oil-water interface, they start to limit the coalescence, and the coalescence stability of sparsely covered emulsion droplets will be governed by the stability of thin film between two droplets.

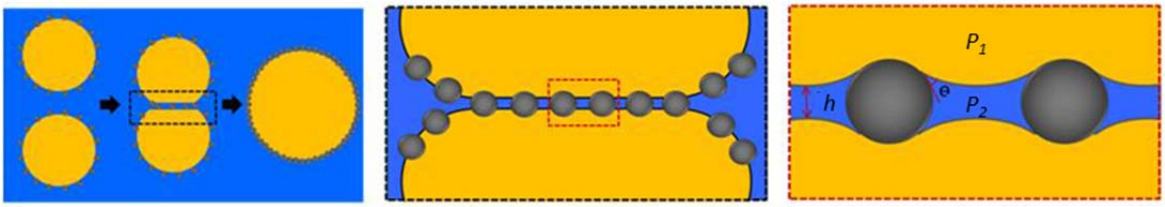

Figure 1.6 Scheme for a capillary mechanism of emulsion stabilization with particles

The meniscus curvature between two particles results in a pressure difference (Laplace pressure) between the emulsion droplets (P_1) and the inter-film fluid (P_2), and this pressure difference is known as the capillary pressure (Fig. 1.6). As the capillary pressure increases, the meniscus profile continues to curve, and the separation h of the thin film will decrease. The highest pressure that the film separating the two droplets can withstand without rupturing, the so-called maximum capillary pressure *Pc,max*, is reached just before the interfaces are deformed to the point of making contact; once the interfaces contact, the film ruptures and the droplets coalesce. A higher *Pc,max* indicates a higher film stability to resist coalescence and also a better emulsion stability. The expressions for *Pc,max* were first discussed by Ivanov and his coworkers[57], and then developed further by others including Kruglyakov[58] and Kaptay[29]. According to the most recent model by Kaptay the maximum capillary pressure is given by[29]:

$$Pc, max = \pm P \frac{2\gamma_{ow} cos\theta_{ow}}{R} \qquad \text{Eq. 1-3}$$

Here, the sign is positive for oil-in-water (o/w) emulsions and negative for water-in-oil emulsions (w/o); P is a theoretical packing parameter, associated with the structure configuration of the particle layer; γ_{ow} is the oil-water interfacial tension; θ_{ow} is the contact angle and R is the particle radius. The equation first implies that *Pc,max* is inversely proportional to particle size, indicating smaller particles give better coalescence stability as a result of their higher packing efficiency. We also notice that *Pc,max* suggests highest emulsion stability at the contact angle of 0° in the case of o/w emulsions and 180° in the case of w/o emulsions. It makes sense here that the more the particles

reside in the film, the better the film resists coalescence, but this is an opposing implication to what the detachment energy suggests: for any given particle size the maximum detachment energy favoring the emulsion stability corresponds a contact angle of 90°. Kaptay[29] looked at the combined effects of the detachment energy and the capillary pressure, and concluded the optimum contact angle for stabilization by a particle monolayer was 70° for o/w emulsions and 110° for w/o emulsions (Fig. 1.7).

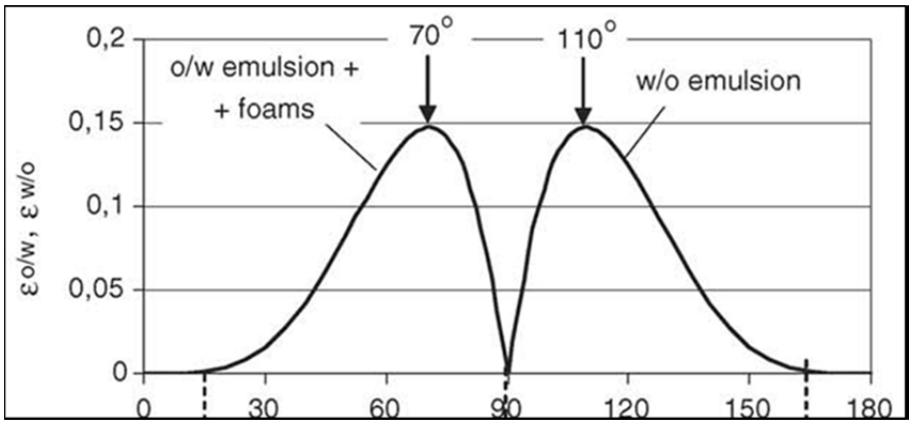

Figure 1.7 Probability of emulsion stabilization by a particle monolayer as a function of contact angle via combining effects of the detachment energy and the maximum capillary pressure of coalescence[29].

The current theoretical models of maximum capillary pressure have their limitations, and predict maximum pressures that are one order of magnitude of larger than the experimentally determined ones. One important reason for this discrepancy is due to the idealized assumption of homogeneous particle layers in all models. In fact, some flocculated or incomplete structures of particle layers might result in some "weak area" with low maximum capillary pressure of coalescence in the absence of particle coverage.

The actual packing structure of particle layers at interfaces will be most affected by particle-particle interactions.

1.2.2.3 Particle-particle interactions at interfaces

When particles adsorb to the interface, their movements in the normal direction is greatly confined by their high adsorption energy. They are more likely to move laterally, and the final packing structure is determined by the balance of all the particle-particle interactions. The double layer repulsion, dipole-dipole repulsion, van der Waals attraction and capillary attraction are the most important particle-particle interactions at interfaces. When particles reside at oil-water interfaces, their double layer repulsion through the water phase is considered the most important repulsive force at short particle separations[5,59]. The dipole-dipole repulsion becomes especially significant in systems where particles contain ionizable surface groups and the oil has a low dielectric constant[60,61]. The dipole perpendicular to the interface is created by the asymmetric distribution of particle charges with respect to the interface[62,63]. The long range dipole-dipole repulsion acts mainly through the oil phase, and together with the short range double layer repulsion force in the water phase, keeps the interfacial particle apart. The van der Waals force and the capillary force are two well-known attractive forces for particles at oil water interfaces. The van der Waals force plays an important role both for particles in the bulk and at the interface, whereas the capillary force is unique to particles at the interface. When particles reside at the interface, the balance of normal stresses on the interface, due to the osmotic pressure of the particle's counterions and due to the electric force on the particle itself caused by the permittivity gradient, results in a

deformation of the interface that sets up the capillary attraction between the particles. This electrostatically induced capillary interaction has been proposed as the source for an experimentally observed long-range attraction[64], but some controversy over its exact range and magnitude persists[65,66,67,68,69].

1.2.3 Pickering emulsion type

1.2.3.1 Particle wettability and emulsion type

Particle wettability, quantified by measuring the contact angle, is important not only for the particle adsorption and capillary coalescence with respect to the stabilization of Pickering emulsions as discussed above, but is also the most important parameter governing the emulsion type. In accordance with Bancroft's rule, a widely accept view suggests that particles with a contact angle less than 90°, defined as hydrophilic, prefer to stabilize oil in water emulsions, whereas particles with a contact angle above 90°, defined as hydrophobic, prefer to stabilize water in oil emulsions (Fig. 1.8). Here, the "preferred emulsion type" means the emulsion type tending to form under equal mixing of oil and water phases. Otherwise, if the two liquid phases are not mixed at 1:1 ratio, increasing the volume of the disperse phase well above the continuous phase will lead to "catastrophic" phase inversion[6,7], but the resulting emulsions of the "non-preferred type" tend to be unstable against coalescence and show poor long term stability. For the equal volume mixing of liquid phases, an exceptional case was reported by Yan and Masliyah[70]. The authors varied the contact angle of clay particles by controlling the amount of asphaltene adsorption on the particles; they found that modified clay particles with macroscopically measured contact angles greater than 90^0 stabilized o/w emulsions. They did not discuss

any explanation. Our preliminary work also reported the fact that o/w emulsions can be stabilized by charged latex particles with macroscopically measured contact angles greater than 90^0, and we hypothesized that this can be explained by a shift of the particle contact angle to lower values caused by the particle-counterion dipole field when the particles reside at oil water interfaces. Detailed discussions are provided in chapter 4.

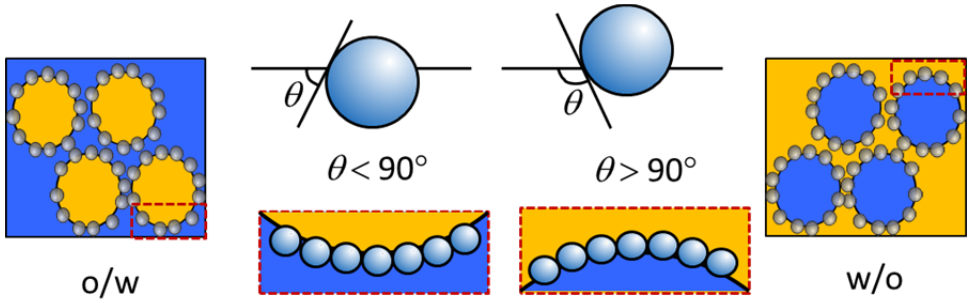

Figure 1.8 Scheme for the relation between the particle contact angle and the emulsion type

The particle wettability can be altered by surface modification. For example, silica particles are intrinsically hydrophilic, and they can be altered to be hydrophobic via grafting of silane groups to their surfaces, where the silanes react with the silanol groups and form Si-O-Si bonds. Alkylchlorosilanes, alkoxysilanes, or alkylaminosilanes are commonly used chemical agents for the surface modification[71]. The particle wettability also depends on their surface charge. Altering the surface charge via changing the pH[72] or ionic strength[73,74] will change the particle wettability and thus the emulsion type. The effect of surface charge on the particle wettability can be indirectly indicated via observing the emulsion type, but the quantitative evaluation of the charge effects on the

particle wettability will depend on the accurate measurements of the three-phase contact angle of particles at the oil water interfaces.

1.2.3.2 Particle contact angle measurements

Several experimental methods have been developed to measure the contact angle of particles at liquid-liquid interfaces. Measuring the three-phase contact angle of a liquid interface with a macroscopic solid surface, coated with a homogeneous layer cast from a solution of dissolved particles in a solvent, is one well-known approach to estimate the three-phase contact angle of particles at interfaces[75], but it can be objected that there is no experimental evidence demonstrating that the created macroscopic proxy surface and the particle surface that it represents indeed have identical surface chemistry. The so-called gel trapping technique (GTT)[76,77,78] is another well-known method for measuring the particles' three-phase contact angle at interfaces. In this method, particles are introduced to the interface via a spreading solvent, typically isopropyl alcohol (IPA); next the water phase is solidified with a non-adsorbing gelling agent. Then, the oil phase is removed and replaced by polydimethylsiloxane (PDMS), which is subsequently cross-linked to produce a solid polymeric replica of the oil-water interface with the embedded particles. In the final step, the position of particles trapped in the PDMS replica, are examined by SEM or AFM to obtain the particle contact angle. A central argument against GTT is its use of IPA as spreading solvent, and a few recent studies have indicated the IPA renders particles more hydrophobic[79,80]. A "film-calliper"[81,82] method allows dynamic measurements of the contact angle of particles at interfaces. A few hydrophilic particles are trapped in a thin and slightly concave water film, supported inside a bulk oil phase by

a hoop-shaped frame. If the minimum film thickness is well below the particle size, capillary forces naturally transport the particles to a location along the film where they can bridge the film and intersect both interfaces at the equilibrium contact angle without deforming the interfaces. If the particle size is known, the contact angle can be inferred from the film thickness at the particle location, which in turn can be determined interferometrically. However, this method is only applicable to contact angle measurements on hydrophilic particles, because hydrophobic particles cannot form stable bridges in the water film. Measuring the contact angle via digital holographic microscopy[83] has been reported recently, where the contact angle is determined by measuring the particle's position at the interface with 2 nm precision. The particle is forced to the interface with a laser trap, and the position of the particle at the decane-water interface is reconstructed from a hologram created by interference of scattered light from the particle and a reference beam. However, 45% glycerol is added to the water phase to match the refractive index of decane, and the effect of added glycerol on the contact angle is not mentioned and remains unknown. Another recently reported method is freeze-fracture shadow-casting cryo-scanning electron microscopy (FreSca cryo-SEM)[80], capable of measuring the contact angle of particles as small as 10 nm in diameter. When a particle-loaded interface is created, both the oil phase and the water phase are shock-frozen into a glassy solid at a cooling rate of 30000 K/s, and therefore particles at the interface are immobilized. The interface preferably fractured at the interface, and the frozen oil phase is removed. The particle height protruding out of the frozen water phase is calculated based on measuring the length and angle of a particle "shadow" created by unidirectional metal deposition from a tilt angle. This method has

several advantages to other techniques, such as no additives, no limitations in the sign of particle charge or wettability, and low size measuring thresholds, but it requires expensive instruments and sophisticated protocols.

1.3 Microencapsulation

Microencapsulation is a process by which targeted "cargos" are enclosed in a microscopic capsule that protects the cargos from the surrounding environment until the delivery conditions are achieved. Research interest in microencapsulation has been renewed due to their many potential applications such as drug delivery systems, microreactors, catalyst supports, toxic indication and energy sensing materials[84]. So far, diverse micro- or nanocapsules have been successfully developed on the lab scale, and some of them have realized commercialization. However, there are still many obstacles to practical applications such as instabilities in large scale productions, complicated multi-step fabrication procedures, cost and environmental restrictions. Ideal capsules will embody improvements in methods and materials along with goals for target applications.

1.3.1 Fabrication of microcapsules

To date, several methods have been developed to generate microcapsules. Here, we generally classified them into two categories: the solid-core template methods and the emulsion template methods. The popular layer by layer (LbL) assembly approach is a typical hard-core template method and was first developed by Decher and his coworkers[85]. Microcapsules based on LbL are formed via an alternate adsorption of two types of polymers or particles to the surface of a sacrificial template particle and

subsequent removal (dissolution) of the template particle. The binding between layers in the LbL deposition can be due to electrostatic interaction, hydrogen bonding, and covalent bonding. Diverse colloidal particles can be used as the hard-core templates in LbL processes such as $CaCO_3$[86,87], $MnCO_3$[88], silica[89,90], magnetic [91]and polymeric particles[92,93]. The inner core particles can be removed by appropriate solvents. For example, the $CaCO_3$ particle can be removed by a strong acid typically, or more recently, by less harsh EDTA[94], and the polystyrene particles can be removed by exposing capsules to THF[95]. The hard-core templated approach can generate capsules with good monodispersity, but the inner core needs to be removed afterwards, and then the active compounds are loaded by diffusion, which is a time-consuming process with low efficiency. By contrast, the emulsion-templated approaches can assemble capsules and load the "cargo" simultaneously. The emulsion droplets are stabilized by either surfactants or particles, and the microcapsule shell forms at the oil-water interface of emulsion droplets via the interfacial polymerization[96], coacervation[97], phase separation[98], or polymer precipitation[99]. Among these methods, interfacial polymerization is most commonly used method because of its simplicity and versatility. Various types of interfacial polymerization including polyaddition[96], polycondensation[100], radical[101] and anionic polymerization[102] have been reported to produce emulsion based microcapsules. The stability of emulsion droplets is very important in the process of preparing microcapsules. In this regard, Pickering emulsions are attractive templates to prepare microcapsules because they are often more stable than surfactant stabilized emulsions.

1.3.2 Colloidosomes

The general definition of a colloidosome is a semi-permeable microcapsule whose external shell is formed by colloidal particles. Colloidosomes were first reported by Velev[103] in 1996, who studied self-assembly of latex particles at a surface of octanol in water emulsion droplets, followed up by adding HCL and $CaCl_2$ as coagulants to lock the particle together. Similar structures have also been obtained by water-in-oil emulsions[104]. The term "colloidosome" was first introduced by Dinsmore et al.[105], who produced colloidosomes by assembly of colloidal particles at the surface of water-in-oil emulsion droplets and a subsequent sintering fusion of the particles into a solid shell. Noble et al.[106] fabricated hairy colloidosomes consisted of aqueous gel core and shells made of polymeric micro-rod particles. Yow et al.[107] created colloidosomes with polystyrene particles based on Pickering emulsions, and controlled the permeability by changing the size of the inter-particle pores by tuning the temperature and time of sintering. Ao et al.[99] fabricated colloidosomes based on oil-in-water emulsions stabilized with polystyrene latex particles. The oil phase was made of octanol, ethyl acetate (EA) and poly(lactic-co-glycolic acid) (PLGA). When the o/w emulsion was diluted with a large amount of water, EA was extracted to the outer aqueous phase. As a result, the EA soluble but octanol insoluble PLGA underwent an outward transport and precipitated within the particle shell as a reinforcing agent. In addition to single emulsions, double emulsion templated colloidosomes have also been reported. Maeda et al.[108] obtained composite colloidosomes from double Pickering emulsions. Lee et al.[12,14] published several papers on achieving monodisperse double emulsion templated colloidosomes via the microfluidic technology.

Sander and Studart[17] assembled monodisperse colloidosomes with a wide range of particles via double emulsions in a microfluidic device.

Colloidosomes represent a promising technique for encapsulations with general advantages such as controllable size, well-defined permeability, mechanical sturdiness and bio-compatibility[105]. The size of colloidosomes depends on the size of the emulsion template, which can be easily controlled by tuning the homogenization speed, concentration of particle emulsifiers, and volume ratio of the oil and water phases. Colloidosome shells can be very sturdy since their building blocks are rigid solid particles instead of soft polymers. Moreover, the permeability of colloidosome, which depends mainly on the pore size, can be tailored by controlling the size of the colloid particles[109].

The main problem of colloidosomes is their incomplete surface coverage of colloidal particles, and such "defects" result in a leakage of inside cargos and thus low encapsulation efficiency[110]. Even with a complete coverage, the intersticial spaces between particles will cause a fast release of small molecules. Several techniques have been investigated to yield better surface coverage and encapsulation efficiency. Appropriate aggregation of particles by adding salt can yield dense coverage of particles in the shell of colloidosomes. Sintering[111] is adopted to tailor the pore size between particles. Mostly, polymers are added to fill the inter-particle space, leading to particle-polymer composite colloidosomes.

1.3.3 Stimulus responsive microcapsules

Stimulus responsive microcapsules are of interest in drug delivery, fragrance release, antimicrobial release, nutrient preservation, sensors and self-healing materials. Many triggering stimuli, such as pH, temperature, UV, electrical field and magnetic field, can initiate changes in a capsule shell and results in the release of capsule cargos[112]. Microcapsules with pH induced release can be appealing for many biomedical applications. San Miguel et al.[39] synthesized pH-responsive particles from Eudragit (copolymer of polymethyl methacrylate and polymethacrylic acid) polymers, and used these particles to stabilize double emulsions as templates to prepare pH-responsive microcapsules. Temperature responsive microcapsules can find useful applications in systems where changes in temperature occur naturally. For example, in agriculture applications, a change in soil temperature can initiate the delivery of nutrients[113]. PNIPAM[114,44,115] is one of the most popular polymers reported to develop thermo-responsive microcapsules. The PNIPAM polymer can contract upon increasing the temperature above their LCST, resulting in the pore formation in the capsule shell and release of inside contents. UV sensitive microcapsules are used in the cosmetic[116] and agriculture industries where solar irradiation triggers the release. For example, Katagiri et al.[117] developed polyelectrolyte microcapsules coated with SiO_2 and TiO_2 particles, and the microcapsules were UV responsive due to the UV adsorption of TiO_2. Fomina et al. [118]reported UV responsive microcapsules based on self-immolative polymers containing a quinone-methide backone, and UV-cleavable nitrobenzyle alcohol groups as triggers. Magnetic responsive microcapsules are developed via embedding the magnetic

nanoparticles into the capsule shell, and the permeability of such capsule shells increases remarkably in the presence of an oscillating magnetic field[119].

In this work, based on the previous knowledge in developing pH-responsive colloidosomes gained in our group, composite pH-responsive colloidosomes from double Pickering emulsions stabilized solely by colloid particles will be designed for sustained cargo release. Also, the low encapsulation efficiency of colloidosomes in encapsulating small molecules due to the inter particle core will be improved by adding a polymer "skin" to the capsule shell via interfacial polymerization. The generated composite microcapsules with hard particles embedded in their shell are expected to demonstrate an improved stiffness and resistance to deformation.

1.4 Thesis motivations and objectives

The growing number of potential applications of Pickering emulsions has boosted both fundamental and applied studies on Pickering emulsions during the recent years. In the fundamental realm, Binks and his coworkers conducted numerous pioneering experimental studies for the factors that influence the stability of the Pickering emulsions, including the particle wettability, the size and concentrations of particles, oil type and electrolyte concentrations[2,7,8,26,72,120,121]. In addition to empirical studies, several theoretical models have been developed to describe the formation and stability of Pickering emulsions. Several recent reviews presented a good summary about fundamental studies of Pickering emulsions[122,123,49,124]. Despite considerable technological and scientific advances, our current fundamental understanding of Pickering emulsions still lags far behind that for classical, surfactant-stabilized

emulsions, and many important factors that might influence significantly the Pickering emulsion stability and the emulsion type still remain poorly understood. Such inadequate understanding will hamper the applications of Pickering emulsions. We are therefore motivated to add new insights into the fundamentals of Pickering emulsification, and specifically, we focus on understanding the effects of particle charge on the formation and stability of Pickering emulsions, and on the emulsion type. The objectives of the fundamental research in this work are to:

- Investigate widely neglected image charge effects on the particle adsorption to oil-water interfaces and on Pickering emulsification, and to include image charge effects in the theoretical description of particle adsorption to liquid interfaces during emulsification
- Investigate effects of the dipole field on the contact angle of particles adsorbed at the interface, which is a crucial parameter not only for the stability of Pickering emulsions, but for the emulsion type.

Recent research interest in Pickering emulsions relates to their use as templates for novel materials, including microcapsules[17], microreactors[125], foams[126] and MOFS[127]. Pickering emulsions are advantageous templates compared to surfactant stabilized emulsions because of their higher stability, reducing droplet breakup during the fabrication process. In the applied part of this work, the objective is to:

- Develop pH-responsive composite microcapsules with sustained release profile from double Pickering emulsion stabilized solely by particles, and to tune the permeability of the microcapsules via interfacial polymerization to make them suitable for encapsulating small molecules.

1.5 Thesis outline

This thesis consists of seven chapters and the thesis structure is outlined in Fig. 1.9.

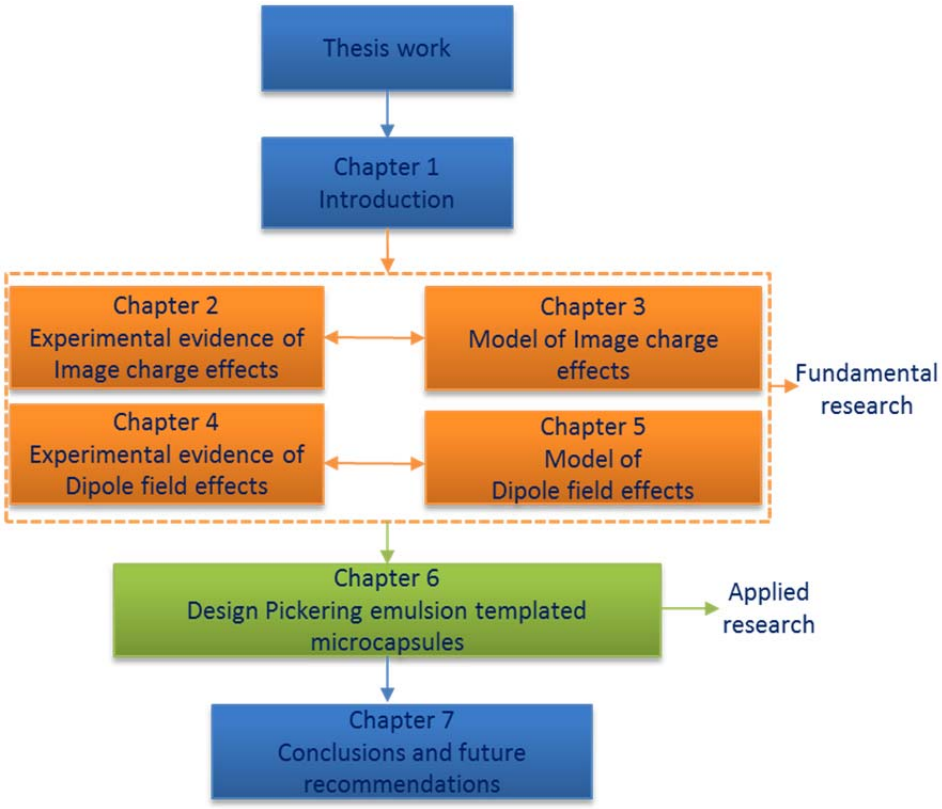

Figure 1.9 Thesis structure outline

Chapter 1 reviews the scientific backgrounds relevant to this thesis work, and underlined the motivation and objective of this work;

Chapter 2 presents the experimental evidence of image charge effects on the particle adsorption associated with the formation of Pickering emulsions, including emulsification experiments and macroscopic observations of the particle adsorption to interfaces.

Chapter 3, closely related to chapter 2, models the particle adsorption to oil-water interfaces with image charge effects included, and compares the model prediction for the outcome of emulsification with the experimental results of chapter 2.

Chapter 4 discusses the experimental evidence of dipole field effects on the particle contact angle by comparing the contact angle of charged polystyrene particles measured with the macroscopic proxy surface method and the Gel Trapping Technique.

Chapter 5, closely related to chapter 4, models the free energy profile of the particle at the interface with the self-energy of dipole field included, to predict the equilibrium position of the particle at the interface, and calculate the particle contact angle; the model predicted contact angle is compared to the experimental one in chapter 4.

Chapter 6 applies the obtained insights from the fundamental study to design pH-responsive composite microcapsules with a sustained release profile from double

Pickering emulsions; tuning the permeability of the obtained microcapsule for small molecules via interfacial polymerization is demonstrated.

Chapter 7 summarizes the conclusions and suggests future work.

1.6 References

1. F.Tadros, T., Emulsion Science and Technology. Wiley-VCH: 2009.

2. Binks, B. P., Particles as Surfactants - Similarities and Differences. Curr. Opin. Colloid Interface Sci. 2002, 7 (1-2), 21-41.

3. Bancroft, W. D., The Theory of Emulsification, V. J. Phys. Chem. 1912, 17 (6), 501-519.

4. Griffin, W. C., Classification of Surface-Active Agents by "HLB". J Soc Cosmetic Chemists 1946, 1, 311-326.

5. Levine, S.; Bowen, B. D.; Partridge, S. J., Stabilization of Emulsions by Fine Particles I. Partitioning of Particles between Continuous Phase and Oil/Water Interface. Colloids and Surf. 1989, 38 (2), 325-343.

6. Binks, B. P.; Lumsdon, S. O., Catastrophic Phase Inversion of Water-in-Oil Emulsions Stabilized by Hydrophobic Silica. Langmuir 2000, 16 (6), 2539-2547.

7. Binks, B. P.; Murakami, R., Phase Inversion of Particle-stabilized Materials from Foams to Dry Water. Nature Mater. 2006, 5 (11), 865-869.

8. Aveyard, R.; Binks, B. P.; Clint, J. H., Emulsions Stabilised Solely by Colloidal Particles. Adv. Colloid Interface Sci. 2003, 100, 503-546.

9. Norton, J. E.; Norton, I. T., Designer Colloids-towards Healthy Everyday Foods? Soft Matter 2010, 6 (16), 3735-3742.

10. Binks, B. P.; Dyab, A. K. F.; Fletcher, P. D. I., Barthel, H. Multiple Emulsions. DE Patent 10211313, 2002

11. Wang, J.; Yang, F.; Tan, J.; Liu, G.; Xu, J.; Sun, D., Pickering Emulsions Stabilized by a Lipophilic Surfactant and Hydrophilic Platelike Particles. Langmuir 2009, 26 (8), 5397-5404.

12. Lee, D.; Weitz, D. A., Double Emulsion-Templated Nanoparticle Colloidosomes with Selective Permeability. Adv. Mater. 2008, 20 (18), 3498-3503.

13. Shah, R. K.; Kim, J.-W.; Weitz, D. A., Monodisperse Stimuli-Responsive Colloidosomes by Self-Assembly of Microgels in Droplets. Langmuir 2009, 26 (3), 1561-1565.

14. Lee, D.; Weitz, D. A., Nonspherical Colloidosomes with Multiple Compartments from Double Emulsions. Small 2009, 5 (17), 1932-1935.

15. Shum, H. C.; Zhao, Y.-j.; Kim, S.-H.; Weitz, D. A., Multicompartment Polymersomes from Double Emulsions. Angew. Chem Int. Ed. 2011, 50 (7), 1648-1651.

16. Romanowsky, M. B.; Abate, A. R.; Rotem, A.; Holtze, C.; Weitz, D. A., High Throughput Production of Single Core Double Emulsions in a Parallelized Microfluidic Device. Lab Chip 2012, 12 (4), 802-807.

17. Sander, J. S.; Studart, A. R.; Monodisperse Functional Colloidosomes with Tailored Nanoparticle Shells. Langmuir 2011, 27 (7), 3301-3307.

18. Pickering, S. U., Emulsions. J. Chem. Soc. 1907, 91, 2001-2021.

19. Ramsden, W., "Separation of Solids in the Surface-Layers of Solutions and 'Suspensions' (Observations on Surface-Membranes, Bubbles, Emulsions, and Mechanical Coagulation). Preliminary Account.". Proc. Royal Soc. London 1903, 72 (479), 156-164.

20. Dickinson, E.; McClements, D. J., Adv. Food Colloids. Chapman & Hall: Glasgow, 1996.

21. Bragg, J. R. Oil Recovery Method Using an Emulsion. U.S. Patent 5927404,1998

22. Sullivan, A. P.; Kilpatrick, P. K., The Effects of Inorganic Solid Particles on Water and Crude Oil Emulsion Stability. Ind. Eng. Chem. Res. 2002, 41 (14), 3389-3404.

23. Eskandar, N. G.; Simovic, S.; Prestidge, C. A., Nanoparticle Coated Emulsions as Novel Dermal Delivery Vehicles. Curr. Drug Deliv. 2009, 6 (4), 367-373.

24. Simovic, S.; Prestidge, C. A., Nanoparticle Layers Controlling Drug Release from Emulsions. Eur. J. Pharm. Biopharm. 2007, 67 (1), 39-47.

25. Tambe, D. E.; Sharma, M. M., Factors Controlling the Stability of Colloid-Stabilized Emulsions: I. An Experimental Investigation. J. Colloid Interface Sci. 1993, 157 (1), 244-253.

26. Binks, B. P.; Whitby, C. P., Nanoparticle Silica-Stabilised Oil-in-Water Emulsions: Improving Emulsion Stability. Colloids Surf., A 2005, 253 (1-3), 105-115.

27. Wang, W.; Zhou, Z., Nandakumar, K., Xu, Z., Masliyah, J. H., Effect of Charged Colloidal Particles on Adsorption of Surfactants at Oil–Water Interface. J. Colloid Interface Sci. 2004, 274 (2), 625-630.

28. Madivala, B.; Vandebril, S.; Fransaer, J.; Vermant, J., Exploiting Particle Shape in Solid Stabilized Emulsions. Soft Matter 2009, 5 (8), 1717-1727.

29. Kaptay, G.; On the Equation of the Maximum Capillary Pressure Induced by Solid Particles to Stabilize Emulsions and Foams and on the Emulsion Stability Diagrams. Colloids and Surf., A: Physicochemical and Engineering Aspects 2006, 282-283, 387-401.

30. Frelichowska, J.; Bolzinger, M.-A.; Chevalier, Y., Pickering Emulsions with Bare Silica. Colloids Surf., A 2009, 343 (1-3), 70-74.

31. Cui, Z. G.; Shi, K. Z.; Cui, Y. Z.; Binks, B. P., Double Phase Inversion of Emulsions Stabilized by A Mixture of $CaCO_3$ Nanoparticles and Sodium Dodecyl Sulphate. Colloids Surf., A 2008, 329 (1-2), 67-74.

32. Wang, X.; Zhou, W.; Cao, J.; Liu, W.; Zhu, S., Preparation of Core–Shell $CaCO_3$ Capsules via Pickering Emulsion Templates. J. Colloid Interface Sci. 2012, 372 (1), 24-31.

33. Ashby, N. P.; Binks, B. P., Pickering Emulsions Stabilised by Laponite Clay Particles. Phys. Chem. Chem. Phys. 2000, 2 (24), 5640-5646.

34. Zhang, H.; Hussain, I.; Brust, M.; Cooper, A. I., Emulsion-Templated Gold Beads Using Gold Nanoparticles as Building Blocks. Adv. Mater. 2004, 16 (1), 27-30.

35. Gelot, A.; Friesen, W.; Hamza, H. A., Emulsification of Oil and Water in the Presence of Finely Divided Solids and Surface-Active Agents. Colloids and Surf. 1984, 12 (0), 271-303.

36. Binks, B. P.; Lumsdon, S. O., Pickering Emulsions Stabilized by Monodisperse Latex Particles: Effects of Particle Size. Langmuir 2001, 17 (15), 4540-4547.

37. Timgren, A.; Rayner, M.; Sjöö, M., Dejmek, P., Starch Particles for Food Based Pickering Emulsions. Procedia Food Science 2011, 1 (0), 95-103.

38. Ngai, T.; Auweter, H.; Behrens, S. H., Environmental Responsiveness of Microgel Particles and Particle-Stabilized Emulsions. Macromolecules 2006, 39 (23), 8171-8177.

39. San Miguel, A.; Scrimgeour, J.; Curtis, J. E.; Behrens, S. H., Smart Colloidosomes with a Dissolution Trigger. Soft Matter 2010, 6 (14), 3163-3166.

40. Horne, D. S., Protein-Stabilized Emulsions. Curr. Opin. Colloid Interface Sci. 1996, 1 (6), 752-758.

41. Van Rijn, P.; Mougin, N. C.; Franke, D.; Park, H.; Boker, A., Pickering Emulsion Templated Soft Capsules by Self-Assembling Cross-Linkable Ferritin-Polymer Conjugates. Chem. Comm. 2011, 47 (29), 8376-8378.

42. Wongkongkatep, P.; Manopwisedjaroen, K.; Tiposoth, P.; Archakunakorn, S.; Pongtharangkul, T.; Suphantharika, M.; Honda, K.; Hamachi, I.; Wongkongkatep, J.; Bacteria Interface Pickering Emulsions Stabilized by Self-Assembled Bacteria–Chitosan Network. Langmuir 2012, 28 (13), 5729-5736.

43. Binks, B. P.; Clint, J. H.; Mackenzie, G.; Simcock, C.; Whitby, C. P., Naturally Occurring Spore Particles at Planar Fluid Interfaces and in Emulsions. Langmuir 2005, 21 (18), 8161-8167.

44. Tsuji, S.; Kawaguchi, H., Thermosensitive Pickering Emulsion Stabilized by Poly(N-isopropylacrylamide)-Carrying Particles. Langmuir 2008, 24 (7), 3300-3305.

45. Ruckenstein, E., The Origin of Thermodynamic Stability of Microemulsions. Chem. Phys. Lett. 1978, 57 (4), 517-521.

46. Sacanna, S.; Kegel, W. K.; Philipse, A. P., Thermodynamically Stable Pickering Emulsions. Phys. Rev. Lett. 2007, 98 (15), 158301.

47. Kraft, D. J.; de Folter, J. W. J.; Luigjes, B.m; Castillo, S. I. R.; Sacanna, S.; Philipse, A. P.; Kegel, W. K., Conditions for Equilibrium Solid-Stabilized Emulsions. J. Phys. Chem. B 2010, 114 (32), 10347-10356.

48. Binks (Ed.), B. P., Colloidal Particles at Liquid Interfaces. Phys. Chem. Chem. Phys. 2007, 9, 6285-6488.

49. Tcholakova, S.; Denkov, N. D.; Lips, A., Comparison of Solid Particles, Globular Proteins and Surfactants as Emulsifiers. Phys. Chem. Chem. Phys. 2008, 10 (12), 1608-1627.

50. Binks, B. P.; Fletcher, P. D. I., Particles Adsorbed at the Oil−Water Interface: A Theoretical Comparison between Spheres of Uniform Wettability and "Janus" Particles. Langmuir 2001, 17 (16), 4708-4710.

51. Tu, F.; Park, B. J.; Lee, D., Thermodynamically Stable Emulsions Using Janus Dumbbells as Colloid Surfactants. Langmuir 2013, 29 (41), 12679–12687

52. Marinova, K. G.; Alargova, R. G.; Denkov, N. D.; Velev, O. D.; Petsev, D. N.; Ivanov, I. B.; Borwankar, R. P., Charging of Oil-Water Interfaces Due to Spontaneous Adsorption of Hydroxyl Ions. Langmuir 1996, 12 (8), 2045-2051.

53. Knecht, V.; Levine, Z. A.; Vernier, P. T., Electrophoresis of Neutral Oil in Water. J. Colloid Interface Sci. 2010, 352 (2), 223-231.

54. Vácha, R.; Rick, S. W.; Jungwirth, P.; De Beer, A. G. F.; De Aguiar, H. B.; Samson, J.-S.; Roke, S., The Orientation and Charge of Water at the Hydrophobic Oil Droplet–Water Interface. J. Amer. Chem. Soc. 2011, 133 (26), 10204-10210.

55. Golemanov, K.; Tcholakova, S.; Kralchevsky, P. A.; Ananthapadmanabhan, K. P.; Lips, A., Latex-Particle-Stabilized Emulsions of Anti-Bancroft Type. Langmuir 2006, 22 (11), 4968-4977.

56. Danov, K. D.; Kralchevsky, P. A.; Naydenov, B. N.; Brenn, G., Interactions between Particles with an Undulated Contact Line at a Fluid Interface: Capillary Multipoles of Arbitrary Order. J. Colloid Interface Sci. 2005, 287 (1), 121-34.

57. Denkov, N. D.; Ivanov, I. B.; Kralchevsky, P. A.; Wasan, D. T., A Possible Mechanism of Stabilization of Emulsions by Solid Particles. J. of Colloid and Interface Sci. 1992, 150 (2), 589-593.

58. Kruglyakov, P. M.; Nushtayeva, A. V.; Vilkova, N. G., Experimental Investigation of Capillary Pressure Influence on Breaking of Emulsions Stabilized by Solid Particles. J. Colloid Interface Sci. 2004, 276 (2), 465-474.

59. Levine, S.; Bowen, B. D.; Partridge, S. J., Stabilization of Emulsions by Fine Particles II. Capillary and Van der Waals Forces between Particles. Colloids and Surf. 1989, 38 (2), 345-364.

60. Stancik, E. J.; Kouhkan, M.; Fuller, G. G., Coalescence of Particle-Laden Fluid Interfaces. Langmuir 2003, 20 (1), 90-94.

61. Stancik, E. J.; Widenbrant, M. J. O.; Laschitsch, A. T.; Vermant, J.; Fuller, G. G., Structure and Dynamics of Particle Monolayers at a Liquid−Liquid Interface Subjected to Extensional Flow. Langmuir 2002, 18 (11), 4372-4375.

62. Hurd, A. J., The Electrostatic Interaction between Interfacial Colloidal Particles. J. Phys. A 1985, 18, L1055 - L1060.

63. Pieranski, P., Two-Dimensional Interfacial Colloidal Crystals. Phys. Rev. Lett. 1980, 45 (7), 569.

64. Nikolaides, M. G.; Bausch, A. R.; Hsu, M. F.; Dinsmore, A. D.; Brenner, M. P.; Gay, C.; Weitz, D. A., Electric-Field-Induced Capillary Attraction between Like-Charged Particles at Liquid Interfaces. Nature 2002, 420 (6913), 299-301.

65. Kralchevsky, P. A.; Denkov, N. D., Capillary Forces and Structuring in Layers of Colloid Particles. Curr. Opin. Colloid Interface Sci. 2001, 6 (4), 383-401.

66. Oettel, M.; Dominguez, A.; Dietrich, S., Effective Capillary Interaction of Spherical Particles at Fluid Interfaces. Phys. Rev. E 2005, 71, 051401.

67. Wurger, A.; Foret, L., Capillary Attraction of Colloidal Particles at an Aqueous Interface. J. Phys. Chem. B 2005, 109 (34), 16435-8.

68. Dominguez, A.; Oettel, M.; Dietrich, S., Absence of Logarithmic Attraction between Colloids Trapped at the Interface of Droplets - Comment on "Capillary Attraction of Charged Particles at a Curved Liquid Interface" by Alois Wurger. Europhys. Lett. 2007, 77 (6), 2.

69. Langevin, D., Electric-field-Induced Capillary Attraction between like-charged particles at liquid interfaces. ChemPhysChem 2003, 4 (10), 1057-8.

70. Yan, Y.; Masliyah, J. H., Solids-Stabilized Oil-in-Water Emulsions: Scavenging of Emulsion Droplets by Fresh Oil Addition. Colloids and Surf., A: Physicochemical and Engineering Aspects 1993, 75, 123-132.

71. Haensch, C.; Hoeppener, S.; Schubert, U. S., Chemical Modification of Self-Assembled Silane Based Monolayers by Surface Reactions. Chem. Soc. Rev. 2010, 39 (6), 2323-2334.

72. Binks, B. P.; Lumsdon, S. O., Influence of Particle Wettability on the Type and Stability of Surfactant-Free Emulsions Langmuir 2000, 16 (23), 8622-8631.

73. Horozov, T. S.; Binks, B. P.; Gottschalk-Gaudig, T., Effect of Electrolyte in Silicone Oil-in-Water Emulsions Stabilised by Fumed Silica Particles. Phys. Chem. Chem. Phys. 2007, 9 (48), 6398-6404.

74. Binks, B. P.; Duncumb, B.; Murakami, R., Effect of pH and Salt Concentration on the Phase Inversion of Particle-Stabilized Foams. Langmuir 2007, 23 (18), 9143-9146.

75. Leunissen, M. E.; van Blaaderen, A.; Hollingsworth, A. D.; Sullivan, M. T.; Chaikin, P. M., Electrostatics at the Oil-Water Interface, Stability, and Order in Emulsions and Colloids. Proc. Nat. Acad. Sci. 2007, 104 (8), 2585-2590.

76. Paunov, V. N., Novel Method for Determining the Three-Phase Contact Angle of Colloid Particles Adsorbed at Air-Water and Oil-Water Interfaces. Langmuir 2003, 19 (19), 7970-7976.

77. Cayre, O. J.; Paunov, V. N., Contact Angles of Colloid Silica and Gold Particles at Air-Water and Oil-Water Interfaces Determined with the Gel Trapping Technique. Langmuir 2004, 20 (22), 9594-9599.

78. Arnaudov, L. N.; Cayre, O. J.; Cohen Stuart, M. A.; Stoyanov, S. D.; Paunov, V. N., Measuring the Three-phase Contact Angle of Nanoparticles at Fluid Interfaces. Phys.Chem. Chem. Phys. 2010, 12 (2), 328-331.

79. Maestro, A.; Bonales, L. J.; Ritacco, H.; Rubio, R. G.; Ortega, F., Effect of the Spreading Solvent on the Three-Phase Contact Angle of Microparticles Attached at Fluid Interfaces. Phys. chem. chem. phys. 2010, 12 (42), 14115-20.

80. Isa, L.; Lucas, F.; Wepf, R.; Reimhult, E., Measuring Single-Nanoparticle Wetting Properties by Freeze-Fracture Shadow-Casting Cryo-Scanning Electron Microscopy. Nat. Commun. 2011, 2, 438.

81. Horozov, T. S.; Braz, D. A.; Fletcher, P. D.; Binks, B. P.; Clint, J. H., Novel Film-Calliper Method of Measuring the Contact Angle of Colloidal Particles at Liquid Interfaces. Langmuir 2008, 24 (5), 1678-81.

82. Reed, K. M.; Borovicka, J.; Horozov, T. S.; Paunov, V. N.; Thompson, K. L.; Walsh, A.; Armes, S. P., Adsorption of Sterically Stabilized Latex Particles at Liquid Surfaces: Effects of Steric Stabilizer Surface Coverage, Particle Size, and Chain Length on Particle Wettability. Langmuir 2012, 28 (18), 7291-7298.

83. Kaz, D. M.; McGorty, R.; Mani, M.; Brenner, M. P.; Manoharan, V. N., Physical Ageing of the Contact Line on Colloidal Particles at Liquid Interfaces. Nat Mater 2012, 11, 138-142.

84. Seok Kwon, O.; Jang, J.; Bae, J., A Review of Fabrication Methods and Applications of Novel Tailored Microcapsules. Curr. Org. Chem.2013, 17 (1), 3-13.

85. Decher, G., Fuzzy Nanoassemblies: Toward Layered Polymeric Multicomposites. Science 1997, 277 (5330), 1232-1237.

86. Saurer, E. M.; Flessner, R. M.; Buck, M. E.; Lynn, D. M., Fabrication of Covalently Crosslinked and Amine-Reactive Microcapsules by Reactive Layer-by-Layer Assembly of Azlactone-Containing Polymer Multilayers on Sacrificial Microparticle Templates. J. Mater.Chem. 2011, 21 (6), 1736-1745.

87. Zhang, L.; Shi, J.; Jiang, Z.; Jiang, Y.; Meng, R.; Zhu, Y.; Liang, Y.; Zheng, Y., Facile Preparation of Robust Microcapsules by Manipulating Metal-Coordination Interaction between Biomineral Layer and Bioadhesive Layer. ACS Appl. Mater. Inter. 2011, 3 (2), 597-605.

88. Jia, Y.; Fei, J.; Cui, Y.; Yang, Y.; Gao, L.; Li, J., pH-Responsive Polysaccharide Microcapsules through Covalent Bonding Assembly. Chem. Comm. 2011, 47 (4), 1175-1177.

89. Becker, A. L.; Zelikin, A. N.; Johnston, A. P. R.; Caruso, F., Tuning the Formation and Degradation of Layer-by-Layer Assembled Polymer Hydrogel Microcapsules. Langmuir 2009, 25 (24), 14079-14085.

90. Huang, C.-J.; Chang, F.-C., Using Click Chemistry To Fabricate Ultrathin Thermoresponsive Microcapsules through Direct Covalent Layer-by-Layer Assembly. Macromolecules 2009, 42 (14), 5155-5166.

91. Rożkiewicz, D. I.; Myers, B. D.; Stupp, S. I., Interfacial Self-Assembly of Cell-like Filamentous Microcapsules. Angew. Chem. Int. Ed. 2011, 50 (28), 6324-6327.

92. Mak, W. C.; Cheung, K. Y.; Trau, D., Influence of Different Polyelectrolytes on Layer-by-Layer Microcapsule Properties: Encapsulation Efficiency and Colloidal and Temperature Stability. Chem. Mater. 2008, 20 (17), 5475-5484.

93. Guo, X.-F.; Kim, Y.-S.; Kim, G.-J., Fabrication of SiO2, Al2O3, and TiO2 Microcapsules with Hollow Core and Mesoporous Shell Structure. J. Phys. Chem. C 2009, 113 (19), 8313-8319.

94. De Geest, B. G.; Van Camp, W.; Du Prez, F. E.; De Smedt, S. C.; Demeester, J.; Hennink, W. E., Degradable Multilayer Films and Hollow Capsules via a 'Click' Strategy. Macromol. Rapid Commun. 2008, 29 (12-13), 1111-1118.

95. Pastoriza-Santos, I.; Schöler, B.; Caruso, F., Core–Shell Colloids and Hollow Polyelectrolyte Capsules Based on Diazoresins. Adv. Funct. Mater. 2001, 11 (2), 122-128.

96. Bouchemal, K.; Briançon, S.; Perrier, E.; Fessi, H.; Bonnet, I.; Zydowicz, N., Synthesis and Characterization of Polyurethane and Poly(ether urethane) Nanocapsules using a New Technique of Interfacial Polycondensation Combined to Spontaneous Emulsification. Int. J. Pharm. 2004, 269 (1), 89-100.

97. Landfester, K.; Musyanovych, A.; Mailänder, V., From Polymeric Particles to Multifunctional Nanocapsules for Biomedical Applications using the Miniemulsion Process. J. Polym. Sci. A: Polym. Chem. 2010, 48 (3), 493-515.

98. Atkin, R.; Davies, P.; Hardy, J.; Vincent, B., Preparation of Aqueous Core/Polymer Shell Microcapsules by Internal Phase Separation. Macromolecules 2004, 37 (21), 7979-7985.

99. Ao, Z.; Yang, Z.; Wang, J.; Zhang, G.; Ngai, T., Emulsion-Templated Liquid Core-Polymer Shell Microcapsule Formation. Langmuir 2009, 25 (5), 2572-2574.

100. Persico, P.; Carfagna, C.; Danicher, L.; Frere, Y., Polyamide Microcapsules Containing Jojoba Oil Prepared by Inter-Facial Polymerization. J. Microencapsulation 2005, 22 (5), 471-486.

101. Scott, C.; Wu, D.; Ho, C.-C.; Co, C. C., Liquid-Core Capsules via Interfacial Polymerization: A Free-Radical Analogy of the Nylon Rope Trick. J. Am. Chem. Soc. 2005, 127 (12), 4160-4161.

102. Musyanovych, A.; Landfester, K., Synthesis of Poly(butylcyanoacrylate) Nanocapsules by Interfacial Polymerization in Miniemulsions for the Delivery of DNA Molecules. In Surface and Interfacial Forces – From Fundamentals to Applications, Auernhammer, G.; Butt, H.-J.; Vollmer, D., Eds. Springer Berlin Heidelberg: 2008; Vol. 134, 120-127.

103. Velev, O. D.; Furusawa, K.; Nagayama, K., Assembly of Latex Particles by Using Emulsion Droplets as Templates. 1. Microstructured Hollow Spheres. Langmuir 1996, 12, 2374 - 2384.

104. Velev, O. D.; Nagayama, K., Assembly of Latex Particles by Using Emulsion Droplets as Templates. 3. Reverse (Water in Oil) System. Langmuir 1997, 13, 1856 - 1859.

105. Dinsmore, A. D.; Hsu, M. F.; Nikolaides, M. G.; Marquez, M.; Bausch, A. R.; Weitz, D. A., Colloidosomes: Selectively Permeable Capsules Composed of Colloidal Particles. Science 2002, 298 (5595), 1006-9.

106. Noble, P. F.; Cayre, O. J.; Alargova, R. G.; Velev, O. D.; Paunov, V. N., Fabrication of "hairy" Colloidosomes with Shells of Polymeric Microrods. J. Am. Chem. Soc. 2004, 126 (26), 8092-8093.

107. Yow, H. N.; Wu, X.; Routh, A. F.; Guy, R. H., Dye Diffusion from Microcapsules with Different Shell Thickness into Mammalian Skin. Eur. J. Pharm. Biopharm. 2009, 72 (1), 62-68.

108. Maeda, H.; Okada, M.; Fujii, S.; Nakamura, Y.; Furuzono, T., Pickering-Type Water-in-Oil-in-Water Multiple Emulsions toward Multihollow Nanocomposite Microspheres. Langmuir 2010, 26 (17), 13727-13731.

109. Hsu, M. F.; Nikolaides, M. G.; Dinsmore, A. D.; Bausch, A. R.; Gordon, V. D.; Chen, X.; Hutchinson, J. W.; Weitz, D. A.; Marquez, M., Self-assembled Shells Composed of Colloidal Particles: Fabrication and Characterization. Langmuir 2005, 21 (7), 2963-2970.

110. Rossier-Miranda, F. J.; Schroën, C. G. P. H.; Boom, R. M., Colloidosomes: Versatile Microcapsules in Perspective. Colloids Surf., A 2009, 343 (1-3), 43-49.

111. Yow, H. N.; Routh, A. F., Release Profiles of Encapsulated Actives from Colloidosomes Sintered for Various Durations. Langmuir 2009, 25 (1), 159-166.

112. Esser-Kahn, A. P.; Odom, S. A.; Sottos, N. R.; White, S. R.; Moore, J. S., Triggered Release from Polymer Capsules. Macromolecules 2011, 44 (14), 5539-5553.

113. Friedman, S. P.; Mualem, Y., Diffusion of Fertilizers from Controlled-Release Sources Uniformly Distributed in Soil. Fert. Res. 1994, 39 (1), 19-30.

114. Cejkova, J.; Hanus, J.; Stepanek, F., Investigation of Internal Microstructure and Thermo-Responsive Properties of Composite PNIPAM/Silica Microcapsules. J. Colloid Interface Sci. 2010, 346 (2), 352-360.

115. Sankaranarayanan, J.; Mahmoud, E. A.; Kim, G.; Morachis, J. M.; Almutairi, A., Multiresponse Strategies To Modulate Burst Degradation and Release from Nanoparticles. ACS Nano 2010, 4 (10), 5930-5936.

116. Tamar Lotan; Eckhouse, S, Methods Compositions and Devices Utilizing Stinging Cells/Capsules for Delivering a Therapeutic or a Cosmetic Agent into a Tissue. US Patent 7338665, 2008.

117. Katagiri, K.; Koumoto, K.; Iseya, S.; Sakai, M.; Matsuda, A.; Caruso, F., Tunable UV-Responsive Organic−Inorganic Hybrid Capsules. Chem.Mater. 2008, 21 (2), 195-197.

118. Fomina, N.; McFearin, C.; Sermsakdi, M.; Edigin, O.; Almutairi, A., UV and Near-IR Triggered Release from Polymeric Nanoparticles. J. Am. Chem. Soc. 2010, 132 (28), 9540-9542.

119. Lu, Z.; Prouty, M. D.; Guo, Z.; Golub, V. O.; Kumar, C. S. S. R.; Lvov, Y. M., Magnetic Switch of Permeability for Polyelectrolyte Microcapsules Embedded with Co@Au Nanoparticles. Langmuir 2005, 21 (5), 2042-2050.

120. Binks, B. P.; Lumsdon, S. O., Stability of Oil-in-Water Emulsions Stabilised by Silica Particles. Phys. Chem. Chem. Phys. 1999, 1 (12), 3007-3016.

121. Binks, B. P.; Philip, J.; Rodrigues, J. A., Inversion of Silica-Stabilized Emulsions Induced by Particle Concentration. Langmuir 2005, 21 (8), 3296-3302.

122. Hunter, T. N.; Pugh, R. J.; Franks, G. V.; Jameson, G. J., The Role of Particles in Stabilising Foams and Emulsions. Adv. Colloid Interface Sci. 2008, 137 (2), 57-81.

123. Leal-Calderon, F.; Schmitt, V., Solid-Stabilized Emulsions. Curr. Opin. Colloid Interface Sci. 2008, 13 (4), 217-227.

124. Chevalier, Y.; Bolzinger, M.-A., Emulsions Stabilized with Solid Nanoparticles: Pickering Emulsions. Colloids and Surf., A: Physicochemical and Engineering Aspects (0).

125. Keating, C. D., Inorganic protocells: Gated Access to Microreactors. Nat. Chem. 2013, 5 (6), 449-451.

126. Blaker, J. J.; Lee, K.-Y.; Li, X.; Menner, A.; Bismarck, A., Renewable Nanocomposite Polymer Foams Synthesized from Pickering Emulsion Templates. Green Chem. 2009, 11 (9), 1321-1326.

127. Huo, J.; Marcello, M.; Garai, A.; Bradshaw, D., MOF-Polymer Composite Microcapsules Derived from Pickering Emulsions. Adv. Mater. 2013, 25 (19), 2717-2722.

CHAPTER 2

IMAGE CHARGE EFFECTS ON THE FORMATION OF PICKERING EMULSIONS

2.1 Introduction

The formation of Pickering emulsions requires that the particles adsorb to the interface in the first place, but this adsorption should not be taken for granted. Current theory suggests there is an electrostatic barrier to particle adsorption, and this barrier is caused by the electric double layer repulsion between a charged particle and a charged oil-water interface. The electric charge of particles stems from dissociable surface groups and can vary in sign and magnitude. The oil-water interface is shown negatively charged above pH 2-3 by electrokinetic and electroacoustic experiments, and it is argued the charge originates from the preferential adsorption of hydroxide ions[1,2,3,4], although this explanation remains controversial[5,6,7].

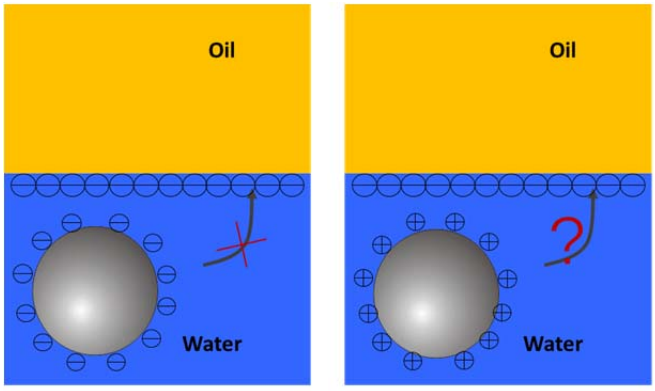

Figure 2.1 Electrical double layer force hinders a anionic particle adsorption (left), and a question is raised about whether a cationic particle can easily adsorb to the oil-water interface when the electric double layer force (right) is attractive.

For a negatively charged oil-water interface, if the double layer repulsion is the only electrostatic barrier to prevent the particle adsorption and the formation of Pickering emulsions, one might expect that only anionic particles should be repelled from the oil−water interface and prevented from adsorbing and stabilizing Pickering emulsions. However, experiments in this chapter suggest some additional electrostatic barrier which can prevent cationic particle adsorption and emulsification, even when the electrical double layer force is attractive in this case**.** We propose this additional electrostatic barrier is caused by image charge effects.

2.2 Materials and Methods

2.2.1 Zeta potential measurements

The zeta potential, associated with the double layer theory, is the electrostatic potential at the "slipping plane", beyond which the ions are free to move relative to the surface. The zeta potential is a function of the surface charge and ionic strength, and plays an important role in governing the electrostatic interactions between two surfaces in colloidal systems[8]. Here, in order to study the particle-interface interactions in the context of the particle adsorption, the particle surface potential is an important parameter required to know. The zeta potential can be determined electrokinetically, by measuring electrophoresis, electro-osmosis, or streaming potentials[9]. In this work, the electrophoretic mobility at varied pH and ionic strength was measured by Laser Doppler Velocimetry using a Zetasizer Nano ZS90, and converted to the zeta potential according to O'Brien and White's method[10,11]. HCl and NaOH were used to adjust pH, and NaCl was used to adjust ionic strength 1.9 μm carboxyl-polystyrene (PS) particles and 0.4 um

amdine-polystyrene (PS) particles were used in this chapter for their large and similar absolute value of maximum surface charge density (−197 mC/m^2 and +192 mC/m$^{2)}$. Both particles, purchased from Life technologies Inc, were washed three times via a centrifuge before use.

2.2.2 Macroscopic contact angle measurements

As discussed in Chapter 1, the particle wettability is important to both the emulsion stability and emulsion type of Pickering emulsions. Unlike inorganic particles which usually have unambiguous wettability, the charged polystyrene particles have a hydrophobic polystyrene bulk, but the charged functional groups on their surface bring uncertainties to the overall wettability. Here, a rough idea of the particle wettability in the emulsion system is obtained by measuring the three-phase contact angle of a macroscopic surface which mimicks the particle surface.

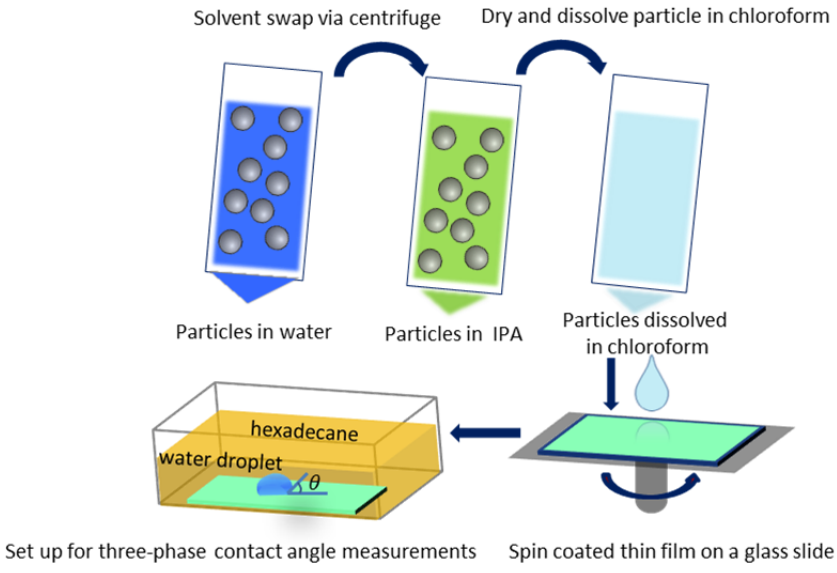

Figure 2.2 Scheme for protocols of preparing macroscopic surface

The macroscopic proxy surface was prepared by a stepwise protocol. Particles were transferred from the initial water dispersion to isopropanol by three-time solvent swap, and then particles were vacuum dried to remove isopropanol. The dried particles were dissolved in chloroform, and a thin film of the obtained solution was spin cast via a spincoater (Laurell WS-650MZ-23NPP) on a glass slide to create a macroscopic surface for the three-phase contact angle measurement. The three-phase contact angle was formed between the solid substrate and the liquid interface of a deposited water droplet and a surrounding oil phase. The three-phase contact angle was measured by the Rame-hart Model 250 contact angle goniometer.

2.2.3 Emulsification experiments

Emulsification experiments are central to our study in this chapter. Emulsification tests were prepared by mixing aqueous 1wt% dispersions of the same particles, used in zeta potential measurements, with an equal volume of hexadecane, using a rotor-stator homogenizer (IKA Ultra-Turrax T10) for 30s at 11000 rpm. The hexadecane (Sigma Aldrich) was purified to remove containments by passing it through a column of activated aluminium oxide (Acros Organics).

Depending on the pH and salt (NaCl) content of the dispersion, we obtained either an oil-in-water(o/w) emulsion, a water-in-oil (w/o) emulsion, or no emulsion at all, where complete phase separation occurred fast and appeared essentially unimpeded by the presence of the particles. In the cases where an emulsion was formed, creaming (o/w) or sedimentation (w/o) occurred over time and revealed the emulsion type, which can be better observed by adding Sudan III to dye the oil phase. The emulsion type was also

further confirmed by conductivity and drop tests. The conductivity of an emulsion is dominated by the conductivity of its continuous phase. If the emulsion is o/w, the outer phase is water and therefore shows a significant conductivity, whereas the outer oil phase in a w/o emulsion exhibits almost no conductivity. In the drop test, a drop of the emulsion was added to water. An o/w emulsion droplet can spread and disperse, whereas a w/o emulsion droplet cannot spread, but remains agglomerated as a lens on the water surface.

2.2.4 Microscopy study of particle adsorption to a macroscopic oil-water interface

We have established a method to test whether particles readily adsorb to a (macroscopic) oil-water interface given an external driving force, or whether some repulsive interaction with the interface prevents them from making contact with it. First, the particles were strongly diluted 1000-fold with solutions of NaCl/HCl or NaCl/NaOH in heavy water (99.9 atom % deuterium oxide, Sigma Aldrich, density 1.107 g/ml) where they experienced a net upward buoyancy force comparable to their net downward gravitational force in regular water (particle density: 1.055 g/ml).

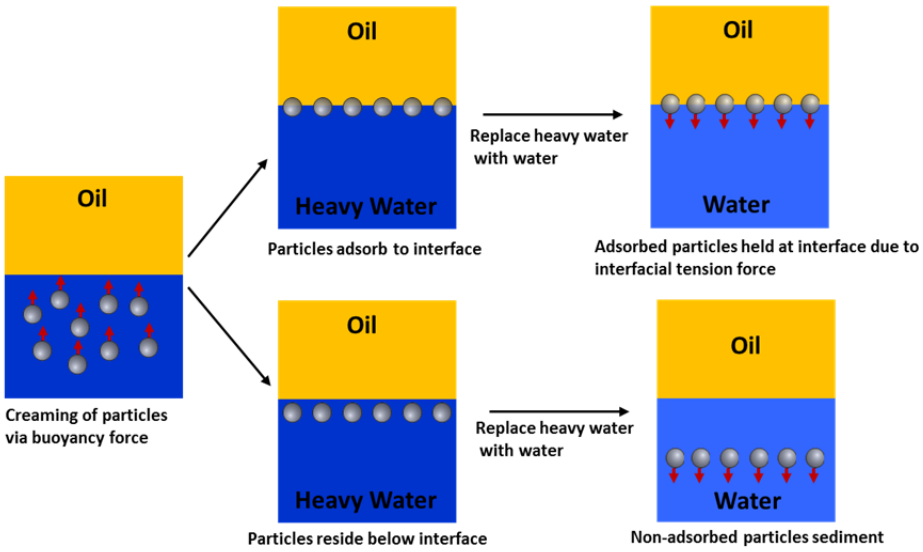

Figure 2.3 Scheme of macroscopic observation of particle adsorption to an oil-water interface

These dilute dispersions were transferred to a glass container for observation on an inverted microscope, and capped with hexadecane to create a macroscopic interface. The particles were observed to slowly cream to the top of the polar phase and accumulate at the interface with the oil. Creaming was allowed to proceed overnight before images of the interface were taken. Then, the heavy water sub-phase was gently pumped out, and replaced by a solution of regular water with the same pH. Now the particles experienced a net gravitational force pointing downward and causing all non-adsorbed particles to slowly sediment to the bottom of the container and while adsorbed particles remained trapped in the interface by the much stronger interfacial tension force. Again, images of the interface were taken the next day.

2.2.5 Macroscopic observation of particle-interface interactions

This experiment is designed to obtain a direct and visual observation of particle-interface interactions via collecting z-stack images using confocal fluorescence

microscopy (Zeiss LSM 510 VIS Confocal Microscope). The particle-interface interaction is expected to be observed in the form of a deformation of the oil-water interface when in close proximity to a charge particle in the case that the interaction is repulsive.

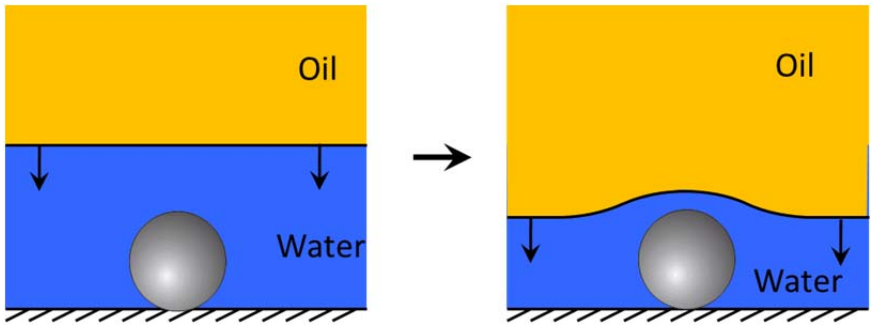

Figure 2.4 Scheme of interface deformation due to repulsive particle-interface interactions

In this experiment, 5.09 μm Carboxyl-nile blue fluorescent polystyrene particles (Spherotech Inc.) were deposited on a glass slide modified with (3-Aminopropyl) triethoxysilane (APTES, Sigma Aldrich), and hexadecane as the oil phase was dyed with Nile red (Sigma Aldrich). The approach of the oil-water interface to the particle was finely controlled by pumping the water out and lowering the interface using a syringe pump (GenTech).

2.3 Results and Discussions

2.3.1 Zeta potential of carboxyl-PS and amidine-PS particles as a function of pH and salt concentration

The results first confirm the expected sign and magnitude of particle charge, seen from Fig. 2.5. Since the two particles have very close maximum surface charge density, they have similar zeta potentials at a highly charged status but opposite sign.

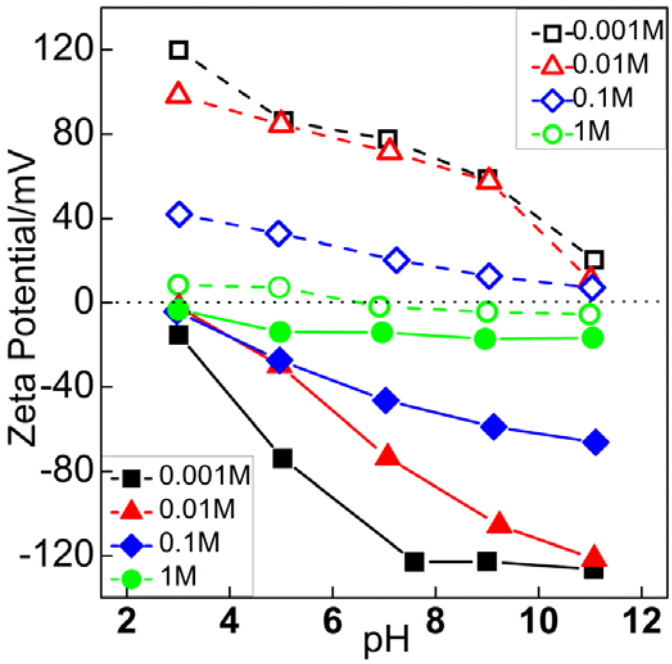

Figure 2.5 Zeta potential of carboxyl-PS (solid markers) and amidine-PS (open markers) particles as a function of pH and salt concentrations.

The data also show the expected qualitative pH dependence. The carboxyl-PS particles exhibit a high zeta potential at high pH because most of their carboxyl groups deprotonate at high pH, and therefore the surface becomes highly charged. Similarly, the amidine-PS particles have a high zeta potential at low pH when the surfaces become

highly charged as more amine groups protonate. The zeta potential decreases for both particles as the salt concentration increases, due to increased charge screening with increasing the salt concentration. At the highest salt content, particles aggregate in the course of the measurements, and thus, caution against a detailed interpretation of the associated results is warranted. The obtained zeta potential here will be used as data inputs for modeling particle-interface interactions in the next chapter.

2.3.2 Particle wettability of carboxyl-PS and amidine-PS particles based on macroscopic contact angle measurements

The measured macroscopic contact angles using proxy surfaces for both particle types range from 132° to 142° over all pH and salt concentrations, indicating a hydrophobic surface. The results show that variations of pH and salt concentrations do not lead to a dramatic change of the macroscopic contact angle. A trend of decreasing contact angle with increasing pH for the PS−carboxyl surface is apparent, and there is an opposite trend for the PS−amidine surface, showing that an increase in the (absolute) surface charge density slightly reduces the hydrophobicity, as one might expect.

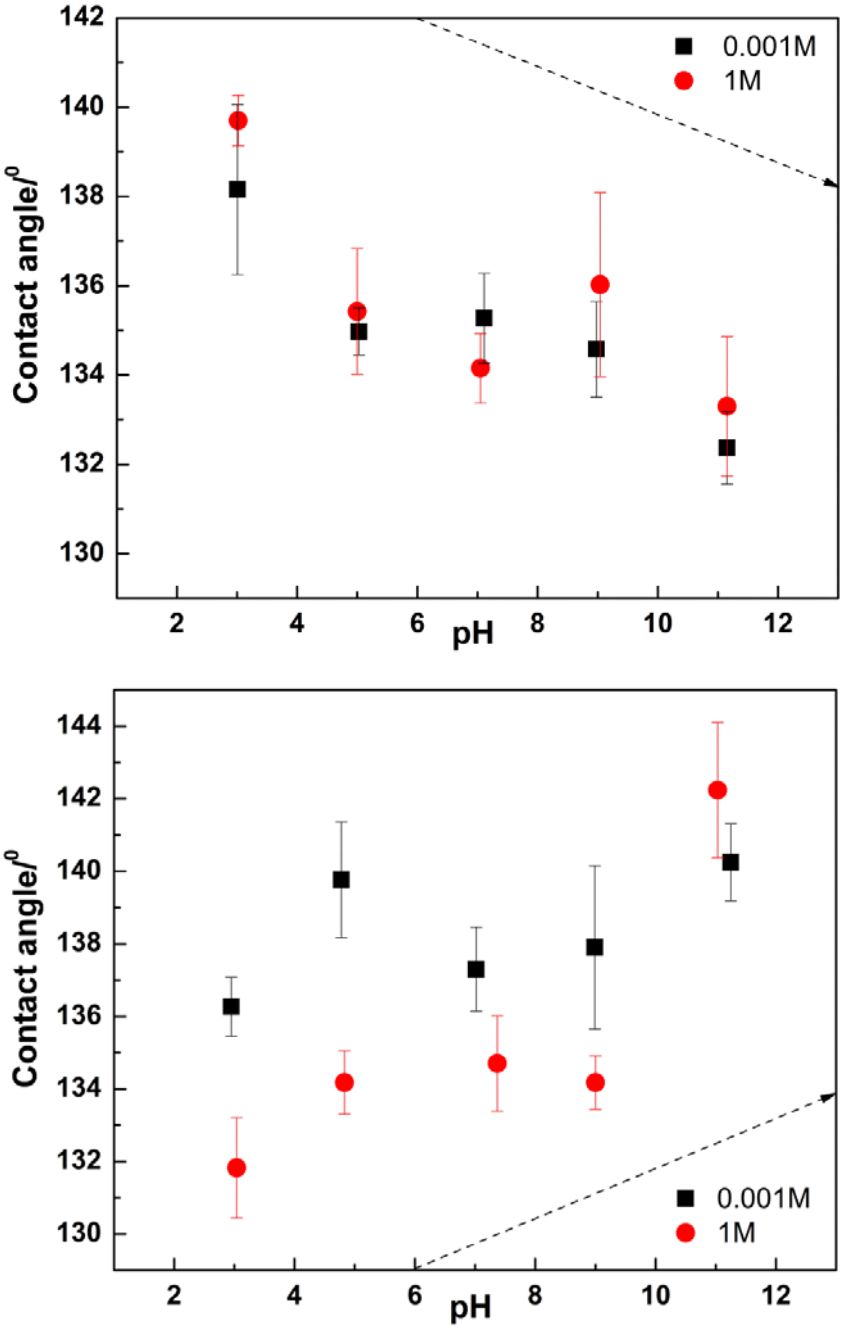

Figure 2.6 Macroscopic contact angles of carboxyl-PS (top) and amidine-PS particles (bottom) versus pH in 0.001M and 1M aqueous NaCl solutions. Data represent averages of four repeated measurements of four contact angles.

No systematic effect of salt concentration on the particle wettability is apparent from our observations of macroscopic contact angles. In the literature, the effect of salt concentrations on the surface wettability has so far remained controversial. For example, Sghaier et al.[12] found the contact angle increased significantly with increasing the salt concentration for all hydrophilic surfaces, but the contact angle variations with salt concentrations were small for tested hydrophobic surfaces. However, Binks et al.[13] reported an increase of salt concentration made carboxyl-PS particles become more hydrophilic, as supported by an observed inversion of the emulsion type from w/o emulsions to o/w emulsion upon increasing the salt concentration. More studies concluded that carboxyl particles adsorbed at an air-water interface protruded further into the water phase and thus appeared more hydrophilic at higher salt concentration[14,15,16]. The macroscopic contact angles shown in Fig. 2.6 would be expected to give a rough idea of the particle wettability, but more research on determining the wettability of charged polystyrene particles at oil-water interfaces will be discussed in chapter 4.

2.3.3 Experimental evidence for image charge effects on the particle adsorption to oil-water interfaces and Pickering emulsification

2.3.3.1 Emulsification test at different pH and electrolyte concentrations

Depending on the pH and electrolyte concentrations of the aqueous phase, we observed three distinct outcomes: no emulsion, water-in-oil (w/o) emulsions and oil-in-water (o/w) emulsions. All these results were recorded in the emulsion phase diagram in Fig. 2.8.

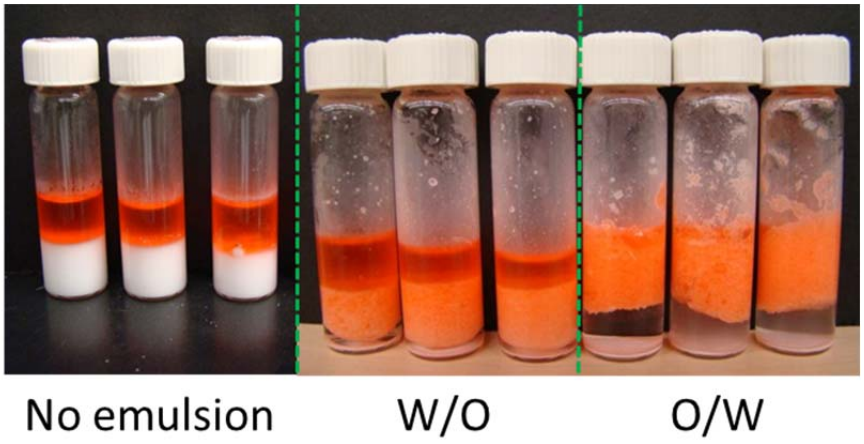

Figure 2.7 Appearances of examples of no emulsion, w/o emulsion and o/w emulsion (after sedimentation/creaming) with carboxyl-PS particles. The hexadecane used as the oil phase was dyed with Sudan III for easy observations of the emulsion type.

No emulsion was stabilized by either particle type at high particle charge (high pH for carboxyl-PS; low pH for amidine-PS) and low electrolyte concentration (low screening). In this "no emulsion" regime (Figure 2.8, solid square), we observed that droplets produced via homogenization underwent rapid coalescence, with no significant retardation by the presence of particles, until complete phase separation into an aqueous particle dispersion and a clear oil phase was achieved in a matter of seconds (Fig. 2.7). We take this complete failure of particles to stabilize any droplets as an indication that the particle adsorption at the oil-water interface is severely restricted. We may further infer from the data in Fig. 2.8 that the forces restricting particle adsorption are probably electrostatic in nature, since emulsions can form when we reduce the particle charge via decreasing the pH or enhance screening effects via increasing the electrolyte concentrations, both of which suppress the electrostatic interactions between particles and oil-water interfaces.

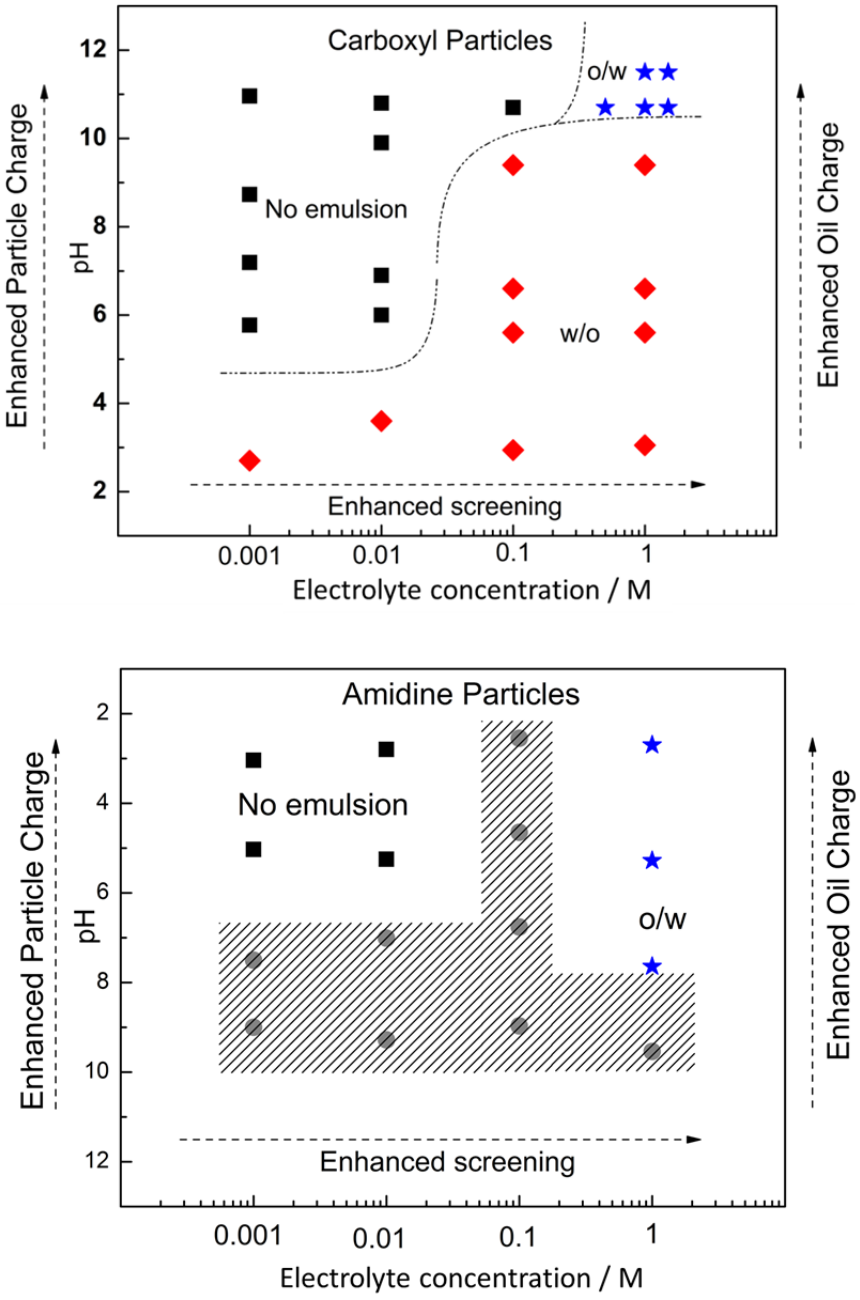

Figure 2.8 Phase diagram of emulsification of hexadecane with aqueous dispersions of carboxyl-PS (top) and amidine-PS (bottom) particles. The shaded area represents an emulsion regime with poor short–term stability, where droplet coalescence proceeded fast until only a few large drops remained stabilized.

One might wonder whether this suppression really stems from the repulsive electrostatic interactions with the interface, or from the interaction with particles already adsorbed at an interfacial concentration too low to prevent droplet coalescence. If it was the repulsion by adsorbed particles that prevented further adsorption, then coalescing emulsion droplets should nonetheless reach good coverage overtime and be stabilized eventually, as illustrated in Fig. 2.9. We therefore believe it is the electrostatic interaction with the interface itself that prevents the particle adsorption and the formation of emulsions.

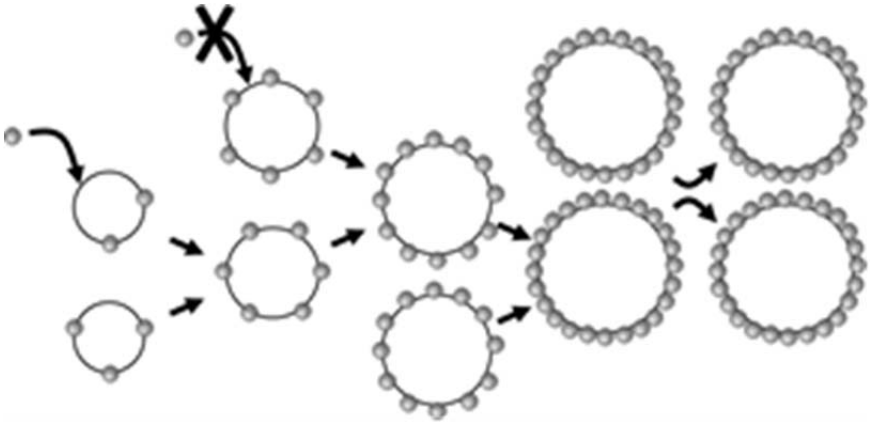

Figure 2.9 Scheme of limited particle adsorption and droplet coalescence. Coalescence reduces the total interfacial area available to the adsorbed particles until the droplet coverage is sufficient for stabilization.

2.3.3.2 Microscopy study of particle – interface interactions

One might also argue, besides the failure of particle adsorption to the oil-water interface, there are other possible explanations for the failure of emulsions, for example, the particle are too hydrophilic to stabilize emulsions[17]. However, our microscopy study of particle adsorption to a macroscopic oil-water interface further confirms our notion

that failure of emulsification at high particle charge and week screening is due to a strong suppression of particle adsorption. In Fig. 2.10, images A and C show carboxyl-PS particles from our emulsification study, gathered at the hexadecane-D_2O interfaces at conditions where particles are highly charged (pH 10), and either weakly screened (1 mM NaCl) or strongly screened (1 M NaCl). In the case of strong screening, the interfacial particles formed aggregates overnight, whereas the weakly screened particles remained dispersed. A more important difference became obvious, when the heavy water sub-phase was gently replaced (slowly and with great care to minimize disturbance of the interface) by a solution of regular water with the same pH. Now, the particles experienced a net gravitational force pointing downward, causing all non-adsorbed particles to slowly sediment to the bottom of the container, while adsorbed particles remained trapped at the interface by the much stronger interfacial tension force. After another day of rest, very few particles were found at the interface with the weakly screened interface(image B), whereas particles at the interface of the high salt system kept aggregating slowly without leaving the interface upon replacement of heavy water with water(image D). These observations confirm strong correlations between “failure of particle adsorption to oil-water interfaces and “failure to emulsify”.

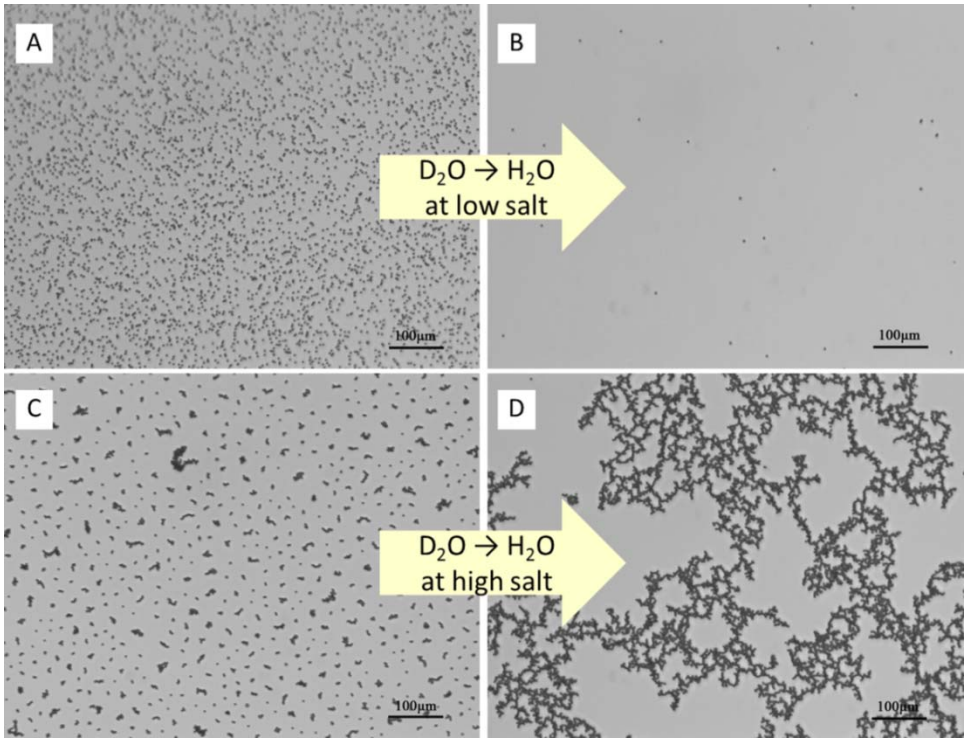

Figure 2.10 Images of carboxyl-PS particles at 1mM NaCl, pH 10, at a D_2O-hexadecane interface before (A) and after (B) replacement of D_2O by H_2O (1mM NaCl, pH10), and the same particles, at 1M NaCl, pH 10, at a D_2O-hexadecane interface before (C) and after (D) replacement of D_2O by H_2O (1mM NaCl, pH 10)[18].

Fig. 2.11 shows the image of a confocal macroscopic observation of particle-interface interactions when the interface slowly descends to approach the 5.09 µm carboxyl-PS particles deposited on a glass surface. An interfacial deformation appeared when the interface was very close to the particle, but we cannot firmly conclude from this observation that the apparent deformation is "real" and due to repulsive particle-interface interactions rather than an optical artefact of the confocal imaging technique.

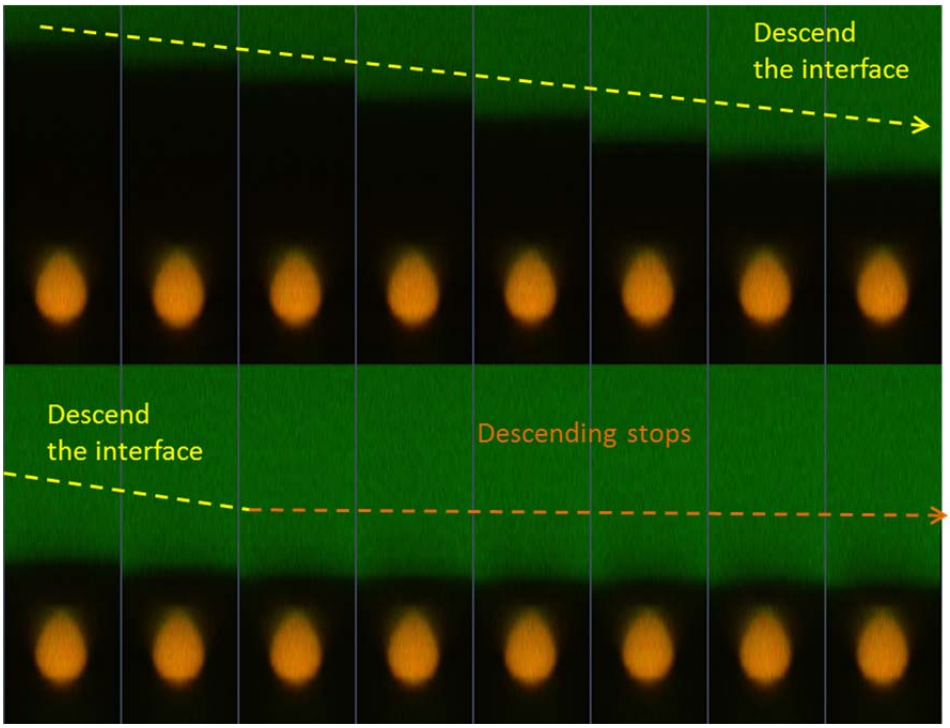

Figure 2.11 Image of a confocal macroscopic observation of particle-interface interactions when the interface slowly descends to approach the 5.09 um carboxyl-nile blue PS fluorescent particles. (The green zone is hexadecane dyed with nile red; the black zone is water; the orange zone is the particle).

We did not make additional efforts to justify this observation, since the above microscopy observation of particle adsorption to a macroscopic oil-water interface already confirms the existence of particle-interface interactions hindering particle adsorption to the oil water interface. For the negatively charged carboxyl particles, such repulsive particle-interface interactions are due to the electric double layer repulsion from the similarly charged oil-water interface[1]. If this was the only interaction preventing the formation of Pickering emulsions, then the positively charged amidine particles, which are attracted to the oil by the electric double layer force, should encounter no such difficulty. Our emulsification experiments suggest otherwise (Fig 2.8 bottom). While emulsions were formed at high salt content, there was again a regime at high and weekly

screened particle charge where no emulsion formed, suggesting the particle adsorption to the oil-water interface is strongly suppressed.

2.3.3.3 Hypothesis of image charge effects on the particle adsorption

We propose that the suppression of particle adsorption for positive charged particles is caused by the repulsion of particles from their electrostatic "image" charge on the oil side of the liquid interface.

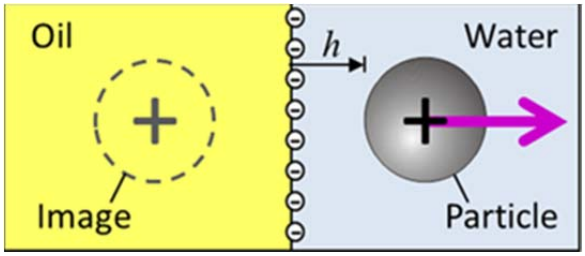

Figure 2.12 Scheme of electrostatic repulsions for positively charged particles from image charge across the oil-water interface

It is well known that an electric charge near an interface between dielectric media of different permittivity sets up a polarization field in which the charge experiences a force pointing towards to the more polarizable medium [19]. Near a large flat interface, the force on a charge q takes the same form as the electrostatic interaction with a second charge located in the position of a mirror image across the interface, carrying an "image charge" of magnitude:

$$q_{image} = q\frac{\varepsilon_1 - \varepsilon_2}{\varepsilon_1 + \varepsilon_2} \qquad \text{Eq. 2-1}$$

Here, ε_1 is the dielectric constant of the medium hosting the real charge, and ε_2 is that of the charge-free medium. For a charge in water ($\varepsilon_1 = 78$) facing a flat surface of hexadecane ($\varepsilon_2 = 2$), the image charge has the same sign and almost the same magnitude as the real charge, and like the interaction between real charges, the charge-image interaction can be screened by salt ions. Similarly, a charged colloid particle near a low-curvature oil-water interface is repelled by its image charge, and it is this repulsion that may result in the suppression of the particle adsorption. While theoretical studies have long hinted at the importance of image forces for the interaction of particles with small ions[20] and even with liquid interfaces[21], considerations of image forces in Pickering emulsions have so far focused only on the image charge *attraction* for particles in the oil phase[22]. To our best knowledge, the work presented in this chapter provides the first experimental evidence of image charge repulsion preventing the formation of Pickering emulsions.

2.4 Conclusions

The work in this chapter presented experimental evidence that the widely neglected image charge repulsion may hinder the particle adsorption and prevent the formation of Pickering emulsions even when the electric double layer interaction with the liquid interface is attractive. However, one might ask: is this image repulsion strong enough to compete with all attraction forces and prevent particle adsorption? A theoretical model of the particle adsorption to oil-water interfaces in the next chapter

confirms that the repulsive image force has the right order of magnitude to successfully compete with other forces acting on the particles and to prevent the particle adsorption and Pickering emulsification.

2.5 References

1. Marinova, K. G.; Alargova, R. G.; Denkov, N. D.; Velev, O. D.; Petsev, D. N.; Ivanov, I. B.; Borwankar, R. P., Charging of Oil-Water Interfaces Due to Spontaneous Adsorption of Hydroxyl Ions. Langmuir 1996, 12 (8), 2045-2051.

2. Zangi, R.; Engberts, J. B. F. N., Physisorption of Hydroxide Ions from Aqueous Solution to a Hydrophobic Surface. J. Amer. Chem. Soc. 2005, 127 (7), 2272-2276.

3. Creux, P.; Lachaise, J.; Graciaa, A.; Beattie, J. K.; Djerdjev, A. M., Strong Specific Hydroxide Ion Binding at the Pristine Oil/Water and Air/Water Interfaces. J. Phys. Chem. B 2009, 113 (43), 14146-14150.

4. Zimmermann, R.; Freudenberg, U.; Schweiß, R.; Küttner, D.; Werner, C., Hydroxide and hydronium ion adsorption — A survey. Curr. Opin. Colloid Interface Sci. 2010, 15 (3), 196-202.

5. Knecht, V.; Levine, Z. A.; Vernier, P. T., Electrophoresis of neutral oil in water. J. Colloid Interface Sci. 2010, 352 (2), 223-231.

6. Vácha, R.; Rick, S. W.; Jungwirth, P.; de Beer, A. G. F.; de Aguiar, H. B.; Samson, J.-S.; Roke, S., The Orientation and Charge of Water at the Hydrophobic Oil Droplet–Water Interface. J. Amer. Chem. Soc. 2011, 133 (26), 10204-10210.

7. Beattie, J. K.; Gray-Weale, A., Oil/Water Interface Charged by Hydroxide Ions and Deprotonated Fatty Acids: A Comment. Angew.Chem. Int. Ed. 2012, 51 (52), 12941-12942.

8. Hunter, R. J., Zeta Potential in Colloid Science: Principles and Applications. Academic Press: New York, 1981.

9. Hunter, R. J., Foundations of Colloid Science. Oxford University Press: Oxford, 1992.

10. O'Brien, R. W.; White, L. R., Electrophoretic Mobility of a Spherical Colloidal Particle. J. Am. Chem. Soc. Faraday Trans. II 1978, 74, 1607 - 1626.

11. Mangelsdorf, C. S.; White, L. R., Effects of Stern-Layer Conductance on Electrokinetic Transport Properties of Colloidal Particles. J. Chem. Soc., Faraday Transactions 1990, 86 (16), 2859-2870.

12. Sghaier, N.; Prat, M.; Ben Nasrallah, S., On the Influence of Sodium Chloride Concentration on Equilibrium Contact Angle. Chem. Eng. J. 2006, 122 (1-2), 47-53.

13. Binks, B. P.; Rodrigues, J. A., Inversion of Emulsions Stabilized Solely by Ionizable Nanoparticles. Angew. Chem. Int. Edit. 2005, 44 (3), 441-444.

14. Dhar, P.; Prasad, V.; Weeks, E. R.; Bohlein, T.; Fischer, T. M., Immersion of Charged Nanoparticles in a Salt Solution/Air Interface. J. Phys. Chem. B 2008, 112 (32), 9565-9567.

15. Gehring, T.; Fischer, T. M., Diffusion of Nanoparticles at an Air/Water Interface Is Not Invariant under a Reversal of the Particle Charge. J. Phys. Chem. C 2011, 115 (48), 23677-23681.

16. Shrestha, A.; Bohinc, K.; May, S., Immersion Depth of Positively versus Negatively Charged Nanoparticles at the Air–Water Interface: A Poisson–Boltzmann Model. Langmuir 2012, 28 (40), 14301-14307.

17. Amalvy, J. I.; Armes, S. P.; Binks, B. P.; Rodrigues, J. A.; Unali, G. F., Use of sterically-stabilised polystyrene latex particles as a pH-responsive particulate emulsifier to prepare surfactant-free oil-in-water emulsions. Chem. Commun. 2003, (15), 1826-7.

18. Wang, H.; Singh, V.; Behrens, S. H., Image Charge Effects on the Formation of Pickering Emulsions. J. Phys. Chem. Lett. 2012, 3 (20), 2986-2990.

19. Israelachvili, J. N., Intermolecular and Surface Forces. 2 ed.; Elsevier: 1992.

20. Messina, R., Image Charges in Spherical Geometry: Application to Colloidal Systems. J. Chem. Phys. 2002, 117 (24), 11062-11074.

21. Grünberg, H. H. v.; Mbamala, E. C., Charged Colloids Near Interfaces. J.Phys.: Conden. Matt. 2001, 13 (21), 4801.

22. Leunissen, M. E.; van Blaaderen, A.; Hollingsworth, A. D.; Sullivan, M. T.; Chaikin, P. M., Electrostatics at the Oil-Water Interface, Stability, and Order in Emulsions and Colloids. Proc. Nat. Acad. Sci. 2007, 104 (8), 2585-2590.

CHAPTER 3

A MODEL OF PARTICLE ADSORPTION TO OIL-WATER INTERFACES WITH IMAGE FORCE INCLUDED

3.1 Introduction

We hypothesize, based on the experimental observations in the previous chapter, that the image repulsive force can be a cause for the electrostatic barrier hindering the adsorption of positively charged particles to oil-water interfaces. We are therefore motivated to quantitatively confirm that this image force is strong enough to impede the particle adsorption by theoretically modeling the particle adsorption to the oil-water interface. In the context of emulsification, particle adsorption under turbulent mixing is governed by the competition of the hydrodynamic mixing force pushing the particle toward the interface with the barrier force hindering particle adsorption, in contrast to the scenario of diffusive adsorption in a quiescent fluid, which involves thermal activation over an interaction *energy* barrier. To predict particle adsorption to oil-water interfaces, the hydrodynamic mixing force F_{mix} has to be compared with the total interaction forces between the particle and the interface, written as the sum of the van der Waals force F_{vdW}, the electric double layer force F_{EDL} (repulsive for anionic particles while attractive for cationic particles), and the image force F_{image} which was newly considered in the previous chapter. We predict that the particle adsorption is suppressed if

$$\max(F_{vdW}+F_{EDL}+F_{image}) > F_{mix} \qquad \text{Eq. 3-1}$$

We will discuss the calculations of each force in detail below. Upon completion of these calculations, we are able to theoretically estimate whether particle adsorption and the formation of emulsions should be expected at given pH and salt concentrations, and will compare such theoretical predictions to the experimental results from chapter 2.

3.2 Methods of force calculation

3.2.1 Hydrodynamic mixing force F_{mix}

For a particle of radius a near a droplet of radius $R \gg a$, the hydrodynamic force under turbulent mixing pushing particle toward the oil-water interface can be estimated as[1]

$$F_{mix} \approx a^2 \rho_c \varepsilon^{2/3} R^{2/3} \qquad \text{Eq. 3-2}$$

Where ρ_c is the density of the continuous liquid and ε is the rate of energy dissipation per unit mass. Here, $\rho_c = 10^3$ kg/m^3 for water, $\varepsilon \approx 10^5$ J Kg^{-1}s^{-1} for a lab-scale rotor-stator mixer, and $R \approx 20$ μm for an estimated droplet radius. We obtained $F_{mix} \approx 1$ nN for the carboxyl particles and 64 pN for the smaller amidine particles.

3.2.2 Particle-interface interaction force

The interaction of a single particle with an oil-water interface includes three components as discussed above: the van der Waals force F_{vdW}, the electric double layer force F_{EDL} and the image force F_{image}. Approximating the oil-water interface as a planar

interface between two semi-infinite media, we calculated all three components of the interaction force using the Derjaguin approximation,[2]

$$F(h) = 2\pi \frac{R_1 R_2}{R_1 + R_2} W(h) \qquad \text{Eq. 3-3}$$

which relates the force F between two body with curved surfaces of curvature radii R_1 and R_2 separated by a gap of width h, to the corresponding interaction energy per unit area between two parallel infinite plates at the same separation. Neglecting the curvature of the large interface against the particle curvature, we use $R_1 = a$ (the particle radius), and $R_2 = \infty$ (infinite oil-water interface) for the van der Waals and electric double layer interaction, whereas $R_2 = a$ (the image charge radius) for the image force. The Derjaguin expression is expected to be a good approximation when the interaction range and the separation h of interest are much smaller than R_1 and R_2. This is certainly the case for the separations at which the force barrier to adsorption is found in our calculations. Details in calculating interactions of W^{vdW}, W^{EDL} and W^{image} will be discussed as follows.

3.2.2.1 Van der Waals interaction

The van der Waals interaction can be calculated by[3]

$$W^{vdW}(h) = -\frac{H_{owp}}{12\pi h^2} \qquad \text{Eq. 3-4}$$

where H_{owp} is a nonretarded Hamaker constant for particle-oil interactions across the water. H_{owp} can be estimated from Lifshiftz theory using the mixing rule[3]

$$H_{owp} = (\sqrt{H_{oo}} - \sqrt{H_{ww}})(\sqrt{H_{pp}} - \sqrt{H_{ww}}) \quad \text{Eq. 3-5}$$

where H_{oo}, H_{ww}, and H_{pp} are the Hamaker constants of the symmetric interaction of oil, water, and polystyrene across vacuum, and the value is given in table 3-1[4]. With all these values known, we obtained H_{owp} of 3.2× 10^{-21} J.

Table 3-1 Values for Hamaker constants of H_{oo}, H_{ww}, and H_{pp} across vacuum

Material	Hamaker constants (10^{-20} J)
Hexadecane	$\mathbf{H_{oo} = 5.2}$
Water	$\mathbf{H_{ww} = 3.7}$
Polystyrene	$\mathbf{H_{pp} = 7.9}$

3.2.2.2 Electric double layer interaction

The double layer interaction between the particle and the oil-water interface is evaluated using the superposition approximation, which evaluates the electric potential by adding the potentials of two non-interacting surfaces (from non-linear Poisson-Boltzmann solutions), with "non-charge regulating" boundary conditions. For surfaces with the same sign of charge, the interaction energy is derived as

$$W^{EDL}(h, \psi_1, \psi_2) = 64nk_BT\kappa^{-1}\frac{1+\frac{E^2(h)}{3}}{(1-E(h))^3}E(h) \quad \text{Eq. 3-6}$$

whereas for surfaces with opposite signs of charge,

$$W^{EDL}(h,\psi_1,\psi_2) = -64nk_BT\kappa^{-1}\frac{E(h)}{1-E(h)} \quad \text{Eq. 3-7}$$

and *E(h)* is the exponentially decaying function,

$$E(h) = \left|\tanh(\frac{\psi_1 e}{4k_BT})\tanh(\frac{\psi_2 e}{4k_BT})\right| \exp(-\kappa h) \quad \text{Eq. 3-8}$$

where *n* is the bulk electrolyte concentration, k_BT is the thermal energy unit, and κ^{-1} is the Debye screening length. $\psi_1 = \psi_p$ is the particles' electrostatic surface potential and $\psi_2 = \psi_{oil}$ is the potential of the oil-water interface.

Table 3-2 Surface potential values (in mV) used to theoretically predict the particle adsorption (carboxyl-PS) and the formation of emulsions at select pH and salt concentrations for which oil data were available in the literature citation.

	1 mM				10 mM		
	ψ_p	ψ_{oil}	ψ_{image}		ψ_p	ψ_{oil}	ψ_{image}
pH 11	-126	-100	-123.4				
pH 8.7	-123	-90	-120.4				
pH 7.2	-121	-70	-118.4				
pH 5.8	-88	-60	-85.6	pH 6	-51	-30	-49
pH 3	-15	-10	-14.3				

Table 3-3 Surface potential values (in mV) used to theoretically predict the particle adsorption (amidine-PS) and the formation of emulsions for select pH and salt concentrations for which oil data were available in the literature citation.

	1 mM				10 mM		
	ψ_p	ψ_{oil}	ψ_{image}		ψ_p	ψ_{oil}	ψ_{image}
pH 3	120	-10	117				
pH 5	86.4	-50	84	pH 6	78.4	-30	76
pH 7.5	74.6	-70	72.3				
pH 9	58.5	-90	56.4				

To theoretically predict the particle adsorption and the formation of emulsions at the corresponding pH and salt concentrations to emulsification experiments, we need to know ψ_p of and ψ_{oil} at these conditions. We use the measured zeta potential as an approximation for the particle surface potential ψ_p, and we estimate the potential of the oil-water interface ψ_{oil} from literature values of the experimental zeta potential of closely related pristine xylene-water interfaces. Xylene-water interfaces are expected to have very similar properties as alkane-water interfaces, but allow for much more accurate characterization because xylene becomes more water-soluble at slightly elevated temperature and can easily be precipitated into small drops at room temperature that remains sufficiently stable without surfactants to allow for high quality electrophoresis measurements. The zeta potential of particles at given pH and salt concentrations can be determined by interpolations of the experimental zeta potential shown in Fig. 2.5. However, our theoretically prediction is limited to pH and salt concentrations where experimental data of ψ_{oil} are available. The available surface potential values used for the theoretical estimates are shown in table 3-2 (carboxyl-PS) and table 3-3(amidine-PS).

3.2.2.3 Image charge interaction

In analogy to the interaction of a point charge with its charge image, we compute the interaction of the charged particle like a double layer interaction with an image particle at separation distance $2h$, using the same approximations as previously for the double layer interaction with the interface:

$$W^{image}(h) = W^{EDL}(2h, \psi_p, \psi_{image}) \quad \text{Eq. 3-9}$$

where, according to Eq. 2-1 and the Grahame equation connecting the charge density and surface potential of isolated surfaces[3], we obtain the surface potential ψ_{image} of the particle image (listed in Tables 3-2 and 3-3) via

$$\psi_{image} = \frac{2k_BT}{e} sinh^{-1}[\frac{\varepsilon_1-\varepsilon_2}{\varepsilon_1+\varepsilon_2} \sinh\left(\frac{e\psi_p}{2k_BT}\right)] \quad \text{Eq. 3-10}$$

Finer details of the image charge interaction, such as effects caused by the curvature of the oil-water interface or the charge images of interfacial ions at the water-particle boundary, are not captured in our simplistic description.

We substitute values of W^{vdW}, W^{EDL} and W^{image} back to Eq. 3-3 and obtain forces of F_{vdW}, F_{EDL} and F_{image}. Finally, we rely on the Eg. 3-1 to predict the particle adsorption and the formation of emulsions at selected pH and salt concentrations upon availability of data inputs (table 3-2 and table 3-3).

3.3 Results and Discussions

3.3.1 Model prediction of electrostatic barrier to particle adsorption

Experimental results in the last chapter suggest an electrostatic barrier hindering the particle adsorption and preventing the formation of emulsions when particles are highly charged at low salt concentrations. The electrostatic barrier to adsorption for negatively charged particles resulting from the electric double layer repulsion has been well known, but current understanding encounters difficulties in explaining the cause of electrostatic barriers to adsorption for the positively charged particles, as the electric double layer is attractive in this case. We propose this widely neglected electrostatic barrier to adsorption is caused by the image force, and include it in our model computation of the forces across oil-water interfaces.

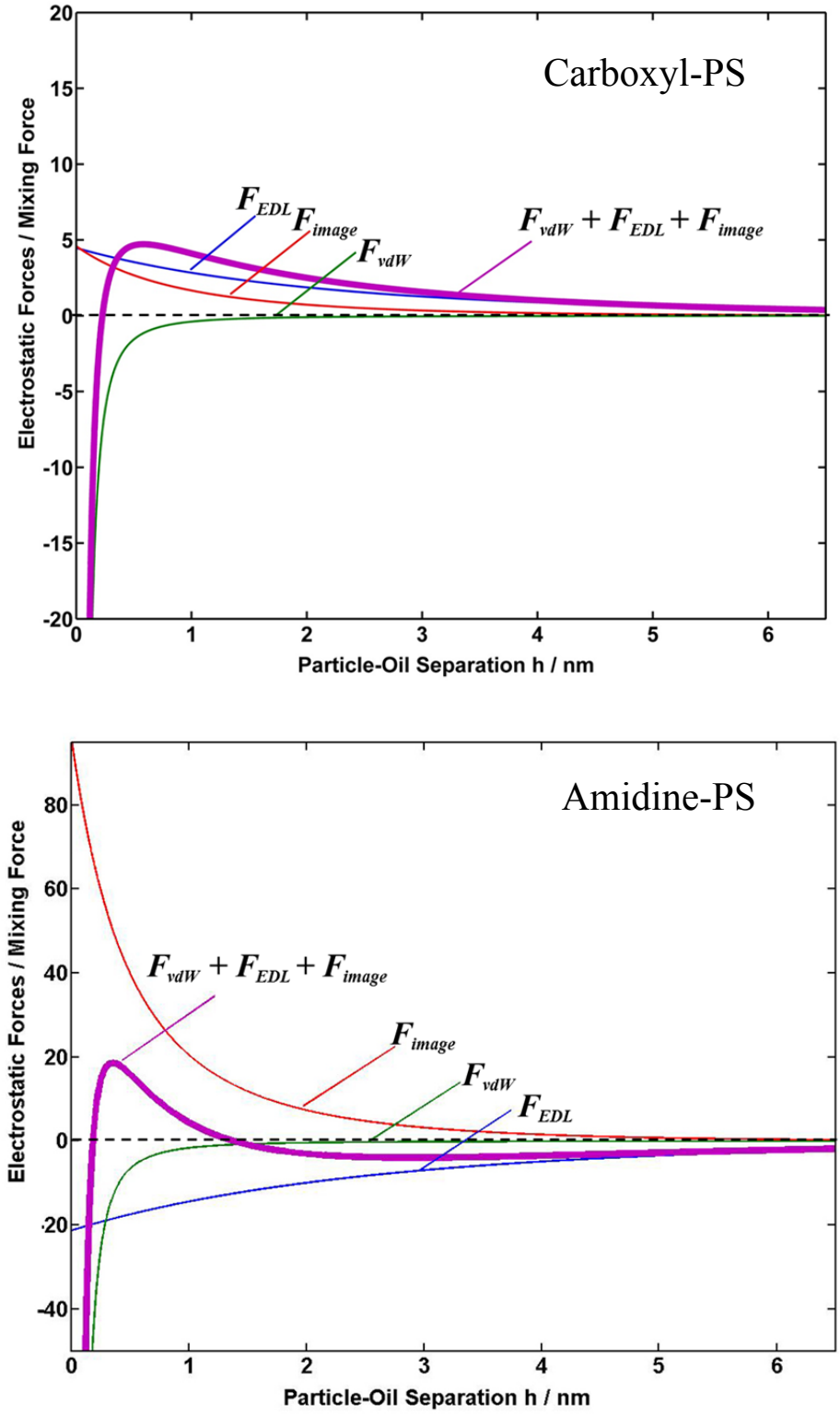

Figure 3.1 Force between a charged particle and a negatively charged interface at pH 6 and 10mM NaCl solutions

Consistently with the experimental suggestion, the model computation confirms the existence of electrostatic barrier for both particles at medium conditions (pH 6 and 10 mM). As shown in Fig. 3.1, the Y-axis is the ratio of total electrostatic force to hydrodynamic mixing force, and the electrostatic barrier exists only if the ratio is greater than one, when the total interaction force outweighs the hydrodynamic mixing force (Eq. 3-1). We attribute the electrostatic barrier to both the electric double layer repulsion and the image force repulsion for negatively charged particles, but only to the image force repulsion for positively charged particles. The height of the estimated electrostatic force barrier is 5 times larger than the hydrodynamic mixing force for anionic carboxyl-PS particles, and is 19 times larger for the small cationic amidine-PS particles. The 0.4 μm amidine-PS particles show a larger relative barrier height than 1.9μm carboxyl-PS particles because carboxyl-PS particles experience a larger hydrodynamic mixing force promoting adsorption, which is proportional to the particle size (Eq. 3-2). In essence, this model computation supports our proposition that image forces can have the right order of magnitude to create an electrostatic barrier impeding the particle adsorption and Pickering emulsification.

According to the model prediction, we should be able to make the particle adsorb and form emulsions by increasing the hydrodynamic mixing force to where it is larger than the maximum electrostatic barrier force. In line with these expectations, we found that a significant increase of hydrodynamic driving force, realized experimentally by increasing the rotor frequency almost 3-fold to 30000 rpm, achieved the formation of emulsions in the cases where weaker mixing failed to produce a Pickering emulsions. By contrast, simply increasing the mixing time by a factor of 2 or 3 did not have that effect.

The model also predicts that an oil with a higher dielectric constant should give rise to a weaker image force and therefore help lower the electrostatic barrier (Eq. 3-9) and promote particle adsorption and emulsification. To test this prediction, we carried out emulsification experiments with 1-octanol, which has negligibly low water miscibility like hexadecane, but a higher dielectric constant (10.3), and we found that mixing always resulted in the formation of Pickering emulsions regardless of the pH and salt concentrations in the aqueous solutions. Such agreements between the model prediction and the experimental observations provide additional support for our arguments about the effects of image charges on the formation of Pickering emulsions.

3.3.2 Comparison of model predictions for the formation of emulsions to experimental results

In addition to the model prediction at medium conditions discussed above, we carried out the similar theoretical estimates for other solution conditions where experimental data of the zeta potential of oil-water interfaces in NaCl solution were available[5]. The model prediction suggesting the failure of particle adsorption and Pickering emulsification are marked with open squares, whereas the model predicted success of the particle adsorption and Pickering emulsification are marked with open circles in Fig. 3.2.

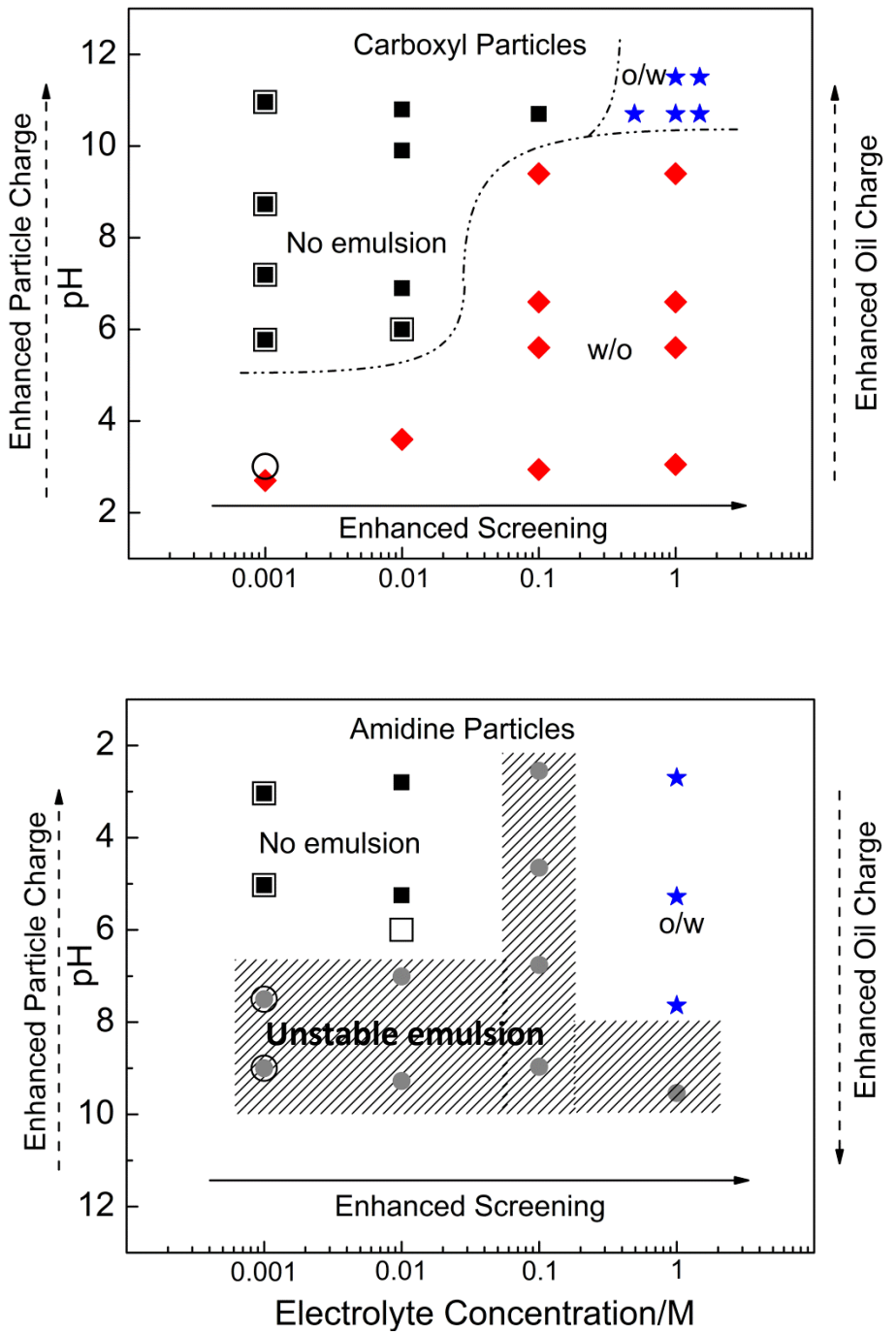

Figure 3.2 Comparison between the model prediction and the experimental results about whether emulsions can form in solution conditions where experimental data for the zeta potential of oil-water interfaces are available. Solid symbols mark experiments, and open symbols mark the model prediction of whether emulsion can form (open square) or not (open circle).

From Fig. 3.2, we see that the model prediction of whether the emulsions can form agrees very well with the experimental observations. Given the crude approximations made in the theoretical estimates, those detailed agreement with experiments seems fortuitous, but it does support our arguments that image forces have the right order of magnitude to impede Pickering emulsification, and including the image force in calculating forces across the interface increases the accuracy of the model prediction.

3.4 Conclusions

The theoretical work in this chapter answers the question left in the chapter 2 about whether the image force repulsion is strong enough to prevent particle adsorption. Our theoretical estimate does support our hypothesis that image repulsive forces have the right order of magnitude to impede the particle adsorption and Pickering emulsification. Further, with the image force included in the model estimating the forces across the oil-water interfaces, we achieved good agreement between the model prediction and the experimental results about whether the particle can adsorb to the interface and produce emulsions at select cases where zeta potential data of oil-water interfaces are available. But, given the use of the superposition approximation and boundary conditions of constant charge and constant potential, the current theoretical model is still quite crude, and further efforts will be made to achieve more accurate theoretical model via solving the full Poisson-Boltzmann equation with boundary conditions of charge-regulating surfaces[6,7] ,where the surface potential and surface charge density is dependent on the surface separation.

3.5 References

1. Tcholakova, S.; Denkov, N. D.; Lips, A., Comparison of Solid particles, Globular Proteins and Surfactants as Emulsifiers. Phys. Chem. Chem. Phys. 2008, 10 (12), 1608-1627.

2. Evans, D. F.; Wennerström, H., The Colloidal Domain: Where Physics, Chemistry, Biology, and Technology Meet. 2 ed.; Wiley-VCH: New York, 1999.

3. Israelachvili, J. N., Intermolecular and Surface Forces. 2 ed.; Elsevier: 1992.

4. Dahneke, B., The Influence of Flattening on the Adhesion of Particles. J. Colloid Interface Sci. 1972, 40 (1), 1-13.

5. Marinova, K. G.; Alargova, R. G.; Denkov, N. D.; Velev, O. D.; Petsev, D. N.; Ivanov, I. B.; Borwankar, R. P., Charging of Oil-Water Interfaces Due to Spontaneous Adsorption of Hydroxyl Ions. Langmuir 1996, 12 (8), 2045-2051.

6. Carnie, S. L.; Chan, D. Y. C., Interaction Free-energy between Plates with Charge Regulation - a Linearized Model. J. Colloid Interface Sci. 1993, 161 (1), 260-264.

7. Behrens, S. H.; Borkovec, M., Electrostatic Interaction of Colloidal Surfaces with Variable Charge. J. Phys. Chem. B 1999, 103 (15), 2918-2928.

CHAPTER 4

ELECTRIC FIELD EFFECTS ON THE PARTICLE CONTACT ANGLE AT OIL-WATER INTERFACES

4.1 Introduction

The particle contact angle θ, used to quantify the particle wettability, is an important parameter for the stability of Pickering emulsions in terms of its effects on the energy of particle adsorption at the oil-water interface (Eq. 1-2) and on the maximum capillary pressure of the liquid film separating two emulsion droplets and stabilizing them against coalescence (Eq. 1-3). The particle contact angle is also the most important parameter governing the emulsion type. Several experimental methods have been advocated to measure the contact angle of particles at liquid-liquid interfaces, including the macroscopic measurement of droplet angles on flat proxy surfaces, the gel trapping technique (GTT), the film-calliper method, and the FreSca cryo-SEM method discussed in the chapter 1. Experimental data from all these methods generally agree on the hydrophilic nature of inorganic particles such as silica particles and gold particles, but they fail to provide a consistent picture about the wettability of charged polystyrene particles. The inorganic particles may be considered inherently hydrophilic, but the charged polystyrene particles exhibit a hydrophobic polystyrene bulk and hydrophilic charged functional groups at the surface, so their resulting overall wettability is not obvious. Our contact angle measurements in chapter 2 reported (macroscopically measured) contact angles for 2 μm carboxyl-PS particles exceeding 130°; Paunov et al[1]

obtained a contact angle around 100° for 3.9 μm sulfate polystyrene particles via GTT. These reports indicate charged polystyrene particles are more hydrophobic. However, the measurements with the film-calliper method[2] showed the contact angle of 2 μm sulfate polystyrene particles was 58°, and recent measurements with FreSca Cryo-SEM[3] reported a contact angle of 85° for 2.8 μm charged polystyrene particles. The charged particles thus appear hydrophilic from these experiments. One might ask: are such differences in suggesting the wettability of charged polystyrene particles caused by differences in the particle functionalization, by a large particle-to-particle or batch-to-batch variability in the particle wettability, by experimental errors, or by other reasons, such as systematic differences in the way that the particle charge affects the contact angle observed in the different experimental geometries[4]? The work in this chapter will help remove much of this uncertainty. We select two well-known methods, the macroscopic surface proxy method and GTT, to measure the contact angle of charged polystyrene particles, and find that details of the sample preparation greatly affect the outcome even when the same analysis is applied. We propose an improved sample preparation protocol for the GTT method, and observe that the (arguably) most reliable data for the particle contact angles and our contact angle data for the macroscopic proxy surfaces suggest opposite wettability for the same material. We attribute this discrepancy to electric field effects on the position of an actual particle at the oil-water interface.

4.2 Materials and Methods

1 μm polystyrene (PS, 64030) particles were purchased from Polysciences Inc. , and 1 μm carboxyl-PS (C37274) and 1 μm sulfate-PS (S37498) particles were purchased

from Life Technologies Corporation. 5 μm Nile-blue fluorescent carboxyl-PS particles were obtained from Spherotech Inc. All particles were purged three times with DI water by centrifuge before use. Some important properties of these particles were summarized in table 4-1. All particles of 1 μm mean diameter have a narrow size distribution (low standard deviation), but the 5 μm particles are polydisperse .

Table 4-1 Properties of charged polystyrene particles for contact angle measurements

Particle	Mean diameter(μm)	STD	Surface charge density (max)
Sulfate-PS1	1 μm	0.03 μm	N.A.
Sulfate-PS2	1 μm	0.026 μm	6.1 μC/cm^2
Carboxyl-PS	1 μm	0.046 μm	12.7 μC/cm^2
Fluorescent carboxyl- PS	5.09 μm	0.437 μm	N.A.

4.2.1 Measurements of macroscopic contact angle and contact angle hysteresis

Measuring the contact angle of a macroscopic surface is widely used to estimate the particle wettability. The procedure of preparing the macroscopic proxy surface mimicking the particle surface is the one described in chapter 2 (Fig. 2.2). To account for the fact that particles are initially dispersed in the water phase and water thus wets the solid first, we revised the set-up for three-phase contact angle measurements by first submerging the polymer coated glass substrate in water rather than in oil. The substrate was held upside down in a sample cell filled with aqueous 1 mM NaCl solution at pH 5.8, and a small drop of hexadecane (Reagent Plus, Sigma-Aldrich), purified via passing through active alum oxide before use, was gently filled and deposited from below on the

substrate by an inverted needle, and the resulting three-phase contact angle was measured through the water phase.

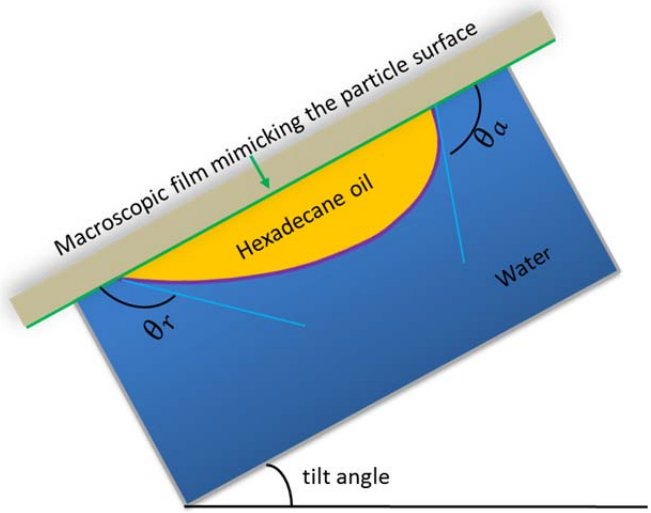

Figure 4.1 Scheme of the tilt plate method for measurements of contact angle hysteresis, where θ_a and θ_r are the advancing contact angle and the receding contact angle respectively.

The contact angle hysteresis, which generally arises from surface roughness or chemical heterogeneity[5], was measured by the tilting plate method[6] (also referred as inclined plate method). As the plate is tilted typically from 0° to 90°, the contact angle on the downhill side increases while the contact angle on the uphill side decreases due to the gravity. Upon the last valid reading when the sessile drop starts to slide, we captured the contact angles on the downhill and uphill sides of the sessile drop as the advancing contact angle θ_a and the receding contact angle θ_r respectively. The difference between them ($\theta_a - \theta_r$) is defined as the contact angle hysteresis. In some cases, the drop will not slide even when the plate tilts all the way to the vertical, and the final static downhill and uphill contact angles were used to represent the θ_a and the θ_r after a rest time of 10 min.

4.2.2 Gel trapping technique (GTT) and revised spreading solvent-free GTT

The GTT protocol reported in the literature for measuring the three-phase contact angle of particles at oil-water interfaces started with the introduction of particles to oil-water interfaces using a spreading solvent like isopropanol, and the water phase consists of an initially warm (50 °C) aqueous solution of 2% gellan gum (CpKelco)/1mM NaCl at pH 5.8, which was purified by passing through a C_{18}-silica chromatographic column before use. When the temperature droped from to 25 °C, the gel sets and immobilizes the particle at oil-water interface. The oil phase was then replaced with polydimethylsiloxane (PDMS), and after curing for 48 hours, the PDMS replica with trapped particles can be peeled off. The protruding height of the particles was measured by AFM (VEECO Dimension 3100) under the tapping mode and was used together with the known particle size to calculate the contact angle. The reported contact angles were averages of contact angles measured for three particles per sample.

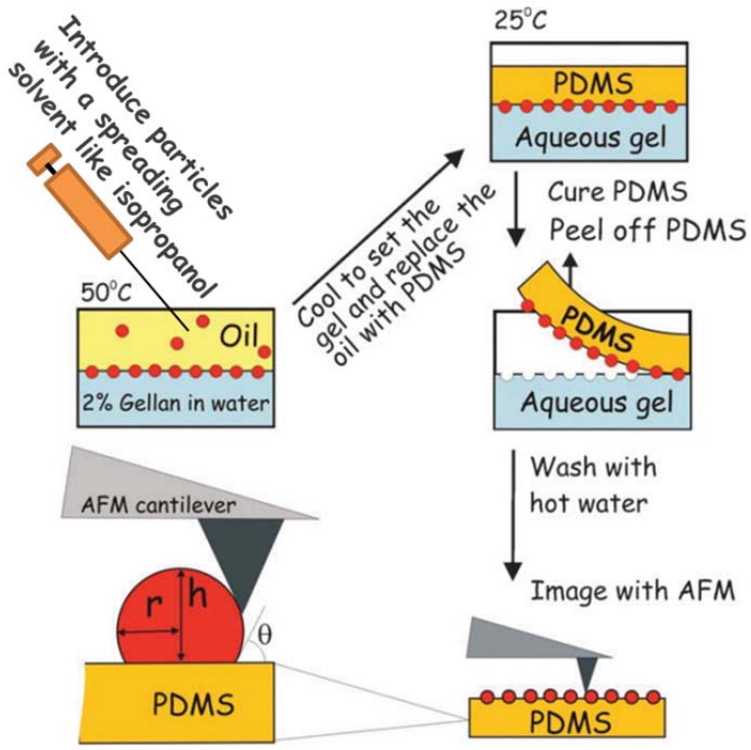

Figure 4.2 Scheme of gel trapping technique (GTT) with a spreading solvent-assisted introduction of particles to oil-water interfaces[1]

A central argument against the classical GTT protocol is the use of a spreading solvent like isopropanol (IPA), and a few recent studies reported that the choice of spreading solvent influences the measured contact angle, with IPA making particles appear more hydrophobic[7]. To remove the effect of IPA on the particle contact angle, we revised the way of introducing the particle to the oil-water interface, and used the buoyancy force on particles in heavy water, combined with mild agitation, to bring particles to the interface. After an overnight rest allowing the particles to reach the interface, we gently added a 3% gel solution to the heavy water and achieved a final gel solution of 2% (w/v) at pH 5.8 and 1 mM NaCl. The rest of protocol was the same as in the classical GTT procedure. The resulting coverage of the interface with particles

achievable with our revised method is much smaller than the one obtained with a spreading solvent, and one might fear that the particle found in the interface may not represent the average particle properties. Given the good size monodispersity of our samples, we nonetheless feel that any sampling flaws possibly introduced in our method are less severe than the artifacts caused by the spreading solvent in the original protocol.

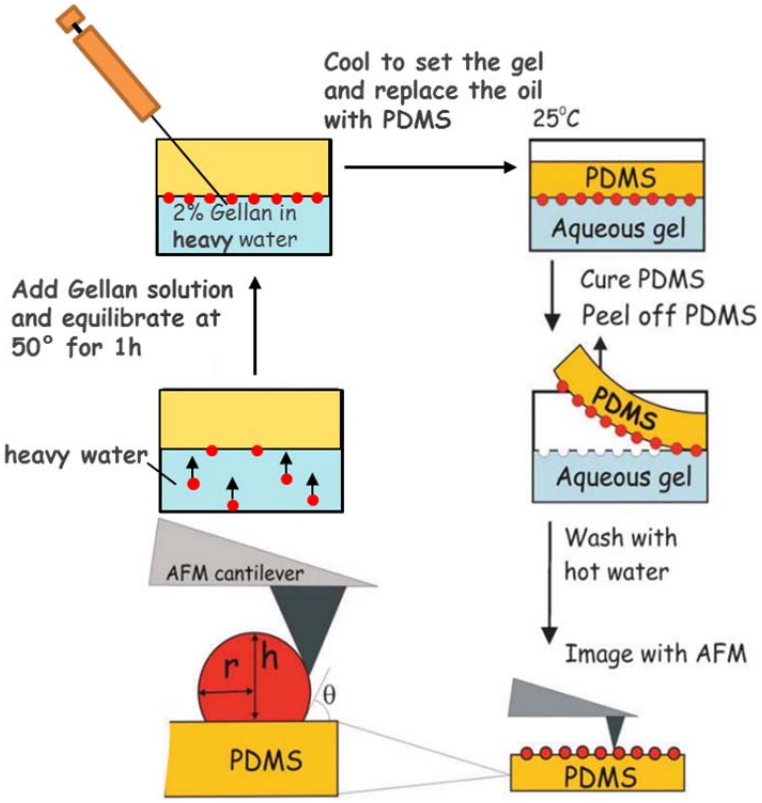

Figure 4.3 Spreading solvent-free GTT with introducing particles via buoyancy force in the heavy water

4.2.3 Confocal microscopy of particles in the oil-water interface

Confocal microscopy observation of the particle position at the oil-water interface was conducted to estimate the particle contact angle, as a complementary approach for the macroscopic contact angle measurement and GTT discussed above. We added 5.09

μm nile-blue fluorescent particles (0.005% w/v) into heavy water and allowed them to reach the interface overnight. The oil phase was labeled with Nile red (Sigma Aldrich) for an observation of the interface. The image showing the particle position in the depth direction (z direction) at the interface was acquired by reconstructing a stack of in-plane images (x-y direction) using a 63X oil-immersion objective lens (numerical aperture: 1.4) on a confocal microscope (Zeiss LSM 510 VIS).

4.2.4 Zeta potential measurements

Zeta potentials of particles as a function of pH at 1 mM NaCl solutions were calculated from experimental electrophoretic mobilities (measured by Malvern zetasizer Nano ZS590) using O'Brien and White's method[8]. Zeta potentials of the macroscopic surface as a function of pH were measured by an electrokinetic analyzer (Anton Paar SurPass electrokinetic analyzer), which analyzes the streaming potential and streaming current generated by solution flow over the surface[9,10]. The reported results for both measurements were averaged from two independently prepared samples at each pH and 4 measurements per sample.

4.3 Results and Discussions

4.3.1Experimental evidence of electric field effects on the particle contact angle at oil-water interfaces

4.3.1.1 Comparison of particle contact angles measured with macroscopic proxy surface method and GTT

For an ideal solid surface, there is no contact angle hysteresis, and the experimentally observed contact angle is the equilibrium θ_E defined by the Young equation. However, for a non-ideal surface, the experimentally observed static contact angle might not be θ_E, and contact angle hysteresis is commonly observed. It has been suggested that the equilibrium angle θ_E can be approximated by the arithmetic mean[11,12]

$$\cos\theta_E = \frac{\cos\theta_a + \cos\theta_r}{2}, \qquad \text{Eq.4-1}$$

where θ_a is the advancing contact angle, and θ_r is the receding contact angle. A typical set up for macroscopic contact angle measurements is shown in Fig. 4.4.

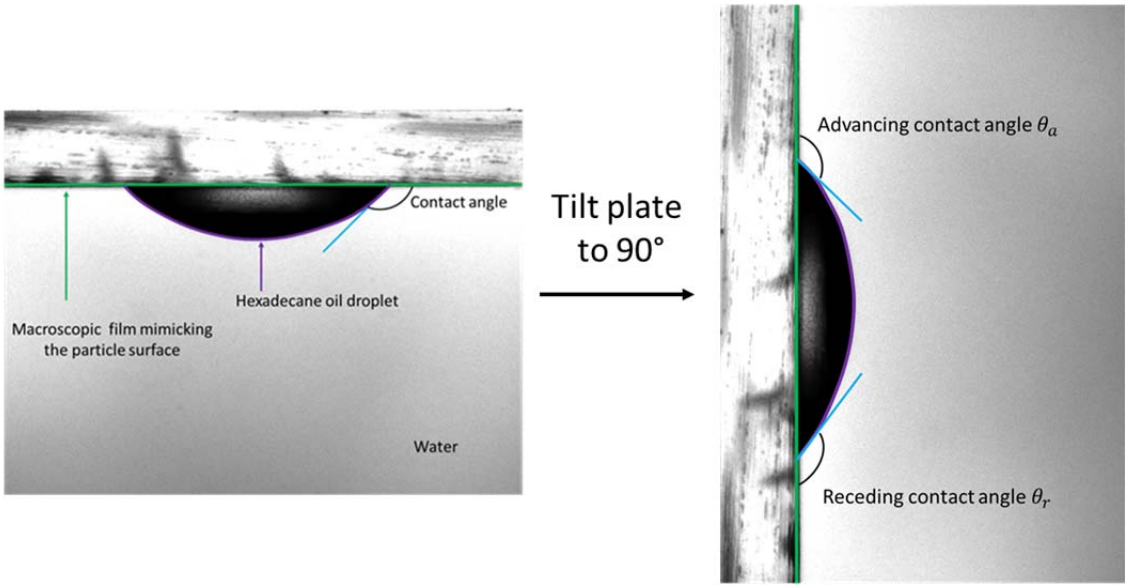

Figure 4.4 Depiction of a macroscopic contact angle and contact angle hysteresis (at a tilt angle of 90°) for the thin film cast from carboxyl-PS particle solutions

In our measurements, the sessile drop did not slide even when the plate was tilted to 90°, and the final static downhill and uphill contact angles were used to represent the θ_a and the θ_r respectively after a rest time of 10 min. Around 6° contact angle hysteresis was observed for all the surfaces, and the θ_E value, calculated according to Eq. 4-1, show all macroscopic surfaces are very hydrophobic with contact angles above 135°, predicting hydrophobicity of all particles. We also find the carboxyl-PS particles appear less hydrophobic (lower contact angle) due to their higher surface charge densities than the other two sulfate-PS particles, as one might expect.

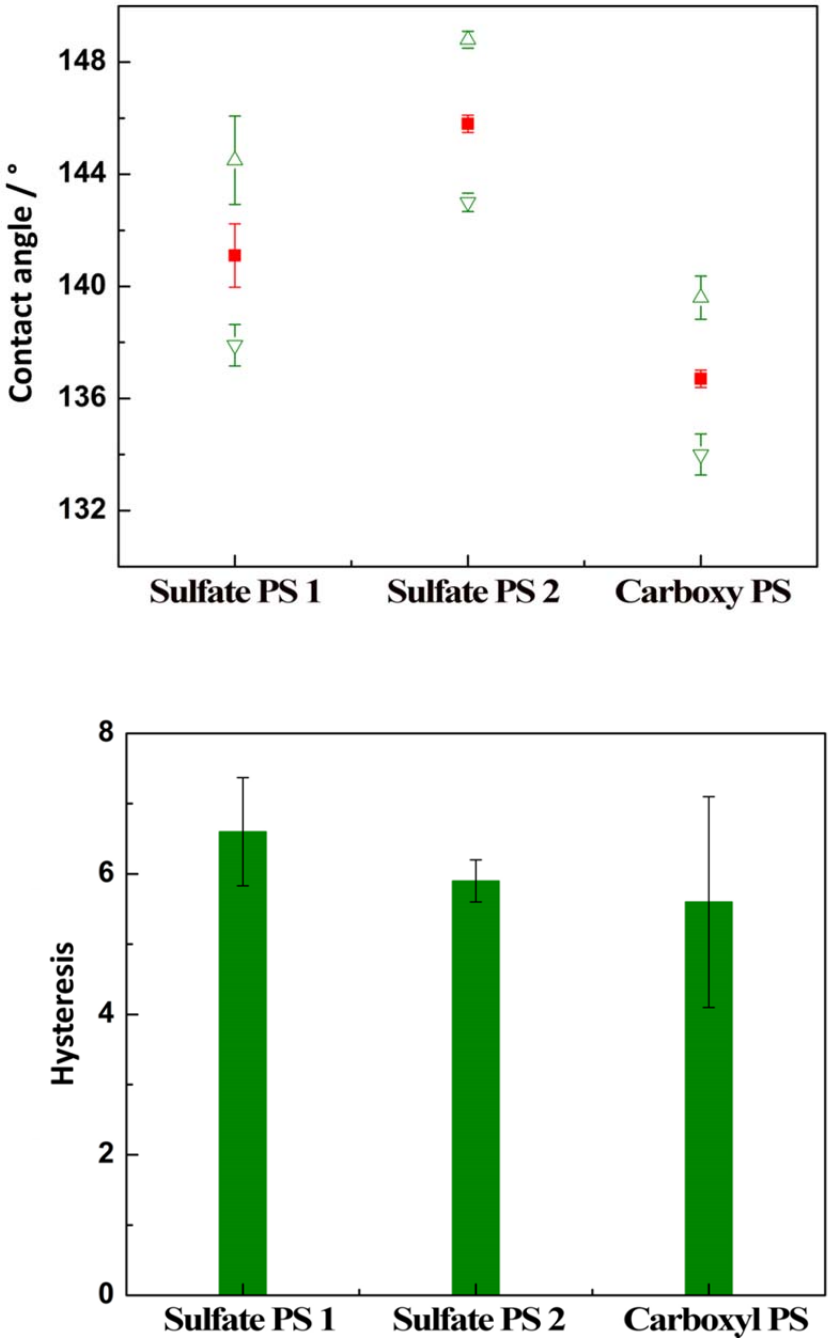

Figure 4.5 Results of θ_a(open triangle) , θ_r (open inverted triangle), and θ_E solid squares and contact angle hysteresis (bottom)

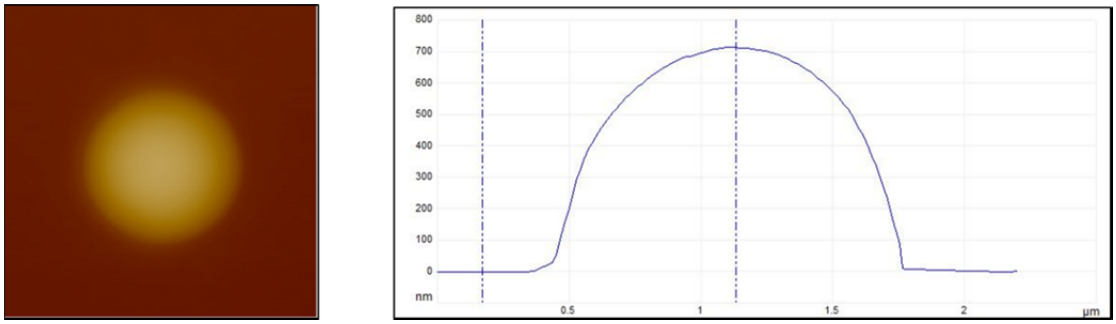

Figure 4.6 A typical AFM scanning image of one polystyrene particle in the PDMS interface (left) and measured protruding height above the PDMS surface (right).

Compared to the macroscopic contact angle measurement, the GTT is a more direct approach to measure the particle contact angle at interfaces. The PDMS replica of the oil-water interface can be examined by scanning electron microscopy, or, for a more accurate determination of contact angles the height of the protruding particles can be measured by atomic force microscopy (AFM). In the latter case the accuracy of measurements is within a few nanometers, determined by the vertical resolution of the AFM. We conducted GTT both with introduction of particles to the interface using the spreading solvent and with buoyancy driven particle adsorption from heavy water. The results, together with data of the macroscopic contact angle measurements above, are summarized in Fig. 4.7.

GTT with spreading solvent yields a significantly lower contact angle for all charged polystyrene particles than observed in the macroscopic measurements on a proxy surface, but both types of measurements agree in the qualitative assessment that the solid surfaces are hydrophobic. Such qualitative agreement in predicting the hydrophobicity of the charged polystyrene particles could distract from the systematic difference in the results, which might in part be blamed on a slightly different surface composition of the

particles and the proxy surfaces. However, in light of the recent suggestions that the spreading solvent can have a hydrophobizing effect[3,7], one may wonder whether particles in the absence of spreading solvent would appear hydrophilic. The answer is yes based on our GTT measurement on particles introduced to the interface from heavy water without the use of spreading solvent – the revised GTT protocol yields contact angles below 90°, indicating that particles are indeed hydrophilic at this low ionic strength, although macroscopic measurements and the widely used original GTT method suggest otherwise.

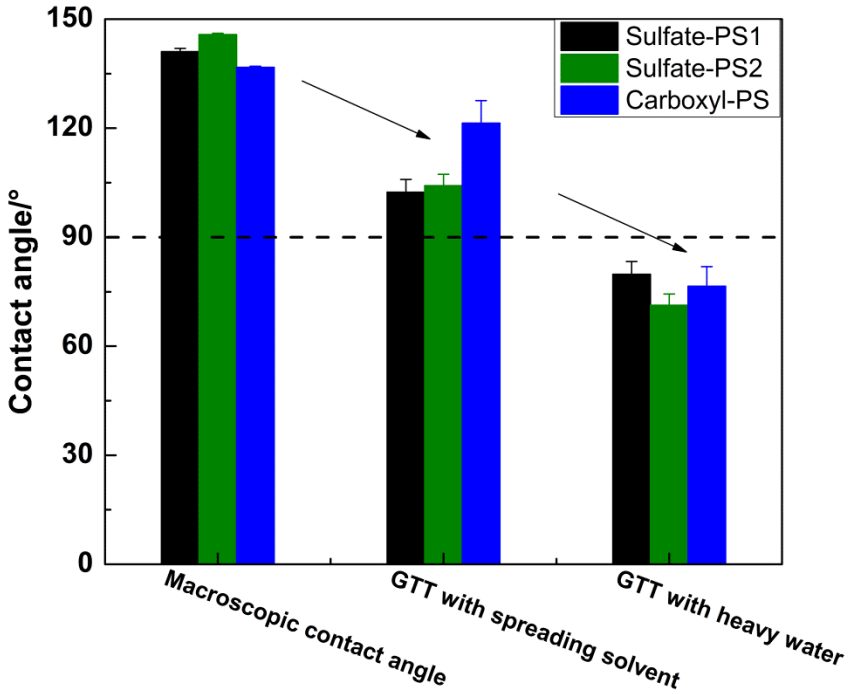

Figure 4.7 Comparison of contact angle measured with macroscopic thin film proxy, GTT with spreading solvent and GTT with heavy water.

For further insights into the true particle wettability, we conducted a confocal microscopy study of the particle position relative to the oil-water interface and estimated the contact angle of the particle with the interface. The confocal observation of a larger

fluorescent carboxyl-PS particle (5 µm) shows the larger part of the particle residing in the water phase, which suggests that particles are hydrophilic in line with the result from the GTT with heavy water.

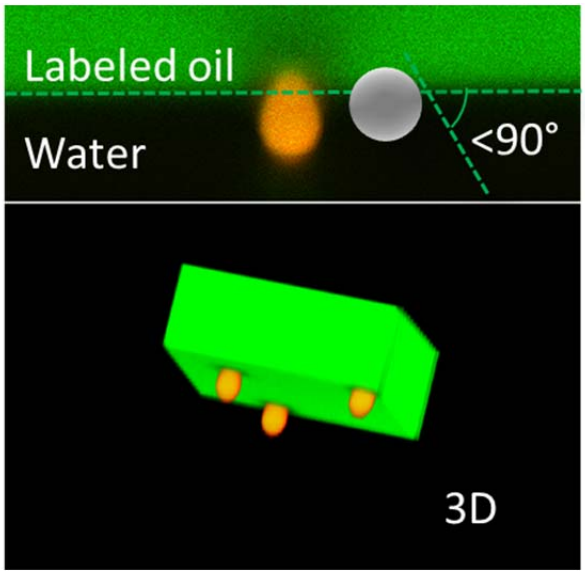

Figure 4.8 Confocal microscope image of a 5 µm fluorescent carboxyl-PS particle at an oil-water interface

4.3.1.2 Comparison of zeta potentials between macroscopic surfaces and particles

While artifacts associated with the spreading solvent explain the hydrophobic appearance in the classical GTT experiments, another explanation is needed for the bigger discrepancy between the macroscopic measurements and the results from the revised GTT method. One might argue that some of the chargeable surface groups on the particles could be lost or modified during the preparation of the macroscopic proxy surface, which involves the transfer of particles from water to IPA, drying, and

dissolution in chloroform for spin coating. Although one might conversely expect a higher surface density of chargeable groups on the macroscopic film, which has lower total surface area than the source particles, we cannot exclude that the temporary exposure to two solvents in the film preparation somehow results in a loss of surface charge. In order to investigate this potential loss of surface charge in the preparation of macroscopic proxy surfaces from the particles, we measured and compared the zeta potentials of the particles and the macroscopic proxy surfaces, shown in Fig. 4.9. For both sulfate-PS particles, the macroscopic surface has a zeta potential about 20 mV ~ 40 mV lower than particles through all pH, whereas for carboxyl-PS particles, the macroscopic surface has a lower zeta potential at high pH and then coincides well with the zeta potential of the particles as pH decreases. A systematic difference in zeta potentials obtained with different experimental techniques has been reported in several previous studies[13,14]. The zeta potential is the potential at the shear plane, and where exactly it is located relative to the charged surface is dependent on the experimental geometry (Fig. 4.10). The shear plane is believed to be closer to the surface in electrophoresis measurements (for the particle zeta potential) than in streaming potential measurements (for the macroscopic surface potential), leading in general to a slightly higher measured zeta potential for particles than for similarly charged macroscopic surfaces.

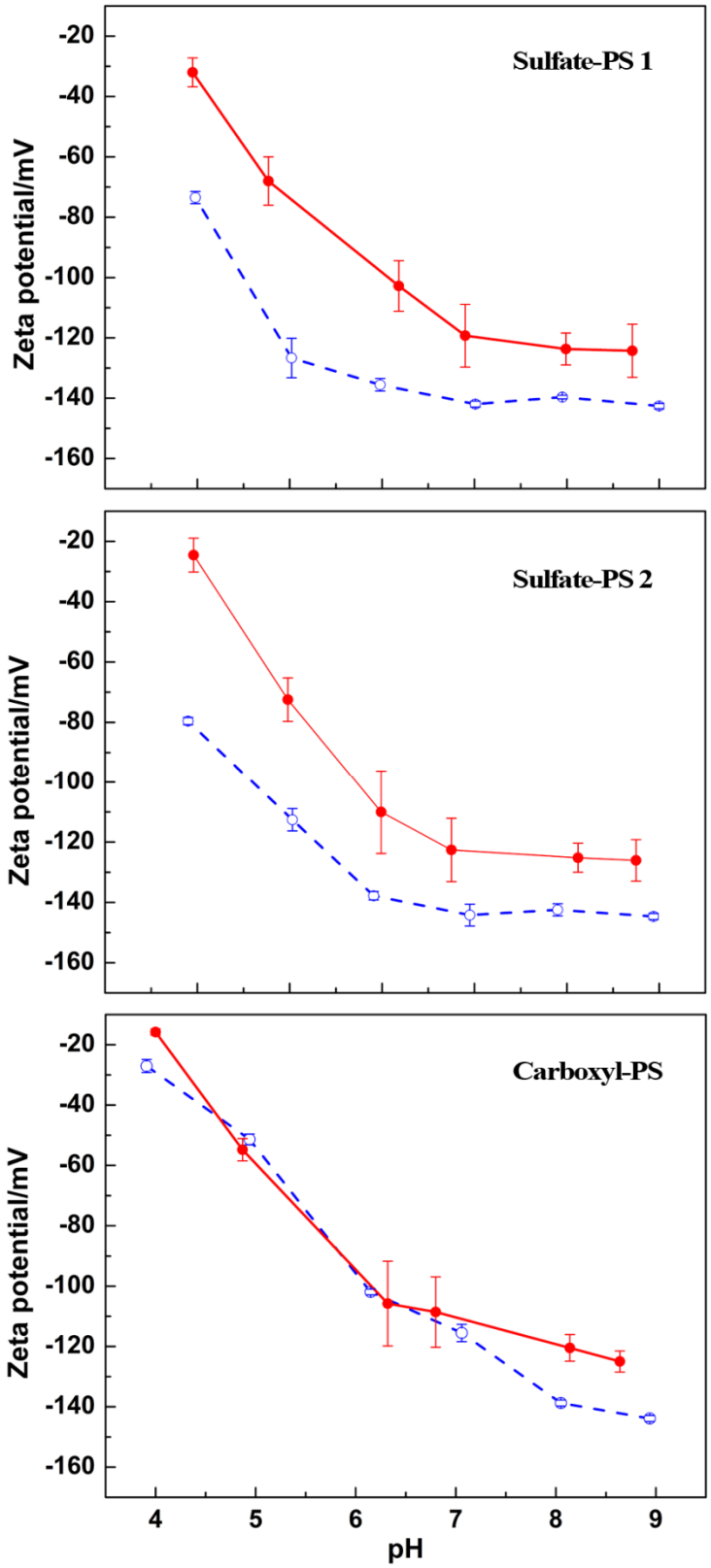

Figure 4.9 Comparisons of zeta potentials as a function of pH between macroscopic surfaces (solid red line) and particles (dashed blue line)

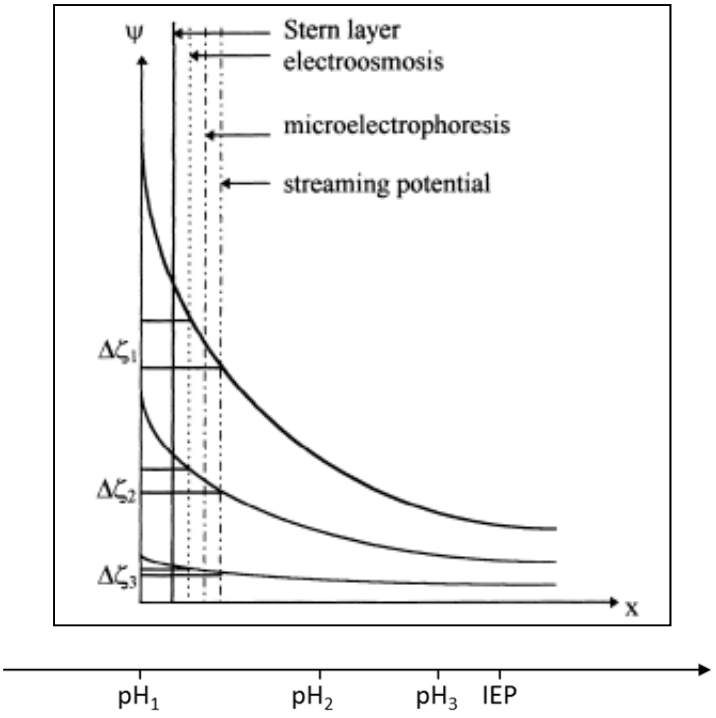

Figure 4.10 Theoretical potential evolution as a function of the distance with respect to the solid surface within the electrical double layer: Influence of the shear plane location on zeta potentials with different electrokinetic methods $\Delta\zeta_i$ is the difference between zeta potentials obtained with different electrokinetic methods at pH_i [14].

According to Fig. 4.10, the difference between different electrokinetic methods becomes especially pronounced when the pH is far from the isoelectric point (IEP), which in the case of our particles is very low, especially for the sulfate particles. One might argue that the 20 mV ~ 40 mV difference observed for the sulfated surfaces may still be due to a loss of charged groups. We cannot eliminate this possibility, but we assure that the macroscopic surface is still highly charged. Therefore, and because of the good consistency in the electrokinetic results for the carboxyl surfaces, it seems implausible that a lack of charges on the macroscopic surfaces is the primary cause for the difference in their contact angles from the particle contact angles.

4.3.1.3 Hypothesis of field effects on the particle contact angle

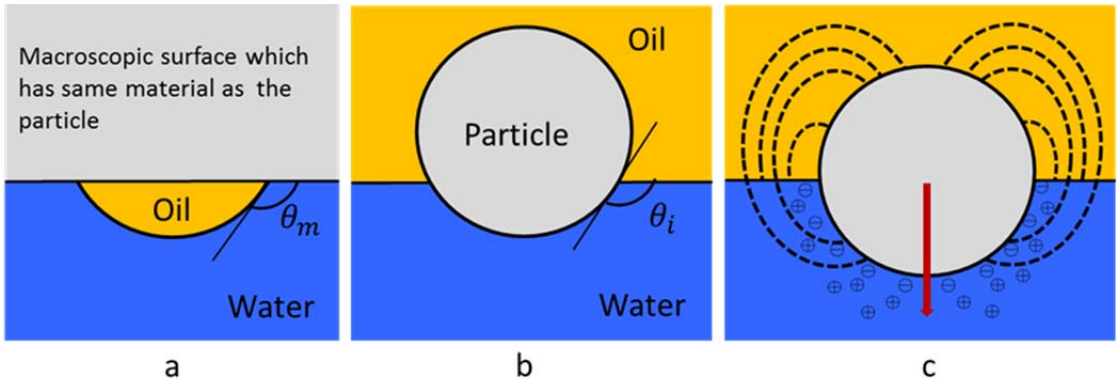

Figure 4.11 Scheme for the macroscopic contact angle θ_m (a), the particle's contact angle θ_i at equilibrium position without the electrostatic field effect (b) and the shifted equilibrium position towards water side including the field effect

Our experimental results above indicate that the contact angle of interfacially adsorbed particles is much smaller than the macroscopic contact angle of chemically similar surfaces. We propose that this is caused by contributions to the particle's free energy from the electric field associated with the charged particle and its asymmetrically distributed counterions. Since these counterions are essentially confined to the far more polarizable aqueous subphase, the overall charge distribution has a strong dipole moment, and in the far field resembles the field of a point dipole, although with significantly reduced strength on the water side due to screening (Fig. 4.11 c). The particle's equilibrium position with respect to the interfaces corresponds to the total free energy minimum, and it is fairly obvious that electrostatic contributions like the energy stored in the dipole field contribute a position dependent free energy term that will influence the equilibrium contact angle and is not accounted for in the standard expression (Eq. 1.2)

relating the free energy to the contact angle. Without the electrostatic effects, the particle's contact angle θ_i at the equilibrium position (Fig. 4.11 b), decided by the interfacial free energy with respect to the interfacial tension, is precisely the macroscopic contact angle θ_m that is formed by an oil droplet on a solid surface which has the same material as the particle, surrounded by the water phase (Fig. 4.11 a).

How far the particle position is shifted because of electrostatic effects – and even the direction of this shift – is far from obvious, but the question naturally arises whether such a shift can possibly explain why polymer particles that produce hydrophobic coatings on macroscopic surfaces can protrude far into the water side of an oil-water interface and preferentially stabilize water-continuous emulsions, much like intrinsically hydrophilic emulsifiers. A simple theoretical model of the total free energy profile for an interfacially adsorbed particle including the self-energy of the dipole field will be discussed in the next chapter.

4.4 Conclusions

By revising the classical Gel Trapping Technique, using particle buoyancy in heavy water to introduce particles to the interface instead of a spreading solvent, we have revealed that charged polystyrene particles can appear hydrophilic with three phase contact angles below 90° measured through the water phase, even when the corresponding flat proxy surfaces are hydrophobic as judged by macroscopic contact angles above 90°. The macroscopic contact angle measurement can still be an effective method to evaluate the inherent wettability of the particle, since the zeta potential of macroscopic surface is found to be comparable to the original particles. However, the

macroscopic contact angle might not truly reflect the position of charged particles in an oil-water interfaces due to the proposed effect of dipole field. The energy stored in the formed dipole field contributes to the total free energy profile, and may shift the particle's equilibrium position toward the water side, yielding a lower contact angle than expected from macroscopic measurements.

4.5 References

1. Arnaudov, L. N.; Cayre, O. J.; Cohen Stuart, M. A.; Stoyanov, S. D.; Paunov, V. N., Measuring the Three-Phase Contact Angle of Nanoparticles at Fluid Interfaces. Phys. Chem. Chem. Phys. 2010, 12 (2), 328-331.

2. Horozov, T. S.; Braz, D. A.; Fletcher, P. D.; Binks, B. P.; Clint, J. H., Novel Film-Calliper Method of Measuring the Contact Angle of Colloidal Particles at Liquid Interfaces. Langmuir 2008, 24 (5), 1678-81.

3. Isa, L.; Lucas, F.; Wepf, R.; Reimhult, E., Measuring Single-Nanoparticle Wetting Properties by Freeze-Fracture Shadow-Casting Cryo-Scanning Electron Microscopy. Nat. Commun. 2011, 2, 438.

4. Shrestha, A.; Bohinc, K.; May, S., Immersion Depth of Positively versus Negatively Charged Nanoparticles at the Air–Water Interface: A Poisson–Boltzmann Model. Langmuir 2012, 28 (40), 14301-14307.

5. Eral, H. B.; 't Mannetje, D. J. C. M.; Oh, J. M., Contact Angle Hysteresis: A Review of Fundamentals and Applications. Colloid Polym Sci 2013, 291 (2), 247-260.

6. Contact Angle Hysteresis. http://www.ramehart.com/contactangle.htm.

7. Maestro, A.; Bonales, L. J.; Ritacco, H.; Rubio, R. G.; Ortega, F., Effect of the Spreading Solvent on the Three-Phase Contact Angle of Microparticles Attached at Fluid Interfaces. Phys. Chem. Chem. Phys. 2010, 12 (42), 14115-20.

8. O'Brien, R. W.; White, L. R., Electrophoretic Mobility of a Spherical Colloidal Particle. J. Am. Chem. Soc. Faraday Trans. II 1978, 74, 1607 - 1626.

9. Werner, C.; Körber, H.; Zimmermann, R.; Dukhin, S.; Jacobasch, H.-J., Extended Electrokinetic Characterization of Flat Solid Surfaces. J. Colloid Interface Sci. 1998, 208 (1), 329-346.

10. Buksek, H.; Luxbacher, T.; Petrinic, I., Zeta Potential Determination of Polymeric Materials Using Two Differently Designed Measuring Cells of an Electrokinetic Analyzer. Acta Chim. Slov 2010, 57.

11. Andrieu, C.; Sykes, C.; Brochard, F., Average Spreading Parameter on Heterogeneous Surfaces. Langmuir 1994, 10 (7), 2077-2080.

12. Korhonen, J. T.; Huhtamäki, T.; Ikkala, O.; Ras, R. H. A., Reliable Measurement of the Receding Contact Angle. Langmuir 2013, 29 (12), 3858-3863.

13. Szymczyk, A.; Fievet, P.; Mullet, M.; Reggiani, J. C.; Pagetti, J., Comparison of Two Electrokinetic Methods – Electroosmosis and Streaming Potential – to Determine the Zeta-Potential of Plane Ceramic Membranes. J. Membr. Sci. 1998, 143 (1–2), 189-195.

14. Kim, K. J.; Fane, A. G.; Nystrom, M.; Pihlajamaki, A.; Bowen, W. R.; Mukhtar, H., Evaluation of Electroosmosis and Streaming Potential for Measurement of Electric Charges of Polymeric Membranes. J. Membr. Sci. 1996, 116 (2), 149-159.

15. Hurd, A. J., The Electrostatic Interaction between Interfacial Colloidal Particles. J. Phys. A 1985, 18, L1055 - L1060.

CHAPTER 5

A MODEL FOR THE PARTICLE CONTACT ANGLE AT OIL-WATER INTERFACES WITH EFFECTS OF DIPOLE FIELD INCLUDED

5.1 Introduction

As a charged particle resides at the oil-water interface, the asymmetric distribution of its counterionic clouds with respect to the interface and to the particle charge gives rise to an electrical dipole moment perpendicularly oriented to the interface, producing an electrical dipole field that is the dominant contribution to the far field in the plane of the oil-water interface ($z = 0$) and anywhere in the nonpolar oil bulk ($z > 0$), which can be considered free of mobile charges[1], whereas in the water phase ($z < 0$) mobile ions, stemming from the autodissociation of water and any dissolved salt, strongly screen the field.

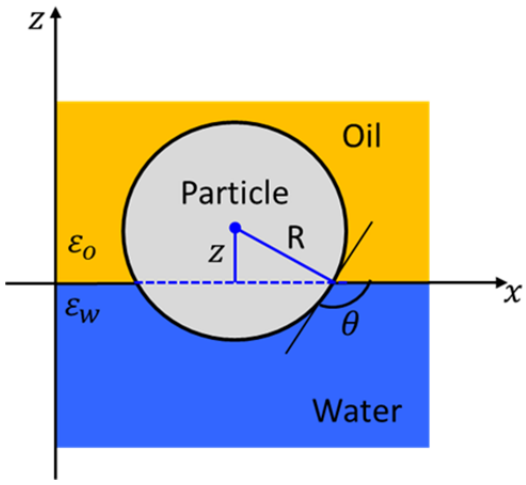

Figure 5.1 Scheme of a single particle at the oil-water interface, z = z_0 and $\theta = \theta_0$ when the particle reaches the equilibrium position.

In principle, the contribution of the entire electric field to the particle free energy can be calculated by integrating the energy density of the field over the entire space:

$$U_{field} = \frac{1}{2}\int \varepsilon_0 \varepsilon \, E^2 \, dV, \qquad \text{Eq. 5-1}$$

where ε_0 is the dielectric constant of the vacuum, ε is the dielectric constant in the medium hosting the field, and E is the magnitude of the electric field $\vec{E} = \nabla\Phi$, with associated electrostatic potential Φ. In the oil phase, this potential must satisfy the Laplace equation (Poisson equation for a charge free medium)

$$\nabla^2\Phi = 0 \quad (z > 0), \qquad \text{Eq. 5-2}$$

whereas for the water phase, the right hand side of this equation must be non-zero to reflect the presence of mobile ions. In mean-field theory, these ions are assumed to spatially arrange themselves according to a Boltzmann distribution dictated by the mean potential $\Phi(\vec{r})$. For low to moderate potential ($\Phi < k_BT$ where k_BT is the thermal energy scale and e the elementary charge), the resulting expression can be linearized and assumes the form of the popular Debye-Hückel equation

$$\nabla^2\Phi = \kappa^2\Phi \quad (z < 0), \qquad \text{Eq. 5-3}$$

where κ^{-1} is the Debye screening length. The potential (and field strength E required for Eq. 5-1) are obtained by solving Eq. 5-2 and 5-3 with the boundary condition Eq. 5-4 potential vanishes at infinite distance from the charged particle

$$\Phi(\vec{r}) \to 0 \text{ for } r \to \infty,$$

that it be consistent with the surface potential of the particle,

$$\Phi \to \Phi_s \text{ for } r = R, \qquad \text{Eq. 5-5}$$

and that the dielectric displacement $\varepsilon\vec{E}$ be continuous at the oil-water interface (assuming no charges bound to the interface):

$$\varepsilon_o \left.\frac{\partial \Phi}{\partial z}\right|_{z>0} = \varepsilon_w \left.\frac{\partial \Phi}{\partial z}\right|_{z<0} \text{ for } r > R. \qquad \text{Eq. 5-6}$$

Despite the linearization in Eq. 5-3 the solution is still far from simple[1], but as mentioned before, the dominant contribution outside of the immediate vicinity of the particle is that of a dipole field, dramatically weakened on the water side through screening by the mobile ions. To obtain a first approximation of the field effects on the particle position with respect to the interface, we will limit our considerations to the dipole field contribution.

Most studies on interfacially adsorbed particles have so far only addressed the role of the dipole field for the inter-particle interactions[2,3,4,5]. At the level of a single charged particle, however, the dipole field can also play a role in influencing the contact angle of the particle with the oil-water interface, and may provide some explanation for our experimental observations discussed in the previous chapter. In the absence of electrostatic effects, the particle's contact angle, associated with its equilibrium position at the interface, is decided by minimizing the interfacial free energy profile governed by

the interfacial tensions and position dependent areas of solid-water, solid-oil and oil-water contact[6]. The interfacial free energy profile with respect to the interfacial tension alone is described by

$$G = U_{ten}(z) = \pi\gamma_{ow}\{(z - z_0)^2 - (R + z_0)^2\} \quad \text{Eq. 5-7}$$

where γ_{ow} is the oil-water interfacial tension, z is the distance from the particle center to the interface (Fig. 5.1) and z_0 is the particle's equilibrium position. z_0 is calculated using the contact angle θ_0 at equilibrium position via the equation

$$z_0 = -R\cos\theta_0 \quad \text{Eq. 5-8}$$

As discussed in the previous chapter, the particle's contact angle θ_0 at the equilibrium position (Fig 4.11 b) without the inclusion of electric field effects is precisely the macroscopic contact angle $\theta_m = \theta_0$.

Now, with contributions of the self-energy of a dipole field U_{dipole} to the total interfacial free energy profile,

$$G = U_{ten} + U_{dipole} \quad \text{Eq. 5-9}$$

we will expect a shifted particle's equilibrium position and contact angle as the free energy profile is modified by the energy stored in the dipole field. In this chapter, we will quantitatively estimate the energy of the dipole field, include it in the model of total

interfacial free energy profile, and compare the model predicted contact angles to the experimentally observed ones.

5.2 Methods for calculating the energy of a dipole field

According to Eq. 5-1, the self-energy of an electric dipole field can be calculated as

$$U_{dipole} = \frac{1}{2}\int \varepsilon_0 \varepsilon E_{dipole}^2 \, dV, \qquad \text{Eq. 5-10}$$

and the dipole field of a charged particle at oil-water interfaces can be estimated by a simple model where the "particle-dipole" is replaced by a "point-dipole" located at the interface[7].

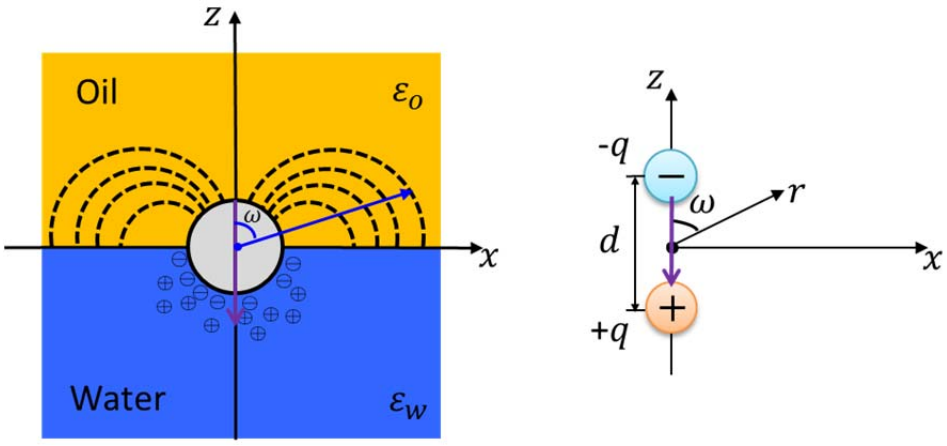

Figure 5.2 Estimate the electric field of "particle-dipole" (left) with a "point-dipole" field (right)

For a "point-dipole" located at the origin of a spherical coordinate (r, ω, φ), in the limit where r ≫ d (far field), the electric field $\vec{E}$ is given by[8]

$$\vec{E}(r,\omega) = \frac{2p\ cos\omega}{4\pi\varepsilon_0\varepsilon r^3}\ \hat{r} + \frac{p\ sin\omega}{4\pi\varepsilon_0\varepsilon r^3}\ \hat{\omega} \qquad \text{Eq. 5-11}$$

and the magnitude of $\vec{E}$ is

$$E = \frac{p}{4\pi\varepsilon_0\varepsilon r^3}\sqrt{1+3\cos^2\omega} \qquad \text{Eq. 5-12}$$

where the magnitude of the dipole moment $p = qd$. In the case of the "point dipole" moment, q is simply the magnitude of the point charge and d is the distance between two opposite charges shown in Fig. 5.2. For the "particle-dipole" at the oil-water interface, we estimate the dipole moment by considering two scenarios suggested by Oettel et al.[7,9]: (i) the particle is only charged on the water side, or (ii) the particle is also charged on the oil side.

5.2.1 Charges only on the water side

When the particle is only charged on the water side, the effective "particle-dipole" moment can be estimated by $p_{eff} \sim q_{eff}\kappa^{-1}$, where κ^{-1} is again the Debye length, and the effective charge q_{eff} can be expressed as $\sigma_c A_w$, where σ_c is the surface charge density of the particle in contact with the water phase, and is calcualted via the measured zeta potential, and A_w is the surface area exposed to the water side, $A_w = 2\pi R^2(1 + cos\,\theta)$ (Fig. 5.1). We insert p_{eff} into Eq. 5-12 and obtain the magnitude of dipole field E. With E known, the self-energy of the dipole field can be estimated

according to Eq. 5-10. Since screening in the water phase side makes the field contribution for $z < 0$ far smaller than the contribution from the oil phase, we neglect the water phase contribution and integrate only over the positive half-space $z \geq 0$. This neglect of the field on the water side is equivalent to treating the water as a perfect conductor (while in reality its conductivity is finite, but orders of magnitude larger than that of the oil).

5.2.2 Charges also on the oil side

It has been suggested that charges also exist at the particle-oil interface[5,10], although this point is somewhat controversial[7] and the charging mechanisms remain unclear. We now consider the charges exist on the oil side, and again approximate the water solution as a perfectly conducting medium for the simplification of the model. The effective dipole moment in this case is dominated by the oil side charge and can be estimated by $p_{eff} \sim q_{eff} R_c$, where R_c is the protruding height of the particle into the oil side[7]. q_{eff} is estimated by $\sigma_c \frac{\varepsilon_o}{\varepsilon_w} A_o$, where $\sigma_c \frac{\varepsilon_o}{\varepsilon_w}$ is the assumed charge density at the particle-oil interface that would give the particle a uniform surface potential throughout (particle surface = equipotential surface), with the factor $\frac{\varepsilon_o}{\varepsilon_w}$ accounting for the larger energy cost of dissociating charges in the low permittivity medium, and A_o is the surface area exposed to the oil phase, $A_o = 2\pi R^2(1 - cos\theta)$. Again, we substitute the p_{eff} in Eq. 5-12, and from Eq. 5-10 we obtain the self-energy of the dipole field by integrating the energy density only over the entire oil space.

5.3 Results and discussions

5.3.1 Model predicted contact angle of the particle at oil-water interfaces

We hypothesize, based on our experimental results in the last chapter, that the self-energy of a dipole field contributes to the total free energy profile, that it shifts the particle's equilibrium position toward the water side, and yields a much lower contact angle than the macroscopic one. The question left is whether this self-energy of the dipole field is large enough to modify the total free energy profile with respect to the interfacial tension contributions and change the contact angle from being hydrophobic to hydrophilic.

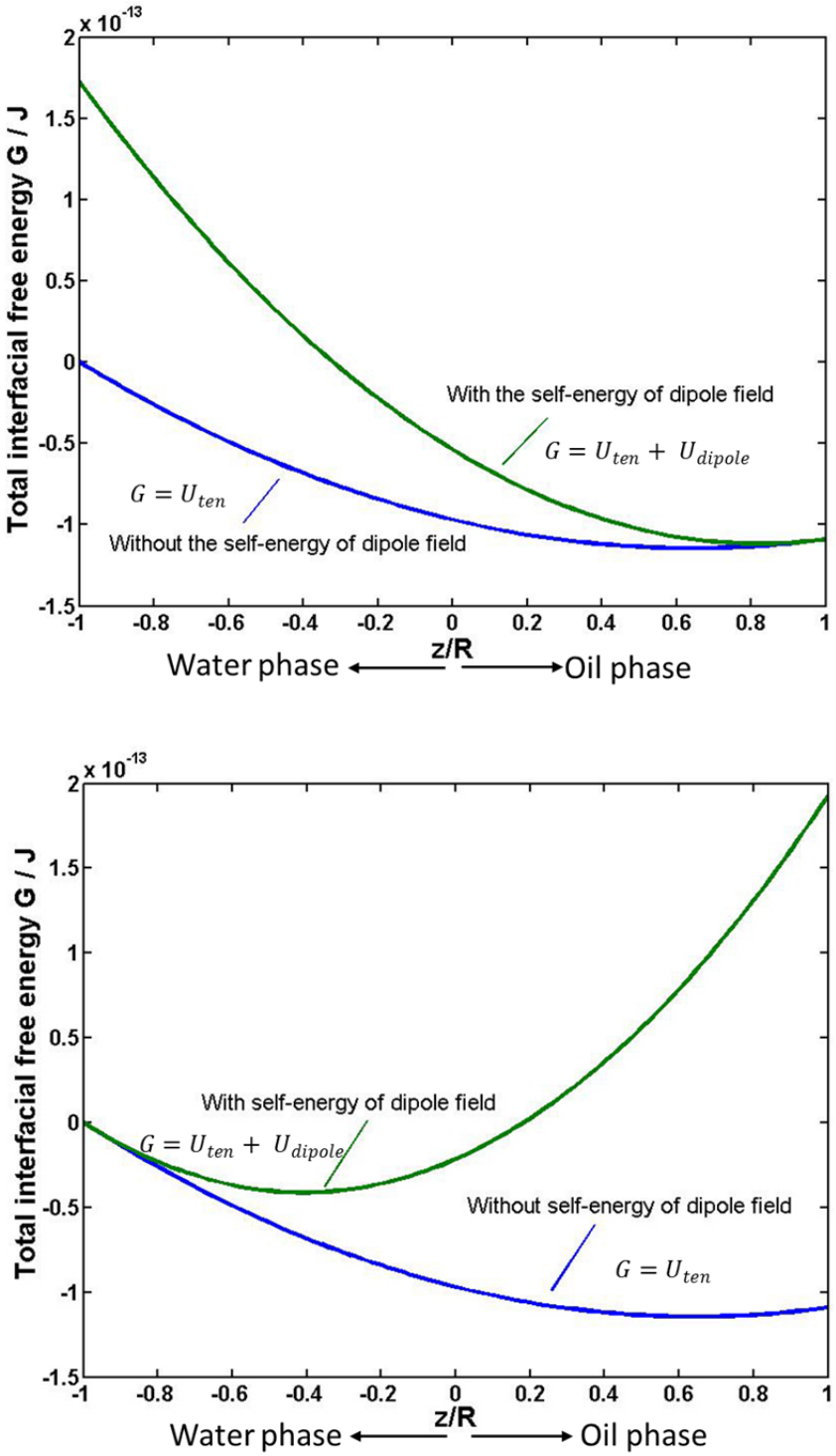

Figure 5.3 Model predicted total free energy profile of a charged particle ($\sigma_c = 9\mu c/cm^2$) of 0.5μm (radius) at the oil –water interface ($\varepsilon_{oil} = 2, \varepsilon_{water} = 78$) as a function of z/R under two scenarios: charges only on the water side (top) and charges also on the oil side (bottom)

In Fig. 5.3, we plot the model predicted total free energy profile as a function of *z/R* (center distance to the interface against particle radius) at the oil-water interface without or with the inclusion of the self-energy of the dipole field. Without the dipole field energy included, the total free energy G relies only on the contribution of the interfacial tension part U_{ten}, and the model predicted contact angle corresponds to the experimental macroscopic contact angle. With the dipole field energy included, the total free energy $(U_{ten} + U_{dipole})$ is expected to be modified if the dipole field energy U_{dipole} has the same order of magnitude as the energy as the interfacial tension part U_{ten}, and the model predicted contact angle should correspond more closely to the contact angle measured by GTT. The particle's contact angle depends on the equilibrium position of the particle at the interface, and that equilibrium position is located where the total interfacial free energy is minimized. In Fig. 5.3, if the minimum of total interfacial free energy is on the water side ($\frac{z}{R} < 0$), the model predicted contact angle is smaller than 90°. In contrast, the model predicted contact angle is larger than 90° if the minimum of total free energy is on the oil side ($\frac{z}{R} > 0$).

In either scenario (charge only at the particle-water interface or also at the particle-water interface), the model estimates a dipole self-energy U_{dipole} in the right order of magnitude to cause an appreciable shift in the position of the total free energy minimum (*i.e.* in the predicted particle position). However, the predicted shift has opposite direction in the two scenarios considered: in the case where the particle is only charged on the water side, the inclusion of dipole field energy shifts the equilibrium position of the particle toward the oil phase and thus makes the particle appear even more hydrophobic, whereas in the case where the charges on the particle-oil interface, the

inclusion of the dipole field energy shifts the equilibrium position from the oil side to the water side and thus mediates a shift in the particle's wetting behavior from hydrophobic to hydrophilic. Therefore, only the model prediction under the second scenario, where we allow for oil-side charges on the particle surface, agrees qualitatively with our experimental observations from the previous chapter.

To further verify which scenario better reflects the "real "case, we investigated effects of the particle size on the contact angle. According to the model prediction, the self-energy of the dipole field is proportional to the cube of the particle radius ($U_{dipole} \sim p \sim q_{eff} R_c \sim R^3$), and increasing the particle size should therefore produce much stronger effects of the dipole field. Based on the results in Fig. 5.3, one might expect that the model for scenario (i) (water-side particle charges only) would predict the smaller particles to appear less hydrophobic, due to their lower dipole field energy, and larger particles to appear more hydrophobic, since their large dipole field energy in this scenario shifts the equilibrium position to the oil side. By contrast, the model for the second scenario (presence of oil-side particle charges) will predict that smaller particles appear more hydrophobic while the bigger particles appear more hydrophilic, since the dipole field energy shifts the equilibrium position toward the water side in this case. In the following section we report experimental tests of this predicted dependence on the particle size. If our particles indeed carry oil-side charges as suggested by the qualitative agreement of Fig. 5.3 (bottom) with our experimental contact angles of Fig. 4.7, then we should expect a significant increase in hydrophilicity (decrease in the particle contact angle) with increasing particle size. This is indeed what we observe.

5.3.2 Effects of the particle size on the particle contact angle

We selected three carboxyl particles of 0.1 μm, 0.5 μm and 1 μm in diameter (life technologies Inc.) to investigate the effect of particle size on the particle contact angle. The zeta potentials for three particle sizes in pH 6 buffer solutions with 1mM or10mM NaCl added are shown in Fig. 5.4. The buffer was used to minimize fluctuations of particle's surface charge. The measurements show a maximum difference of 20 mV in the zeta potentials of particles at 1mM NaCl, and a maximum difference of 10 mV at 10 mM NaCl. Given a small zeta difference (10 mV) at 10 mM NaCl where the zeta potential can be determined more accurately from electrophoresis and should approximate the surface potential fairly well, we consider the three particles to have very similar surface potential and be distinguished primarily by their size difference.

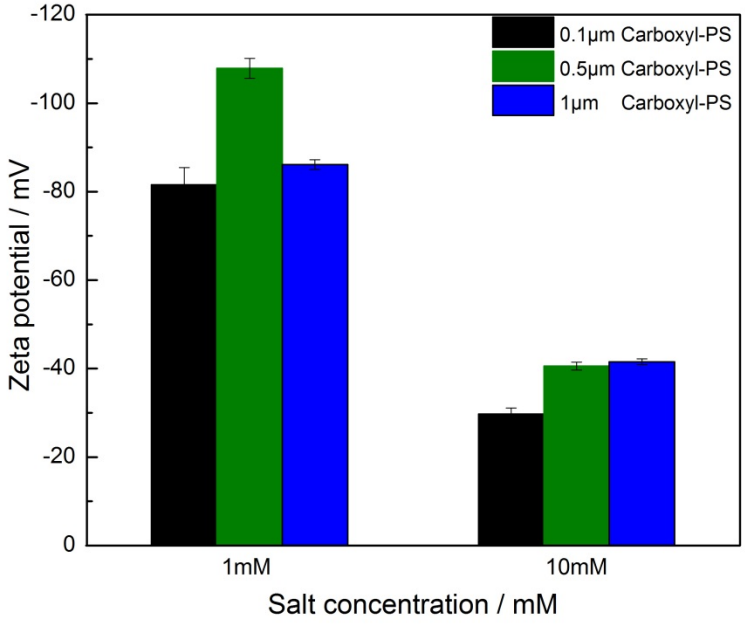

Figure 5.4 Zeta potentials of carboxyl-PS particles at solutions at the pH 6 and 1mM or 10 mM NaCl

The contact angle was measured with solvent-free GTT as discussed in the last chapter. The buffer was added to the water phase to keep the constant pH at 6. Since GTT is limited to relatively low salt solutions (because high salt concentrations cause difficulties in controlling the gel setting temperature and obtaining an uniform gel structure), we measured the contact angle at 1mM and 10mM NaCl solutions. As shown in Fig. 5.5, the results agree with the model prediction for particles with oil-side surface charges that the free energy contribution of the dipole field produces a more significant "hydrophilic shift" for larger particles than for smaller ones.

We also find the effect of particle size on the particle contact angle appears more obvious (slope in Fig. 5.5) at the high salt concentration and in fact bears surprisingly close resemblance to our theoretical prediction, which treated the water phase as a perfect conductor, corresponding to the limit of high salt concentration.

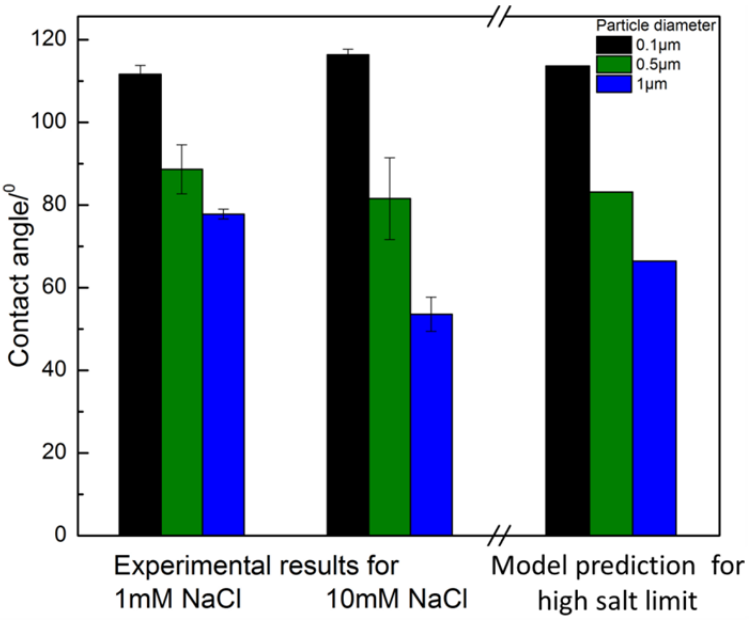

Figure 5.5 Effects of the particle size on the particle contact angle

5.4 Conclusions

The theoretical work in this chapter answers the question left in the previous chapter about whether the self-energy of a dipole field is large enough to modify the total free energy profile and change the contact angle from being hydrophobic to hydrophilic. Our theoretical model confirms that self-energy is comparable in order of magnitude to the free energy from contributions of the interfacial tension, and can modify the total free energy profile and shift the equilibrium position of the particle at oil-interface. However, only the model prediction in the scenario where we assume charges exist on the oil side achieves good agreement with our experimental observations that the self-energy of dipole field shifts the particle equilibrium position to the water side and makes the particle more hydrophilic. The experimental observations of effects of the particle size demonstrate the smaller particle with less dipole field energy appears hydrophobic, whereas the bigger particle with higher dipole field energy appears hydrophilic, in agreement with the model prediction in the scenario where the particle is also charged in the oil phase. Our findings therefore only support the notion that

I. electric field effects due to the particle charge can indeed shift the equilibrium position of particles in oil-water interfaces from the oil side to the water side,
II. as a consequence, particles from an intrinsically hydrophobic material can act as hydrophilic emulsifiers if the surface charge and size of the particles is sufficiently large, and that
III. the still controversial occurrence of electric surface charges at the particle-oil interface may indeed be real and have a strong effect on the particle contact angle.

Since our model only estimates the self-energy of a dipole field in the "far field" and assumes the water phase to be a perfect conductor for simplicity, the current model might underestimate the contributions of the self-energy of the dipole field to the total free energy and in particular the influence of water-side particle charges. Further efforts will be made to achieve a more accurate theoretical model with a consideration of the self-energy in the "near field" close to the particle surface on the oil side, and the finite energy contribution from the field in the water phase, when the "perfect conductor" assumption is released.

5.5 References

1. Hurd, A. J., The Electrostatic Interaction between Interfacial Colloidal Particles. J. Phys. A 1985, 18, L1055 - L1060.

2. Danov, K. D.; Kralchevsky, P. A., Interaction between Like-Charged Particles at a Liquid Interface: Electrostatic Repulsion vs. Electrocapillary Attraction. J. Colloid Interface Sci. 2010, 345 (2), 505-514.

3. Danov, K. D.; Kralchevsky, P. A., Electric Forces Induced by a Charged Colloid Particle Attached to the Water–Nonpolar Fluid Interface. J. Colloid Interface Sci. 2006, 298 (1), 213-231.

4. Park, B. J., Pantina, J. P.; Furst, E. M., Oettel, M.; Reynard, S., Vermant, J., Direct Measurements of the Effects of Salt and Surfactant on Interaction Forces between Colloidal Particles at Water-Oil Interfaces. Langmuir 2008, 26, 1686 - 1694.

5. Aveyard, R., Binks, B. P., Clint, J. H.; Fletcher, P. D. I., Horozov, T. S.; Neumann, B.; Paunov, V. N.; Annesley, J.; Botchway, S. W., Nees, D., Parker, A. W., Ward, A. D., Burgess, A. N., Measurement of Long-Range Repulsive Forces between Charged Particles at an Oil-Water Interface. Phys. Rev. Lett. 2002, 88 (24), 246102.

6. Aveyard, R., Binks, B. P., Clint, J. H., Emulsions Stabilised Solely by Colloidal Particles. Adv. Colloid Interface Sci. 2003, 100, 503-546.

7. Oettel, M., Dietrich, S., Colloidal Interactions at Fluid Interfaces. Langmuir 2008, 24 (4), 1425-1441.

8. Blinder, S. M., Singularity-Free Electrodynamics for Point Charges and Dipoles: a Classical Model for Electron Self-Energy and Spin. Eur. J. Phys. 2003, 24 (3), 271.

9. Domínguez, A., Frydel, D., Oettel, M., Multipole Expansion of the Electrostatic Interaction between Charged Colloids at Interfaces. Phys. Rev. E 2008, 77 (2), 020401.

10. Leunissen, M. E., van Blaaderen, A., Hollingsworth, A. D., Sullivan, M. T., Chaikin, P. M., Electrostatics at the Oil-Water Interface, Stability, and Order in Emulsions and Colloids. Proc. Nat. Acad. Sci. 2007, 104 (8), 2585-2590.

CHAPTER 6

DESIGN OF DOUBLE PICKERING EMULSION TEMPLATED COMPOSITE MICROCAPSULES

6.1 Introduction

While previous chapters have focused on fundamentals of particle adsorption to oil-water interfaces and the stabilization of Pickering emulsions, the remainder of this thesis shall explore a more practical side of such emulsions. Particle stabilized emulsions have been used for many applications such as food technology, oil recovery, surfactant-free cosmetics and skin care products, and more recent research interest in Pickering emulsions has been sparked by their use as a template for microcapsules with controlled release performance. In this chapter, we will explore double Pickering emulsions as precursors to design pH responsive composite microcapsules with a sustained release profile, which are potentially useful for sustained protection of encapsulated "active cargos". For example, with antimicrobial substances encapsulated, these microcapsules can be embedded in paper and packaging materials for sustained antimicrobial protection[1]; with herbicide or pesticide encapsulated, these microcapsules can be applied to agriculture solutions for sustained crop protection.

Here the focus will be on double Pickering emulsions, which offer a particularly promising route toward controlled delivery of common water-soluble or water-dispersible cargoes. Emulsion droplets are an extremely versatile template for capsules, because most successful protocols to encapsulate a droplet will work independently of the precise

chemical nature of the dissolved active. W-o-w double emulsion droplets as a capsule template have several distinct advantages. First they allow for a high loading efficiency: when a solution of dispersion of the aqueous active is emulsified in oil and the resulting is emulsion re-emulsified in water, the entire active content in principle ends up encapsulated in the inner droplet phase, whereas alternative encapsulation routes often rely on preparation and subsequent diffusive loading of a capsules, in which much of the active remains unencapsulated in the outer liquid phase. Second, the presence of a continuous aqueous phase facilitates release into aqueous environments such those found in living organisms. By comparison, aqueous core capsules prepared in water-immiscible liquids first need to be transferred into a different medium, and the associated passage of phase boundaries or solvent exchanges often lead to capsule damage and a reduced overall yield. Third, the presence of a middle oil phase and two liquid interfaces separating the aqueous core of a w/o/w droplet from the aqueous outer medium allows offers many opportunities for controlling the mass transfer resistance.

Similarly, the use of particulate emulsifiers, rather than surfactants, offers important benefits. The inclusion of particles as building blocks for a capsule shell may be expected to improve the mechanical properties. Moreover, particles with a great variety of physicochemical properties and surface functionality are readily available and can be used to impart some desired functionality to the capsule shell. Most importantly, however, the stabilization of double emulsions calls for two types of emulsion stabilizers, a hydrophobic one for the inner w/o interface, and a hydrophilic one for the outer o/w interface. Multiple emulsions stabilized with two types of surfactant tend to have poor long-term stability. For surfactant stabilized emulsions, as we discussed before, the

adsorbed surfactant molecules desorb easily from the interface due to the small desorption energy, and there fluctuate in and out of the interface in a dynamic equilibrium. As a result, the inside surfactant molecules (purple) used to stabilize w/o emulsion can leave the inner interface and adsorb to the outer o/w interface, where they will act as demulsifiers for the the o/w emulsion; similarly, the outer surfactant molecules can adsorb to the inner interface as a demulsifier. The interchange of surfactant molecules between two interfaces is detrimental to the stability of double emulsions, and the double emulsion with surfactants often evolves into single emulsions over time[2]. The large desorption energy of particulate emulsifiers, by contrast, prevents such instability due to "flipping" of the emulsifier between the two liquid interfaces.

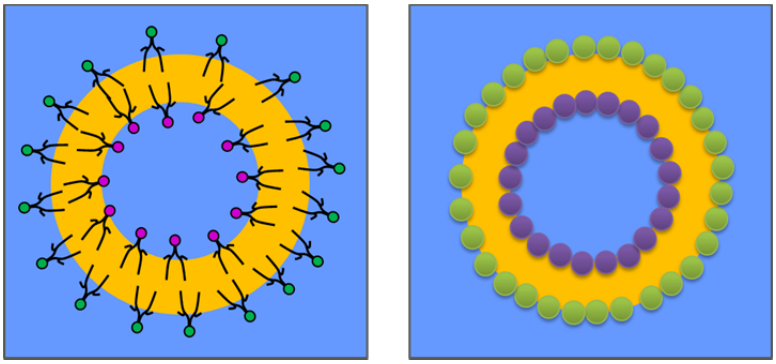

Figure 6.1 Scheme of surfactant stabilized double w/o/w emulsion (left) and particle stabilized double w/o/w emulsion (right), with w/o emulsifier (purple) and o/w emulsifier (green).

Microcapsules prepared from single Pickering emulsions, either oil-in-water or water-in-oil emulsions, have been widely reported[3,4,5,6], and the first example of double shell microcapsules based on double Pickering emulsions with polymer particles via bulk emulsification is also reported by our group recently[7]. However, double Pickering emulsion templated composite microcapsules with a combination of multiple types of

particles are rarely reported. A use of multiple types of particles can help generate functional microcapsules with customized properties. In this work, a unique combination of inorganic particles and stimulus responsive polymer particles into the shell endows the generated microcapsules with targeted properties. The work pursues the following three application-oriented targets:

- Design of microcapsules from double emulsion stabilized solely by silica particles
- Design of pH-responsive microcapsules with sustained release profile from double Pickering emulsions with both inorganic and polymer particles.
- Design of composite microcapsules with high encapsulation efficiency for small molecules

6.2 Materials and methods

6.2.1 Design microcapsules from double emulsion stabilized solely by silica particles

6.2.1.1 General design approach

Commercial silica particles are selected as an inorganic particle candidate because they are very cheap, and have been well studied in Pickering emulsions. Microcapsules from double Pickering emulsions with silica particles have been generated via microfluidic emulsification[8], but rarely via bulk emulsification. Here, the adopted process started with creating a w/o emulsion with hydrophobically modified silica particles (HDK H30, Wacker). The water phase contained 2% (w/v) particles and 0.2 mol/L NaCl, and toluene was used as the easily extractable oil phase. The water and oil were mixed at a ratio of 1:2, and homogenized at 20500 rpm (IKA Ultra-Turrax). The resulting w/o emulsions were transferred to an outer water phase containing 2% hydrophilic silica particles (Bangs lab, Inc) and 0.1 mol/L NaCl at a 1:3 ratio of w/o emulsion to water, and

the system was homogenized at 14500 rpm. Once the double emulsion was achieved, the oil phase (toluene) was extracted by copious dilution in water and subsequent solvent evaporation at room temperature. When the oil phase was removed, the particles originally adsorbed at the interfaces, remained connected by van der Waals forces, forming the microcapsule shells (colloidosomes).

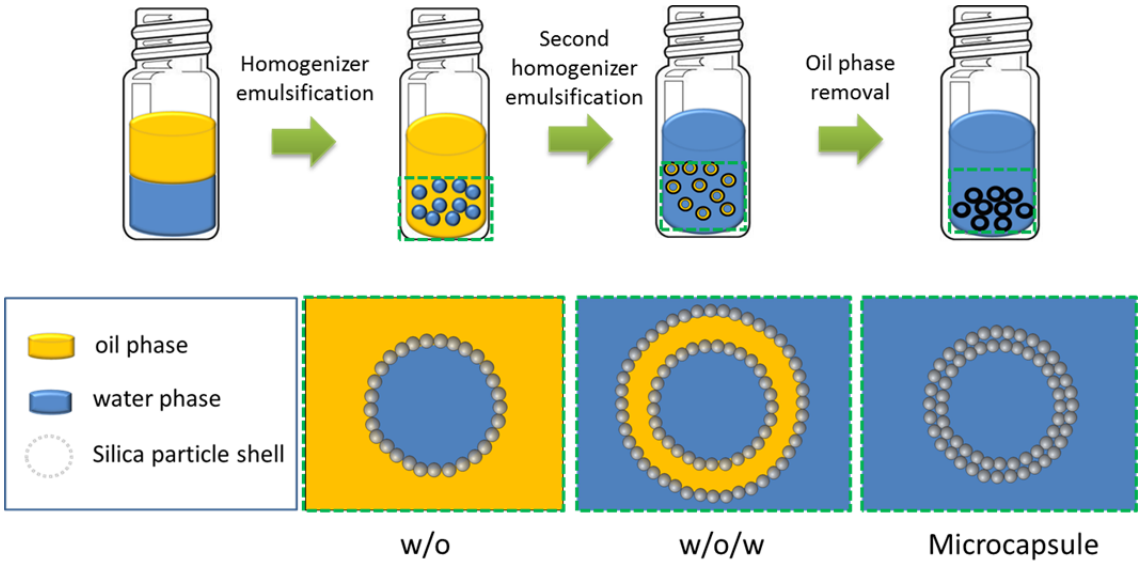

Figure 6.2 Protocol for preparing double Pickering emulsion templated microcapsules

6.2.1.2 Surface modification of silica particles

Silica particles without surface modification (150nm, Bangs lab) were found too hydrophilic to stabilize o/w emulsions. Silanization is a common approach to hydrophobize the surface. Alkylchlorosilanes, alkoxysilanes, or alkylaminosilanes are commonly used chemical agents for the surface modification[9]. We chose methyltrimethoxysilane (MTMS) as a chemical agent capable of completing the

modification in aqueous solution. 2% (w/v) hydrophilic silica particles were dispersed in 10 ml water and stirred at 400 rpm with a magnetic stirrer. 1% (w/v) MTMS was then added to the silica particle solution in a dropwise fashion, and continuously stirred at 400 rpm for 30 mins, allowing MTMS to hydrolyze. After the hydrolysis of MTMS, the pH of the solution mixture was adjusted to 9.6 via NaOH, and this basic condition allowed the silane groups to condensate on the surface of silica particles where the silanes react with the silanol groups to form Si-O-Si bonds. After an overnight reaction under 400 rpm stirring, the resulting modified particles were washed twice with fresh water to remove unreacted MTMS by centrifuge. In the final step, the pH of particle solution was adjusted back to neutral via HCl, ready for use.

6.2.2 Design pH-responsive microcapsules with sustained release profile from double Pickering emulsions

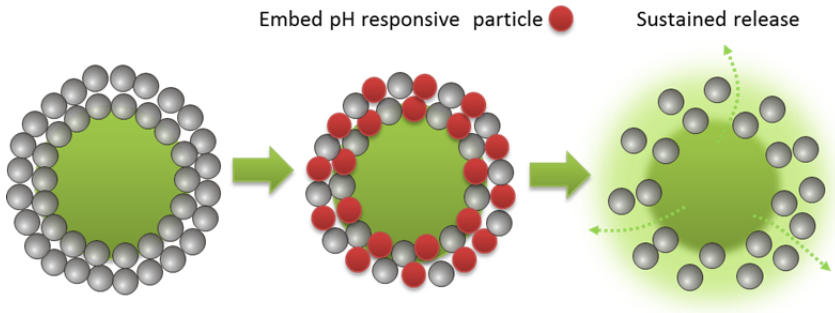

Figure 6.3 Scheme of the microcapsule composed of pH responsive and silica particles for the pH responsive and sustained release control

Upon first achieving the targeted microcapsule from double Pickering emulsion with silica particles alone, we are motivated to target in the next step pH responsive microcapsule with a sustained release profile. A general approach towards this target is to embed pH responsive particles into the shell, where those particles dissolve in response to the pH change and initiate the cargo release from the capsule, while the silica particles do not respond to the pH change and maintain the structural integrity of the microcapsule, assured a sustained release profile beyond the triggered release burst (Fig. 6.3). The pH responsive particles were prepared from a co-polymer of methyl methacrylate-co-methacrylic acid (Eudragit-S100, Evonik) based on the well-know "Ouzo effect" [10], with a dissolution pH of 7. The procedure of synthesizing these pH responsive particles was developed by a former lab member, and details were discussed elsewhere[7]. The obtained pH responsive particles have an average size of 179 nm as determined by dynamic light scattering (Malvern Nano ZS90). Fluorescently (FITC-) labeled dextran (10 kDa, Sigma-Aldrich at a concentration of 5μg/ml) was used as a model cargo for evaluation of the release under the confocal microscopy.

6.2.3 Design composite microcapsules with high encapsulation efficiency for small molecules

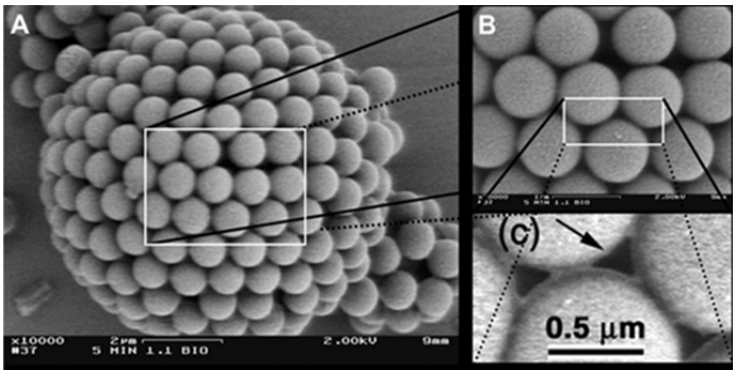

Figure 6.4 Image of microcapsule whose shell is composed of colloidal particles and the inter-particle pores (c)[11]

The main hindrance to sustained release from microcapsule shells composed of colloidal particles ("colloidosomes") is the porosity arising from incomplete particle coverage or packing "defects" that can easiliy result in fast cargo leakage and correspondingly low encapsulation efficiency[6]. Even in the case of dense particle packing, the interstitial spaces between particles provide sufficiently large pores to allow for undesirably fast loss of small cargo molecules (Fig. 6.4).

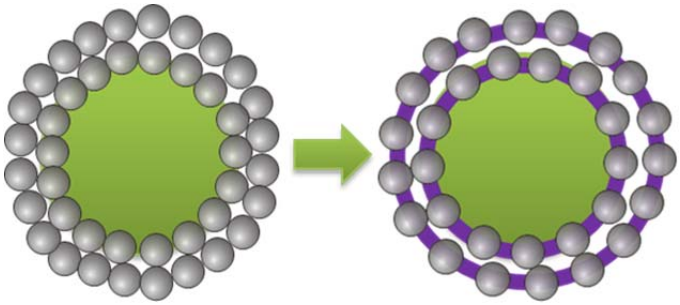

Figure 6.5 Scheme of adding polymer "skin" to the shell via interfacial polymerization for improving encapsulation efficiency for small molecules

To resolve this problem, we added a polymer "skin" to the shell by interfacial polymerization. Generally following the protocol in the Fig. 6.2, we added additional 1mol/L glycerol (Sigma Aldrich) to the inner water phase and 1.2 mol/L Methylene diphenyl diisocyanate (MDI, BASF) to the oil phase at the first step of preparing the w/o emulsion, and added 1mol/L ethylene glycol to the outer water phase at the second step of preparing the w/o/w emulsion. At the interface, the glycerol and ethylene glycol reacted with MDI to form polyurethane "skin". The final "skin" thickness will rely on the interplay of diffusion through bulk, diffusion through the formed polymer shell, and interfacial reaction[12]. The reaction proceeds steadily until all monomers are consumed or their diffusion becomes severely impeded by the formed polymer shell.

6.2.4 Microcapsule characterization

6.2.4.1 SEM observation

The shape and surface morphology of the microcapsules were observed by SEM (Zeiss SEM Ultra 60). The microcapsules were mounted onto a double-sided carbon stub

and dried in a vacuum overnight. The sample was coated with gold prior to SEM observation.

6.2.4.2 Confocal microcopy observation

The water phase was labeled with 5μg/ml FITC-dextran (10 kDa, Sigma-Aldrich). The formed emulsions were observed using 10X objective lenses of confocal microscopy (Zeiss LSM 510 VIS confocal microscopy).

6.2.4.3 Shell permeability

Shell permeability was evaluated by Fluorescence Recovery After Photobleaching (FRAP). Fluorescently labeled molecular probes in the volume inside the microcapsules were photobleached by a short light pulse, and then the bleached volume was monitored to record the kinetics of fluorescence recovery due to the diffusion of unbleached dye into the microcapsules. Obviously, the more permeable the shell, the less time the recovery time takes. The permeability *P* of the shell can be calculated as[7,13]:

$$P = \frac{R}{3\tau_2} \qquad \text{Eq. 6-1}$$

where R is the capsule radius, and τ_2 is the time constant associated with the probe permeation through the shell and can be obtained by fitting the recovering fluorescence intensity $f(t)$ to the equation:

$$f(t) = \alpha \left[\exp\left(-\frac{\tau_1}{t}\right) \times \left\{I_0\left(\frac{\tau_1}{t}\right) + I_1\left(\frac{\tau_1}{t}\right)\right\}\right] + (1-\alpha)\left[1 - \exp(-\frac{t}{\tau_2})\right] \qquad \text{Eq. 6-2}$$

Here, by a weigh factor α, two mechanisms contributing to fluorescence recovery in the bleached region are combined: permeation of the probe through the capsule wall depicted by the Möhwald equation (τ_2 part) [14] and the free diffusion of unbleached probe inside the capsule depicted by Soumpasis' expression (τ_1 part) involving the zero (I_0) and first order (I_1) modified Bessel functions[15].

6.2.4.4 Encapsulation efficiency

Encapsulation efficiency was calculated according to the equation:

$$Encapsulation\ efficiency = \frac{Amount\ of\ substance\ encapsulated}{Total\ amount\ loaded} \qquad \text{Eq. 6-3}$$

A known amount of targeted substance was added to the water phase, and then the encapsulation of substance was completed in accordance to the procedure depicted in Fig. 6.2. The obtained microcapsules were separated from solution via centrifugation, and the supernatant was taken and analyzed by HPLC to quantify the amount of unencapsulated substance, and the encapsulated amount of substance can be calculated by subtracting the unencapsulated amount from the amount initially added to the system. Results were averaged based on three measurements.

6.2.4.5 Mechanical properties

Nanoindentation processes with high resolution and depth sensing ability has become an important tool to assess mechanical properties of microcapsules[16]. Here,

mechanical properties of the microcapsules were studied using a Nano-indenter (Hysitron Triboindenter) with a 1μm conospherical tip. The microcapsules were fixed to a glass surface by a waxy adhesive (Tempfix), and then one randomly selected microcapsule was compressed, and the force versus displacement curves were recorded to calculate the reduced Young modulus and the hardness. They are both defined to depict the resistance of a microcapsule to deformation under an applied force load.

6.3 Results and discussions

6.3.1 Microcapsules from double emulsion stabilized solely by silica particles

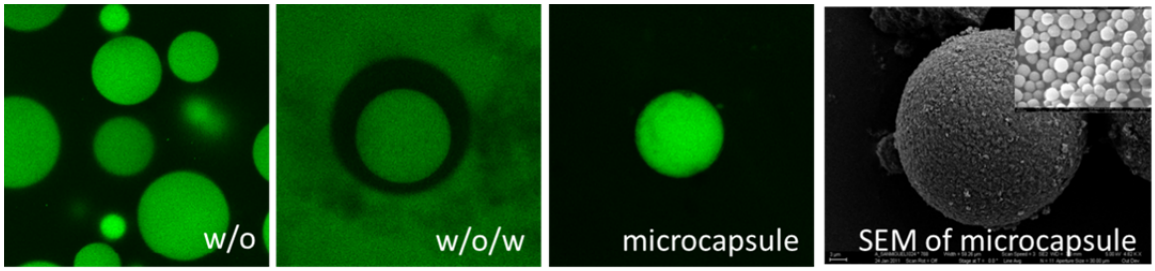

Figure 6.6 Confocal microscopic observations of the process to prepare double Pickering emulsion templated microcapsules, and SEM of the microcapsule (the inlet image is a local magnification showing the shell composed of silica particles).

We successfully generated the targeted emulsions and microcapsules by using only silica particles with rational wettability, and using toluene as the extractable oil phase. The fluorescent images in Fig. 6.6 (Water phase was labeled with FITC-dextran) show the obtained w/o emulsions, w/o/w emulsions, microcapsules and SEM of microcapsules, prepared via the procedure in Fig. 6.2. In order to take SEM pictures of

the microcapsules in the dry condition, polyvinyl acetate (PVAc, Sigma-Aldrich) a polymer of with low glass transition temperature T_g was embedded into the microcapsule shell, offering the microcapsule some elasticity and resistance to fracture under drying condition. The typical diameter of the obtained microcapsules ranges from 30 μm to 80 μm as shown in Fig. 6.7. After a success of preparing microcapsules from double Pickering emulsions with only silica particles via bulk emulsification, we move to the second target: preparing pH responsive microcapsules with sustained release profiles from double Pickering emulsions with both silica particles and polymer pH responsive particles.

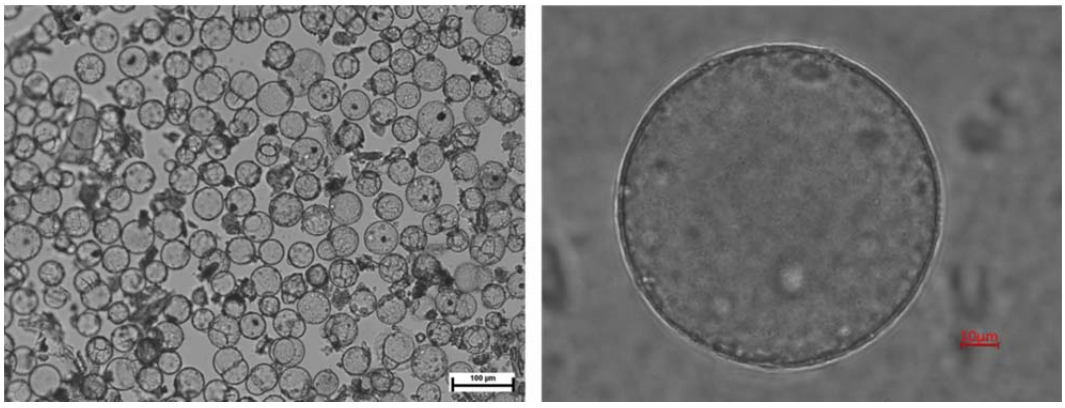

Figure 6.7 Bright-field microscopic observations of multiple microcapsules (left) and one single microcapsule (right) in aqueous solution, synthesized from double Pickering emulsions.

6.3.2 pH-responsive microcapsules with a sustained release from double Pickering emulsions

To achieve pH responsive and sustained release microcapsules, we incorporated both silica particles and pH responsive particles to yield composite microcapsules. The pH responsive particles endow the microcapsules with pH-responsive properties, while

the silica particles guarantee the integrity of the microcapsule shell upon dissolution of pH responsive particles and allow for the slower release of the enclosed cargo. For FITC-dextran (10 kDa, Sigma-Aldrich) as the encapsulated cargo, the image in Fig. 6.8 shows that the microcapsule composed of only pH responsive particles complete the cargo release within 4 seconds as the pH is raised above pH 8 (the dissolution threshold being ~pH 7 for the polymer particles), but in contrast to this fast release, the microcapsule composed of both silica particles and pH responsive particles exhibits a slower release that is sustained for more than 40 seconds. The release time can be well tuned by rationally designing the thickness and composition of the shell according to customized requirements.

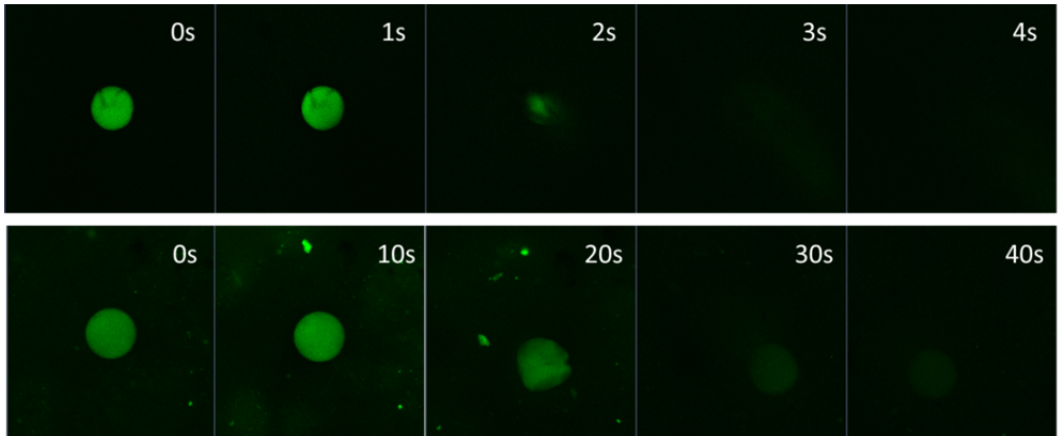

Figure 6.8 Images for a fast release of microcapsule composed of only pH responsive particles (top) and a sustained release of the composite microcapsule composed of pH responsive particles and silica particles (bottom)

The shell permeability of microcapsules was evaluated by FRAP. A typical FRAP curve for a composite pH responsive microcapsule before and after a pH change is shown in Fig. 6.9. As one might expect, the microcapsule is less permeable and therefore takes a

long time to recover the fluorescence intensity before the pH change, but becomes much permeable as the pH responsive particles are dissolved and open "holes" in the shell upon increased pH. The shell permeability can be further quantified by the fit of the experimental recovery curve (line in Fig. 6.9) using Eq. 6-2, from which the time scales τ_1 and τ_2 of confined diffusion in capsule volume and of shell permeation can be deduced, and the shell permeability can be calculated according to Eq. 6-1. The shell permeability of the microcapsule is roughly 48nm/s and 654nm/s before and after the pH changes. Here, we notice that the microcapsules whose shells consist only of particles are still very permeable for 10 kDa FITC-dextran, and will be even more permeable for smaller molecules as a result of leaking from the inter-particle pores. We can expect these microcapsules to achieve very poor encapsulation efficiency for small molecules, which will limit their potential applications.

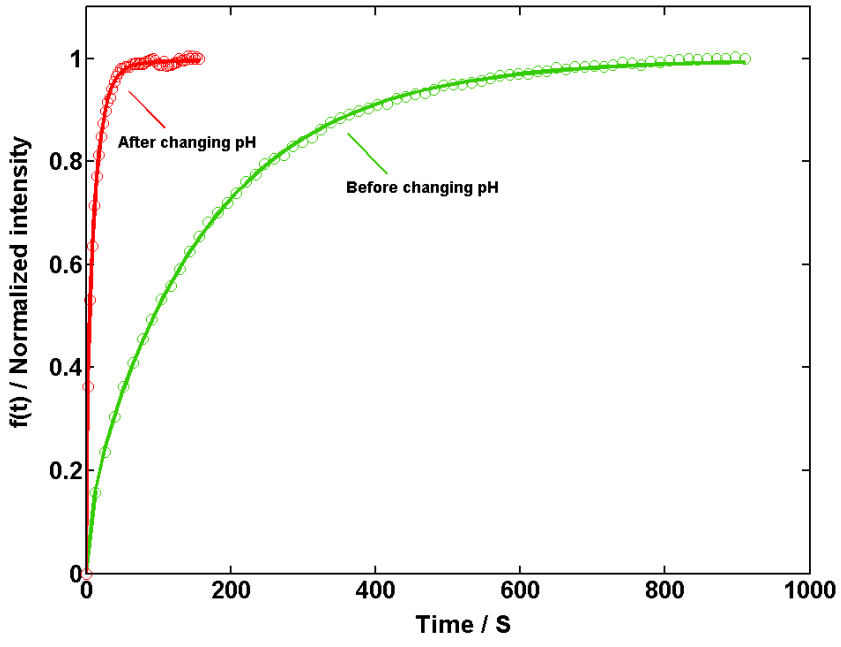

Figure 6.9 Fluorescence recovery curves (circle) and their fitting curves (line) for a composite microcapsule with 10kDa FITC-dextran encapsulated before and after changing pH.

6.3.3 Composite microcapsules with improved encapsulation efficiency for small molecules

To make Pickering emulsion template microcapsules suitable for encapsulating small molecules, as our third target, we filled the inter-particle pores by adding polymer "skins" to the shell via interfacial polyurethane formation at both interfaces. The SEM images in Figure 6.10 show the distinctly different appearance of microcapsules without and with interfacial polymerization, with the polymerized shell indeed appearing wrapped in an out "skin". Measurements of the encapsulation efficiency for these two types of capsules reveal the practical benefits of this polymer skin for controlling the release kinetics.

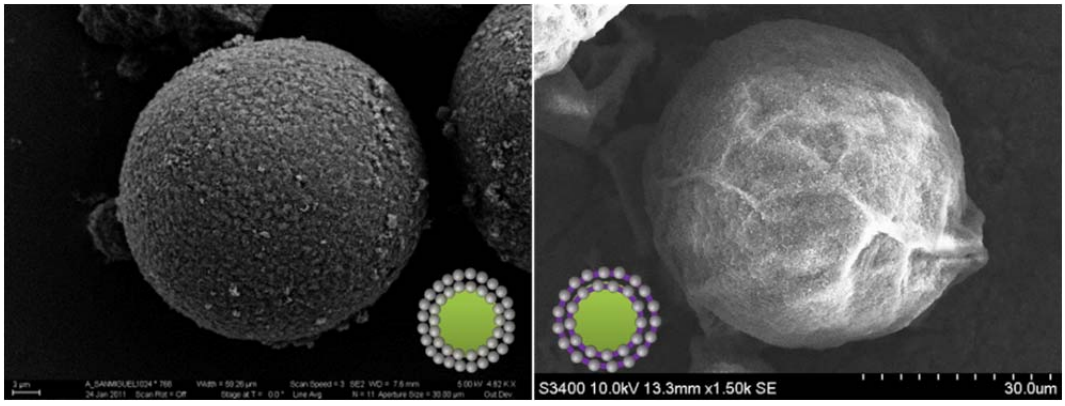

Figure 6.10 SEM images of microcapsules without and with a polymeric "skin" added via interfacial polymerization

A small model cargo molecule of molecular weight 221g/mol (the herbicide dicamba) was used as the "active cargos" to test encapsulation efficiency of the obtained microcapsules for small molecules. As shown in Fig. 6.11, the microcapsules with a

polymer “skin” added via interfacial polymerization present a dramatic increase of encapsulation efficiency from 2% to 51%.

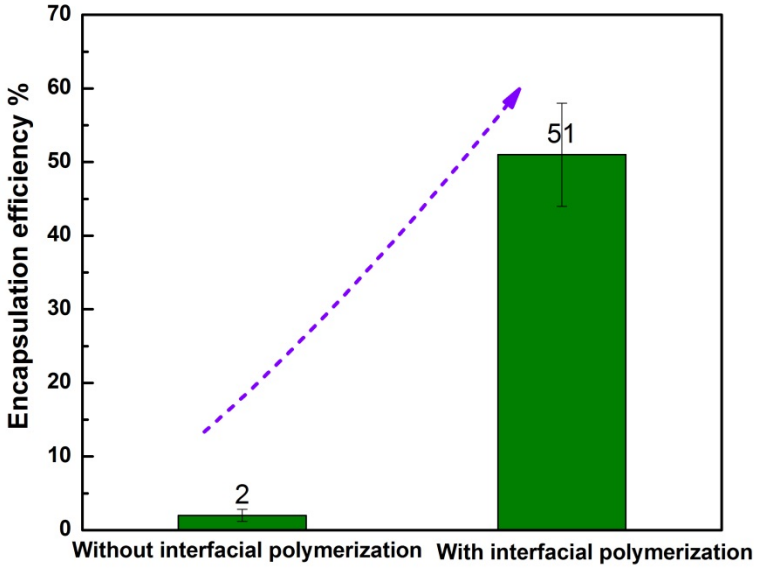

Figure 6.11 Encapsulation efficiency of microcapsules for one herbicide of molar mass 221 g/ mol without and with interfacial polymerization, measured by HPLC.

It is noteworthy that encapsulation efficiencies well above 90 % for the same cargo were achieved by Abiola Shitta in our group using a similar double Pickering emulsification approach combined with double interfacial polymerization, that was inspired by the present study and further exploits the barrier properties of a retained oil phase as well as an optimized protocol for the interfacial polymerization. Abiola has also demonstrated that the composite character of such capsule shells is indeed beneficial for the encapsulation efficiency: particle-free capsules prepared from surfactant stabilized double emulsions of similar droplet structure, using the same double interfacial polymerization, were found to achieve significantly lower encapsulation efficiency than

their Pickering emulsion templated counterparts with particles in the polymer shell. To the best of our knowledge the present study was the first to implement interfacial polymerization at both interfaces of a double emulsion template and the first to produce capsules with two shells of a particle-polymer composite material[10].

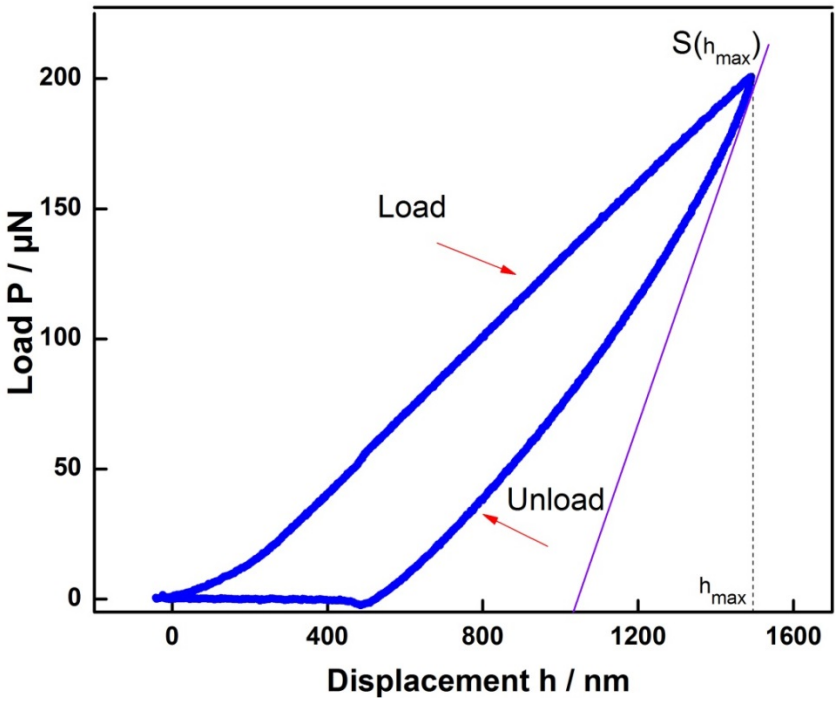

Figure 6.12 Typical loading versus displacement curve of a composite microcapsule (45µm)

Mechanical properties of our composite microcapsules with a double shell composed of silica particles and polyurethane were probed with the nano-indenter. The measurement acquired loading force-displacement data as the indenter compressed the microcapsule (Fig. 6.12). The plotted curve represents the loading and unloading branch. As the loading force is applied, the indenter tip compresses the sample and produces a complex combination of elastic and plastic deformation. In the unloading part, the force

on the tip is released, and the elastic response of the material is detected. The slope S at the point of initial unloading is the "contact stiffness" and considered to reflect the elastic behavior of the sample. The unloading slope at the point of maximum load is given by[16]:

$$S(h_{max}) = \frac{dp}{dh}(h_{max}) = \frac{2}{\pi} E_r \sqrt{A_c(h_{\max})} \qquad \text{Eq.6-4}$$

Where E_r is the reduced Young modulus and $A_c(h_{\max})$ is the contact area between the indenter and the sample at h_{max}. The hardness of material is defined by the equation:

$$H = \frac{P(h_{max})}{A_c(h_{max})} \qquad \text{Eq.6-5}$$

Hardness can be interpreted as a mean pressure that the material can resist.

We expect that embedding inorganic particles to the polymer shell will offer microcapsules better mechanical properties. To support these arguments, we initially intended to compare the mechanical properties of these composite microcapsules to pure polyurethane microcapsules synthesized from surfactant stabilized double emulsions via the nano-indenter. However, unlike the composite microcapsules which still keep their spherical shape in the dry condition, the generated pure polyurethane microcapsules cannot withstand the osmosis pressure under drying and collapse, and cannot be measured under the nano-indenter. The survival of composite microcapsules under drying indicates their better mechanical properties than pure polyurethane microcapsules.

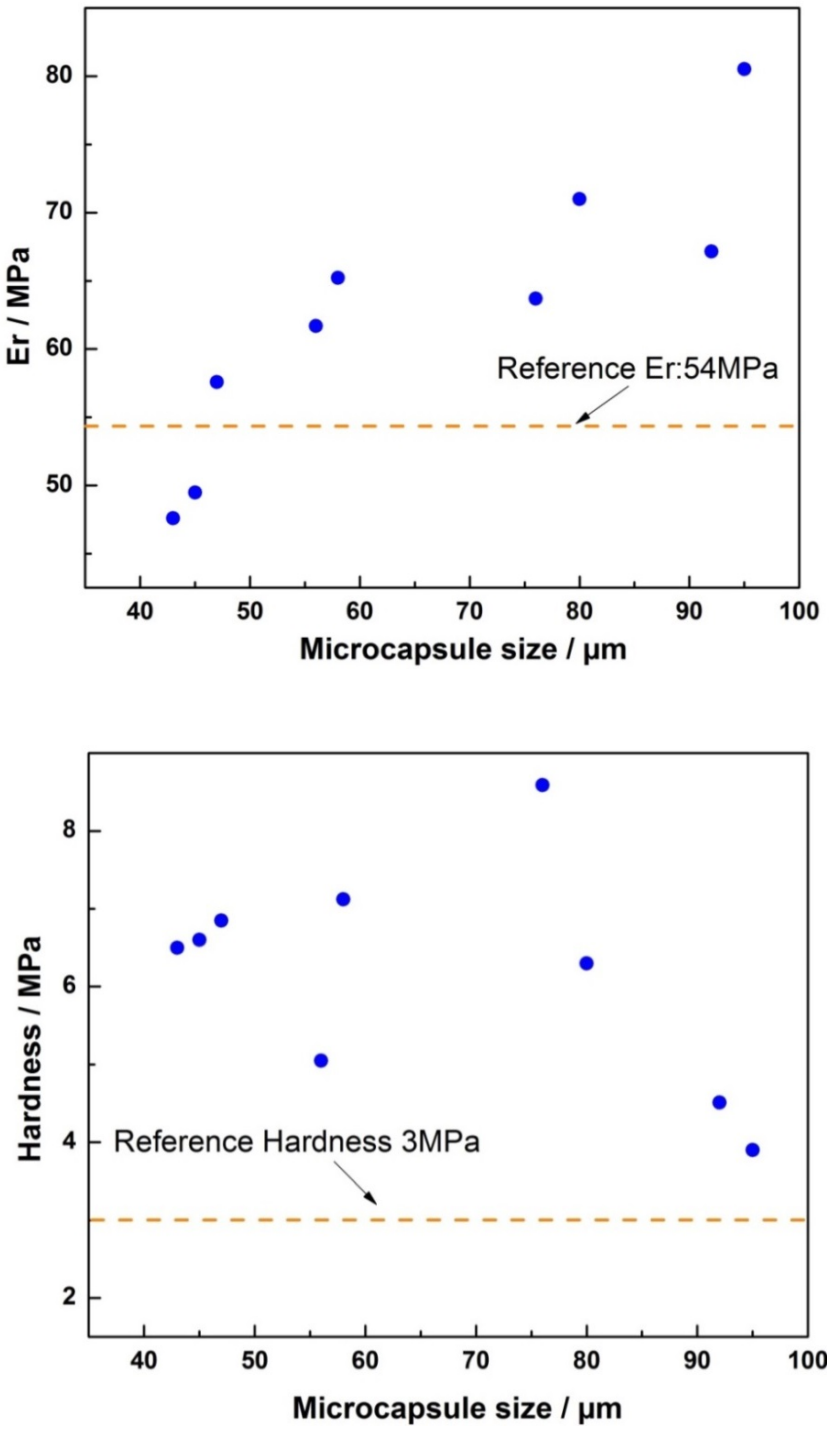

Figure 6.13 Reduced Young modulus (top) and hardness (bottom) versus size of composite microcapsules. Reference data (dash line) is average value for microcapsules whose shell consists of only polymers.

To quantitatively assess the comparison between composite microcapsules and pure polymer capsules, we compared Er and hardness H of our composite microcapsules with the inclusion of silica particles in the shell, to microcapsules from one recent reference[17], where their poly(urea-formaldehyde) microcapsules were also synthesized via emulsion based interfacial polymerization, but without silica particle included. The modulus Er and hardness H of our composite microcapsules whose shell consists of silica particles and polyurethane are shown in Fig. 6.13. The results show most of our tested composite microcapsules exhibit a higher Er and Hardness H than microcapsules with pure polymeric shell (dash line), and indicating embedding particles into the shell benefits the mechanical properties of microcapsules, as one might expect.

6.4 Conclusions

The work in this chapter completed three tasks: we first successfully generated microcapsules from double Pickering emulsion with only silica particles via bulk emulsification; second, we presented the first example of combining multiple type of particles to develop pH responsive and sustained releasing microcapsules; third, we improved the encapsulation efficiency of obtained microcapsules for small molecules by adding a polymer "skin" to the shell via interfacial polymerization. The obtained knowledge in this chapter partially contributes to a project on developing composite microcapsules from double Pickering emulsions to control the release of herbicide for agriculture applications, sponsored by BASF.

6.5 References

1. Ocepek, B.; Boh, B.; Šumiga, B.; Tavčer, P. F., Printing of Antimicrobial Microcapsules on Textiles. Coloration Technology 2012, 128 (2), 95-102.

2. Norton, J. E.; Norton, I. T., Designer Colloids-towards Healthy Everyday Foods? Soft Matter 2010, 6 (16), 3735-3742.

3. Velev, O. D.; Furusawa, K.; Nagayama, K., Assembly of Latex Particles by Using Emulsion Droplets as Templates. 1. Microstructured Hollow Spheres. Langmuir 1996, 12, 2374 - 2384.

4. Velev, O. D.; Nagayama, K., Assembly of Latex Particles by Using Emulsion Droplets as Templates. 3. Reverse (Water in Oil) System. Langmuir 1997, 13, 1856 - 1859.

5. Sahiner, N.; Ozay, O., Responsive Tunable Colloidal Soft Materials Based on p(4-VP) for Potential Biomedical and Environmental Applications. Colloids and Surf. A: Physicochemical and Engineering Aspects 2011, 378 (1-3), 50-59.

6. Rossier-Miranda, F. J.; Schroën, C. G. P. H.; Boom, R. M., Colloidosomes: Versatile Microcapsules in Perspective. Colloids Surf. A 2009, 343 (1-3), 43-49.

7. San Miguel, A.; Scrimgeour, J.; Curtis, J. E.; Behrens, S. H., Smart Colloidosomes with a Dissolution Trigger. Soft Matter 2010, 6 (14), 3163-3166.

8. Lee, D.; Weitz, D. A., Double Emulsion-Templated Nanoparticle Colloidosomes with Selective Permeability. Adv. Mater. 2008, 20 (18), 3498-3503.

9. Haensch, C.; Hoeppener, S.; Schubert, U. S., Chemical Modification of Self-Assembled Silane Based Monolayers by Surface Reactions. Chem. Soc. Rev. 2010, 39 (6), 2323-2334.

10. Vitale, S. A.; Katz, J. L., Liquid Droplet Dispersions Formed by Homogeneous Liquid - Liquid Nucleation: "The Ouzo Effect". Langmuir 2003, 19 (10), 4105-4110.

11. Aveyard, R.; Binks, B. P.; Clint, J. H., Emulsions Stabilised Solely by Colloidal Particles. Adv. Colloid Interface Sci. 2003, 100, 503-546.

12. Yadav, S. K.; Khilar, K. C.; Suresh, A. K., Microencapsulation in Polyurea Shell: Kinetics and Film Structure. AIChE J. 1996, 42 (9), 2616-2626.

13. Scrimgeour, J.; San-Miguel, A.; Curtis, J.; Behrens, S., A Generalized Approach for Measuring Microcapsule Permeability with Fluorescence Recovery After Photobleaching. J Mater Sci 2013, 48 (5), 2215-2223.

14. Ibarz, G.; Dahne, L.; Donath, E.; Mohwald, H., Controlled Permeability of Polyelectrolyte Capsules via Defined Annealing. Chem. Mater. 2002, 14 (10), 4059-4062.

15. Soumpasis, D. M., Theoretical Analysis of Fluorescence Photobleaching Recovery Experiments. Biophys. J. 1983, 41 (1), 95-97.

16. Lee, J.; Zhang, M.; Bhattacharyya, D.; Yuan, Y. C.; Jayaraman, K.; Mai, Y. W., Micromechanical Behavior of Self-Healing Epoxy and Hardener-Loaded Microcapsules by Nanoindentation. Mater. Lett. 2012, 76 (0), 62-65.

17. Wang, W.; Xu, L.; Liu, F.; Li, X.; Xing, L., Synthesis of Isocyanate Microcapsules and Micromechanical Behavior Improvement of Microcapsule Shells by Oxygen Plasma Treated Carbon Nanotubes. J. Mater. Chem. A 2013, 1 (3), 776-782.

CHAPTER 7

CONCLUSIONS AND FUTURE OUTLOOK

Particle stabilized emulsions, also known as Pickering emulsions, have been known for more than a century. To date, Pickering emulsions have been widely used in many industry applications, such as food industry, oil recovery, cosmetic and household products. Recent research interest in Pickering emulsions has been renewed by their novel uses as templates to develop new materials such as microcapsules, microreactors, and MOFS. Though the potential applications of Pickering emulsions keep growing, our current fundamental understanding of Pickering emulsions is still limited, and often fails to offer good theoretical guidance for practical control of the stability of Pickering emulsions. The work in this thesis aims at improving our understanding of the mechanisms responsible for the stability of Pickering emulsions, and in particular to clarify the effects of particle charge. Since these effects can be significant and particle charge is ubiquitous in aqueous systems, we expect that relevant insights in this arena could have a significant impact on the application of Pickering emulsions and facilitate the rational design of new emulsion-based materials.

The stabilization of Pickering emulsions requires that particles adsorb to the oil-water interface in the first place, but this should not be taken for granted. The possibility of electrostatic barriers to particle adsorption is widely acknowledged, but so far, theoretical descriptions of this barrier only focus on the electric double layer repulsion between a particle and a liked-charged oil water interface. Our work provides the first experimental hint that the additional, widely overlooked image charge repulsion can

hinder the adsorption of highly charged and weakly screened particles regardless of their sign of charge, and prevent the formation of Pickering emulsions.

Our theoretical estimate of the image force on water-borne particles near an oil-water interface confirms that the image charge repulsion has the right order of magnitude, relative to the other forces known to act on the particle, to impede the particle adsorption and Pickering emulsification. With the image force included, our theoretical model prediction of the force barrier to particle adsorption under typical conditions of turbulent mixing, and the inferred expectation for the short term stability of emulsion droplets agrees well with our experimental observations. However, given the crude estimate used for the hydrodynamic force scale of turbulent mixing and our use of the superposition approximation with boundary conditions of constant charge and constant potential for the electrostatic interaction, our current theoretical model leaves much room for improvement. Future efforts will be made to achieve theoretical model with better accuracy via solving the full Poisson-Boltzmann equation with boundary conditions of charge-regulation[1,2]. In addition, our current calculation for the magnitude of image charge is based on the "method of image charge" with the boundary condition that the charge at the interface must be zero, which does not satisfy our real case where the oil-water interface is negatively charged as discussed. The correct calculation of "image charge" with boundary conditions of a charged interface will be employed in future, and it will not only improve the accuracy of our model in the context of Pickering emulsions, but will be useful for models of ubiquitous cases where image charge exists across charged interfaces.

After particles manage to adsorb to interfaces under sufficiently high mixing force or high screening (high salt), the particle contact angle will play an important role in influencing the stability and type of Pickering emulsions. Our experimental work shows that the equilibrium contact angle of particles at interfaces and the type of emulsions preferentially stabilized by these particles can be strongly affected by the particles' charging state, which we attribute to a free energy contribution from the electric field set up by the charged particle and its asymmetric counterion cloud[3]. A very simplistic calculation considering only the dipole field as the leading contribution and treating the water phase as a perfect conductor, finds that the energy stored in the field is indeed strong enough and shows sufficient variation with the particle position to shift the equilibrium position significantly from where it would be based on interfacial tension alone. Only when assuming the existence or particle charges on the particle-oil interface did our model predict the field-induced shift in the particle position to have the experimentally observed direction: toward the water phase, effectively rendering the particles more hydrophilic.

Similarly, the assumption of particle charges on the oil side in our model for the self-energy of the dipole field also led to a qualitatively correct prediction of how the "hydrophilic shift" depends on the particle size (larger particles experiencing a larger shift toward the water phase). This agreement with measured particle contact angles lends further support both to the insight that the electric field around a charged particle in an oil water interface introduces a particle charge and size dependence to the particle's contact angle, as well as the notion that surface charges can exist at the particle-oil interface (which has been championed by others[6], but it still controversial[7]).

For a fully predictive model, future theoretical studies should release the crude approximations made in our simplistic model, and numerically solve for the electrostatic potential everywhere inside and outside a charged particle in an oil-water interface. Calculating the complete electrostatic component of the particle's free energy will yield a far more accurate prediction of the particle's contact angle. In particular it will allow to predict the contact angle dependence on the ionic strength of the aqueous phase, which our toy model for perfectly conducting water obviously could not address. With the availability of trustworthy predictions for the effect of screening, a systematic experimental verification will be called for. Since the gel trapping method applied in the present study is not applicable to a wide range of salt concentrations (the available non-adsorbing gels being incompatible with elevated salt concentrations), it will be necessary to employ alternative experimental techniques for the contact angle assessment, such as the freeze-fracture shadow-casting cryo-scanning electron microscopy[4] championed by the Behrens group collaborator Lucio Isa at the ETH Zurich.

The applied part of this thesis work explored the potential of Pickering emulsions as templates for colloidosome microcapsules with controllable permeability, mechanical properties and response to environmental stimuli. The work presented the first example of combining both inorganic silica particles and stimulus responsive polymer particles to achieve targeted stimulus responsive microcapsules with sustained release profile from double Pickering emulsions. We first successfully prepared microcapsules from double Pickering emulsions with only silica particles via bulk emulsification; second, we presented the first example of incorporating both silica particles and pH responsive particles into the microcapsule shell as a proof of principle for achieving pH responsive

and sustained releasing microcapsules; third, we further demonstrated the first double Pickering emulsion templated capsules in which interfacial polymerization was carried out at both emulsion interfaces, yielding a capsule with two composite shells, suitable for practical encapsulation of small molecules. The work partially contributes to a BASF sponsored project on developing composite microcapsules from double Pickering emulsions to control the release of herbicide for agriculture applications. We will also be looking for options to use the scheme developed in this thesis to prepare antimicrobial microcapsules with sustained release profile, and embed them into paper and packaging products for durable antimicrobial protections[5].

References

1. Behrens, S. H.; Borkovec, M., Electrostatic Interaction of Colloidal Surfaces with Variable Charge. J. Phys. Chem. B 1999, 103 (15), 2918-2928.

2. Borkovec, M.; Behrens, S. H., Electrostatic Double Layer Forces in the Case of Extreme Charge Regulation. J. Phys. Chem. B 2008, 112 (35), 10795-10799.

3. Hurd, A. J., The Electrostatic Interaction between Interfacial Colloidal Particles. J. Phys. A 1985, 18, L1055 - L1060.

4. Isa, L.; Lucas, F.; Wepf, R.; Reimhult, E., Measuring Single-Nanoparticle Wetting Properties by Freeze-Fracture Shadow-Casting Cryo-Scanning Electron Microscopy. Nat. commun. 2011, 2, 438.

5. Ocepek, B.; Boh, B.; Šumiga, B.; Tavčer, P. F., Printing of Antimicrobial Microcapsules on Textiles. Color. Technol. 2012, 128 (2), 95-102.

6. Aveyard, R.; Binks, B. P.; Clint, J. H.; Fletcher, P. D. I.; Horozov, T. S.; Neumann, B.; Paunov, V. N.; Annesley, J.; Botchway, S. W.; Nees, D.; Parker, A. W.; Ward, A. D.; Burgess, A. N., Measurement of Long-Range Repulsive Forces between Charged Particles at an Oil-Water Interface. Phys. Rev. Lett. 2002, 88 (24), 246102-4.

7. Oettel, M.; Dietrich, S., Colloidal Interactions at Fluid Interfaces. Langmuir 2008, 24(4):1425-1441.